Exact inversion of the quasistatic electric potential field to retrieve the complex permittivity of a dielectric cylinder

Armand Wirgin *

January 2, 2015

Abstract

This study concerns the 2D inverse problem of the retrieval, using external field data, of either one of the two physical parameters, constituted by the real and imaginary parts of the permittivity, of a z-independent cylindrical dielectric specimen subjected to an external, z-independent, quasistatic electric field. Six other parameters enter into the inverse problem. They are termed nuisance parameters because: 1) they are not retrieved during the inversion and 2) uncertainty as to their actual values can adversely affect the accuracy of the retrieval of the permittivity. This inverse problem is shown to have an exact, mathematically-explicit, solution, both for continuous and discrete input data, whose properties, with respect to the various nuisance parameter uncertainties, are analyzed, first in a mathematical, and subsequently in a numerical manner for noiseless data. It is found that: a) optimal inversion requires data registered at only a small number of sensors, b) the inverse solution, satisfying pre-existing physical constraints, exists and is unique. Moreover, the inverse solution is shown to be unstable with respect to three nuisance parameter uncertainties, the consequence of which is large retrieval inaccuracy for small nuisance parameter uncertainties, acting either individually or in combination.

Keywords: quasistatic electricity, exact solution of inverse problem, parameter retrieval, real and imaginary parts of permittivity, nuisance parameter uncertainty-induced instabilities.

A shorter version of this study can be found in: Wirgin A., *An exactly-solvable quasistatic electricity inverse problem: retrieval of the complex permittivity of a cylinder taking account of nuisance paramter uncertainty*, Prog.In Electromag.Res. B, 62, 1-16 (2015).

*wirgin@lma.cnrs-mrs.fr, LMA, CNRS, UPR 7051, Aix-Marseille Univ, Centrale Marseille, F-13402 Marseille Cedex 20, France

Contents

1 Introduction

The retrieval of the complex permittivity (or related physical parameters such as the dielectric constant, index of refraction, absorption coefficient,...) of a homogeneous, isotropic material is a theoretical and experimental electromagnetic *inverse* (although only relatively-recently recognized as such) problem of considerable importance. The reason for this is that permittivity is a sensitive indicator of the chemical [9] and physical identity of natural and man-made materials and of their state (notably in quality control and health monitoring [52] applications) [48, 54]. The materials of interest cover a wide range: liquids and colloids (such as industrially-produced organic materials), organic solids (e.g., food [33, 44], live tissue [52]), polymers [26], ceramics, inorganic solids with interesting electronic and optical properties (insulators, conductors, semiconductors, geophysical materials,...) [40, 3].

The DC dielectric constant is usually determined by the comparison of the capacity of an empty or air-filled capacitor with that of the capacitor filled with the dielectric material of interest. At low frequencies ($10^2 - 10^7$ Hz), use is made, for this purpose, of a device similar to the Wheatstone bridge. At higher (10-100 MHz) frequencies, the resonant circuit method is employed, whereas in the range 100 MHz-1 GHz the transmission line technique as well as dielectrometry [28] are used. At still higher (microwave) frequencies, appeal is made to the transmission line technique and the detection of perturbations (shift of frequency and modification of the Q) of a resonant cavity [52]. Finally, at optical frequencies, reflectometry [3], refractometry [1, 2, 9, 3], and ellipsometry [49] are the dominant techniques for the determination of the complex permittivity.

The aforementioned techniques rely (to match theory to measurement) on the possibility of obtaining homogeneous specimens of prescribed (usually-simple) shape (usually a block, slab, thin film, sphere, cylinder, etc.) and size (e.g., films). In naturally-occurring materials, this is not always possible. For instance, in studies of natural phenomena connected with the scattering of light (interstellar dust, air-borne pollution, powder, granular media [41] and other divided matter characterizations, material characterization of living bodies (cells, phytoplancton, etc.), the specimens can have complicated shapes (although they are often considered to be spherical or cylindrical [36, 14, 10]) and are too small (e.g., films so thin that the matter therein appears to be divided) to be examined by the previously-mentioned techniques [34, 14, 10, 36, 49]. It is thus increasingly recognized that discrepancies between the assumed and actual: size, shape and composition of the specimen (divided versus homogeneous, such as in colloids and metamaterials [41, 42, 13, 43, 12]) have to be taken into account in connection with the meaning that is attached to the permittivity determined from the response of the specimens to quasistatic or dynamic (wave-like) electric fields (the latter response incorporates diffraction and/or collective effects, not ordinarily accounted-for in methods relying on reflective or refractive response fields). A second trend of permittivity retrieval inverse problems is the recognition of the necessity of taking into account the *uncertainty* (of the experimental results [49], of certain parameters (and their sensitivity [13]) that enter into the retrieval model, of the mathematical ingredients of the retrieval model itself [50, 37]) in order to evaluate the accuracy of the retrieved parameters, e.g., [49, 17, 19, 20].

The present investigation is inspired by these two trends.

More specifically, we shall be concerned with quasistatic electrical phenomena [29, 21, 35, 5] occurring in $\mathbb{R}^n$ $(n = 1, 2, 3)$ occupied by a heterogeneous, isotropic medium $\mathcal{M}$. Electromagnetic fields are governed, in the space-time framework, by the Maxwell equations ([45])

$$\nabla \times \hat{\mathbf{E}}(\mathbf{x}, t) + \hat{\mathbf{B}}_{,t}(\mathbf{x}, t) = \mathbf{0} \ , \tag{1}$$

$$\nabla \times \hat{\mathbf{H}}(\mathbf{x}, t) - \hat{\mathbf{D}}_{,t}(\mathbf{x}, t) = \hat{\mathbf{J}}(\mathbf{x}, t) \ , \tag{2}$$

wherein $\hat{\mathbf{E}}$ and $\hat{\mathbf{H}}$ are the intensities of the electric and magnetic fields respectively, $\hat{\mathbf{D}}$ the displacement, $\hat{\mathbf{B}}$ the magnetic induction, $\hat{\mathbf{J}}$ the current density, $\mathbf{x}$ the vector from the origin O to a generic point of space, t the time variable, and $,t$ the symbol of partial differentiation with respect to t.

The current density $\hat{\mathbf{J}}$ is the sum of a conduction current density $\hat{\mathbf{J}}^c$ related to the electric field, and an impressed current density $\hat{\mathbf{J}}^i$ connected with the impressed charge density $\hat{\rho}^i$ by the conservation of charge relation

$$\nabla \cdot \hat{\mathbf{J}}^i(\mathbf{x}, t) + \hat{\rho}^i_{,t}(\mathbf{x}, t) = 0 \ . \tag{3}$$

In the *quasistatic electrical regime*, $\hat{\mathbf{B}}_{,t} \approx \mathbf{0}$ so that (1) becomes

$$\nabla \times \hat{\mathbf{E}}(\mathbf{x}, t) = \mathbf{0} \ , \tag{4}$$

whence, by virtue of the identity (for an arbitrary scalar $\hat{S}$) $\nabla \times \nabla \hat{S} = \mathbf{0}$,

$$\hat{\mathbf{E}}(\mathbf{x}, t) = -\nabla \hat{\psi}(\mathbf{x}, t) \ , \tag{5}$$

in which $\hat{\psi}$ designates the quasistatic electrical potential. Taking the divergence of (2), and applying the identity (for an arbitrary vector $\hat{\mathbf{V}}$) $\nabla \cdot \nabla \times \hat{\mathbf{V}} = 0$, gives

$$-\nabla \cdot \hat{\mathbf{D}}_{,t}(\mathbf{x}, t) = \nabla \cdot \hat{\mathbf{J}}(\mathbf{x}, t) \ . \tag{6}$$

The vector and scalar quantities are expressible as the Fourier integrals

$$\hat{\mathbf{V}}(\mathbf{x}, t) = \Re \int_{-\infty}^{\infty} \mathbf{V}(\mathbf{x}, \omega) \exp(-i\omega t) d\omega \ , \ \hat{S}(\mathbf{x}, t) = \Re \int_{-\infty}^{\infty} S(\mathbf{x}, \omega) \exp(-i\omega t) d\omega \ , \tag{7}$$

(wherein ω is the angular frequency), so that (3), (5) and (6) yield the frequency domain partial differential equations

$$\nabla \cdot \mathbf{J}^i(\mathbf{x}, \omega) - i\omega \rho^i(\mathbf{x}, \omega) = 0 \ . \tag{8}$$

$$\mathbf{E}(\mathbf{x}, \omega) = -\nabla \psi(\mathbf{x}, \omega) \ , \tag{9}$$

$$i\omega \nabla \cdot \mathbf{D}(\mathbf{x}, \omega) = \nabla \cdot \mathbf{J}(\mathbf{x}, \omega) = \nabla \cdot \left(\mathbf{J}^i(\mathbf{x}, \omega) + \ \mathbf{J}^c(\mathbf{x}, \omega) \right) \ . \tag{10}$$

In an isotropic, generally-inhomogeneous, medium, the displacement and the conduction current density are related to the electric field by a dielectric constant $\varepsilon'(\mathbf{x},\omega)$ and loss factor $\varepsilon''(\mathbf{x},\omega)$ respectively via the constitutive relations:

$$\mathbf{D}(\mathbf{x},\omega) = \varepsilon'(\mathbf{x},\omega)\mathbf{E}(\mathbf{x},\omega) \ , \tag{11}$$

$$\mathbf{J}^c(\mathbf{x},\omega) = \omega\varepsilon''(\mathbf{x},\omega)\mathbf{E}(\mathbf{x},\omega) \ . \tag{12}$$

wherein ε' and ε'' are generally positive (or zero) scalar functions for $\omega \geq 0$. It ensues that

$$i\omega\nabla\cdot(\varepsilon'(\mathbf{x},\omega)\mathbf{E}(\mathbf{x},\omega)) = \nabla\cdot\mathbf{J}^i(\mathbf{x},\omega) + \nabla\cdot(\varepsilon''(\mathbf{x},\omega)\mathbf{E}(\mathbf{x},\omega)) \ , \tag{13}$$

or

$$\nabla\cdot\left[\left(\varepsilon'(\mathbf{x},\omega) + i\varepsilon''(\mathbf{x},\omega)\right)\mathbf{E}(\mathbf{x},\omega)\right] = \frac{\nabla\cdot\mathbf{J}^i(\mathbf{x},\omega)}{i\omega} \ , \tag{14}$$

whence

$$\nabla\cdot[\varepsilon(\mathbf{x},\omega)\mathbf{E}(\mathbf{x},\omega)] = \rho^i(\mathbf{x},\omega) \ , \tag{15}$$

or

$$\nabla\cdot[\varepsilon(\mathbf{x},\omega)\nabla\psi(\mathbf{x},\omega)] = -\rho^i(\mathbf{x},\omega) \ , \tag{16}$$

wherein

$$\varepsilon(\mathbf{x},\omega) = \varepsilon'(\mathbf{x},\omega) + i\varepsilon''(\mathbf{x},\omega) \ , \tag{17}$$

is the (complex) permittivity such that $\varepsilon(\mathbf{x},-\omega) = \varepsilon^*(\mathbf{x},\omega)$; $\omega > 0$. For For passive materials, $\varepsilon' \geq 0$ and $\varepsilon'' \geq 0$. Usually, $\varepsilon'' << \varepsilon'$ at low frequencies. The quasistatic electric field is thus seen to be governed by an inhomogeneous Poisson equation, which, in a homogeneous medium, devoid of impressed sources, becomes the (homogeneous) Laplace equation.

Let $\mathbb{R}^n$ be divided into two domains $\mathfrak{D}_0$ and $\mathfrak{D}_1$, separated by the interface $\mathfrak{I}$ the unit vector normal to which is $\boldsymbol{\nu}$, and let $\mathfrak{M}_0$ and $\mathfrak{M}_1$ be two homogeneous, isotropic dielectric media (filling $\mathfrak{D}_0$ and $\mathfrak{D}_1$ respectively) in which the position-independent permittivities are ε_0 and ε_1 respectively.

If all space (i.e., $\mathfrak{D}_0+\mathfrak{D}_1$) is occupied solely by $\mathfrak{M}_0$, and to be devoid of impressed charges (i.e., $\rho^i = 0$), but subjected to a uniform electric field $\mathbf{E}^i$ satisfying

$$\mathbf{E}^i = -\nabla\psi^i \ , \tag{18}$$

then

$$\nabla\cdot(\varepsilon_0\nabla\psi^i) = 0 \quad \text{ in } \mathfrak{D}_0 \subset \mathbb{R}^n \ . \tag{19}$$

The introduction of $\mathfrak{M}_1$ into $\mathfrak{D}_1$ induces a potential ψ_0^d in $\mathfrak{D}_0$ so that the total potential is now

$$\psi_0 = \psi^i + \psi_0^d \quad \text{ in } \mathfrak{D}_0 \ , \tag{20}$$

whereas the induced and total potentials in $\mathfrak{D}_1$ are

$$\psi_1 = \psi_1^d \quad \text{ in } \mathfrak{D}_1 \ . \tag{21}$$

Then the problem of the prediction of ψ_l ; $l = 0, 1$, for given $\mathbf{E}^i$ or ψ^i, can be cast in the three-relation form (equivalent to (12))

$$\nabla \cdot (\nabla \psi_l) = 0 \quad \text{in } \mathfrak{D}_l \ , \ l = 0, 1 \ , \tag{22}$$

$$\psi_0 - \psi_1 = 0 \quad \text{on } \mathfrak{I} \ , \tag{23}$$

$$\varepsilon_0 \boldsymbol{\nu} \cdot \nabla \psi_0 - \varepsilon_1 \boldsymbol{\nu} \cdot \nabla \psi_1 = 0 \quad \text{on } \mathfrak{I} \ , \tag{24}$$

with uniqueness assured by the condition:

$$|\psi_l^d| < \infty \quad \text{in } \mathfrak{D}_l \ ; \ l = 0, 1 \ . \tag{25}$$

In the preceding lines, the emphasis has been on the *forward problem* of the prediction of the potential field ψ, assuming that all other ingredients of the configuration and of the solicitation (via ψ^i) are known. Actually, the present investigation is more specifically concerned with the *inverse problem* (examples of which can be found in [14, 8, 24, 29, 31, 6, 17, 39, 23, 51, 11, 53, 19, 5, 27, 5, 38, 19]) of the retrieval of ε (or, more precisely, of ε_1) from data relative to ψ (more precisely, ψ_0), assuming that all other parameters of the configuration as well as of the solicitation (i.e., the nuisance parameters [17]) are more or less well-known (i.e., uncertain to some degree).

The chosen physical configuration (in which $\mathfrak{D}_1$ is an infinitely-long circular cylinder) will be shown to enable both the forward and inverse problems to be solved in explicit, exact manner so as to make possible a thorough analysis (somewhat in the spirit of [19, 20, 17]) of the influence of nuisance parameter uncertainty on retrieval accuracy. This point merits to be emphasized because it is not often that an other-than-academic inverse problem can be solved exactly (see [50] for another example), and it is not commonplace in parameter retrieval problems to be able to evaluate analytically the influence of nuisance prior uncertainty on the accuracy of the retrievals.

At this point, it is necessary to give a definition of *uncertainty*. Let us first assume that the potential field (i.e., the input data required for the inversion) is the output of a real experiment. In order to conceptualize this experiment, and/or eventually simulate (by a computer code, rather than physically-generate) the data, we need a mathematical model of the physics involved in the experiment. This model, includes, among other things, a set of parameters $\mathbf{p} = \{p_1, p_2, ...\}$ to which we must assign values. A way to do this is by measurement. Assume that one of these parameters, say p_j is what (we think) is actually measured. It is common to repeat the measurement of p_j several times (call these: realizations) while keeping all the other parameters (hopefully) constant. If these various realizations lead to different values of p_j then we say that there is some error in the measurement of p_j, and the inclination is strong to class these as *random errors* [17, 15]. If, on the other hand, the various realizations lead to the same value P_j, then the question arises as to whether this value is the true value or something else. If it is something else, then its departure from the true value can be qualified as *systematic error* [15]. If systematic error is thought to exist, but cannot be corrected (with the means available to the experimentalist) then a way

of taking this error into account is to say that p_j lies somewhere within a *range of values* including P_j. If, on the other hand, we don't even go to the trouble of actually measuring p_j, then a common way of assigning a value to it is either by guessing, or borrowing the value from a publication. Again, the question arises as to whether this (guessed or borrowed) value P_j is the true value. If, as it is reasonable to expect, P_j is not the true value of p_j (all the more so than we don't know (the true) p_j), then we can take into account this error by saying that p_j lies somewhere within a *range of values* including P_j. In what follows, we qualify a parameter as being uncertain by the fact that its assigned value, resulting from experiment, guessing or borrowing from a published result, is incorrect in a sense akin to systematic measurement error.

2 Description of the physical configuration

A circular cylinder, occupied by the homogeneous, isotropic medium $\mathfrak{M}_1$ (in which the permittivity is ε_1) is introduced into another homogeneous, isotropic medium $\mathfrak{M}_0$ (in which the permittivity is ε_0) of infinite extent and is submitted to an electric field $\mathbf{E}^i$ whose direction is assumed to be constant at all points of space. The z axis (of the cartesian coordinate system $Oxyz$ forms the axis of the cylinder and the circular disk Ω_1, with center at O, constitutes the support of the cylinder in the $x-y$ plane. The unbounded region exterior to Ω_1 (in the $x-y$ plane) is Ω_0.

The incident electric field vector $\mathbf{E}^i$ is assumed to lie in the $x-y$ plane and to be independent of z. The circular boundary of Ω_1 is Γ, the outward unit vector normal to which is $\boldsymbol{\nu}$. Consequently, the incident and induced fields are independent of z, i.e., *the problem is two-dimensional, with z the ignorable coordinate* (fig. 1).

The effect of the primary field $\mathbf{E}^i = -\nabla\psi^i$ on the cylinder is to induce a secondary field $\mathbf{E}^d = -\nabla\psi^d$. In the so-called forward problem, the task is to predict this secondary field, whereas in the inverse problem, the associated potential ψ^d (combined with ψ^i) constitutes the data, which, by means of an inversion scheme, is analyzed to enable the retrieval of the constitutive parameter ε_1 of $\mathfrak{M}_1$.

The units of $\mathbf{E}$, ψ, ε, a, θ^i, b and θ are: $volt/m$, $volt$, $farad/m$, m, $^\circ$ or rad, m, $^\circ$ or rad respectively.

Let r, θ designate the polar coordinates of a point P in the $x-y$ plane and let $\mathbf{x}$ designate the vector joining O to P. The parametric equation of Γ is $r = a\ ;\ \forall\theta \in [0, 2\pi[$, with a (m) the radius of the circular disk Ω_1. The (incident) angle between $\mathbf{E}^i$ and the x axis is θ^i ($^\circ$ or rad).

The total (primary plus secondary) potential field is assumed to be sensed at various points on a circle (concentric with Γ) of radius $b > a$. The polar angle ($^\circ$ or rad) at which a generic point-like sensor is located is θ (with respect to the positive x axis).

In the first part of this document, the objective will be: given e^i (amplitude of ψ^i), θ^i, a and $\varepsilon_l\ ;\ l = 0, 1$, find the total potential fields at one or more positions (starting with $\theta = \theta^b$) on the circle $r = b$. It is assumed that the location of the axis of the cylinder is known (and coincides with the $z-$axis) and that the number, and angular, positions of the point-like (in

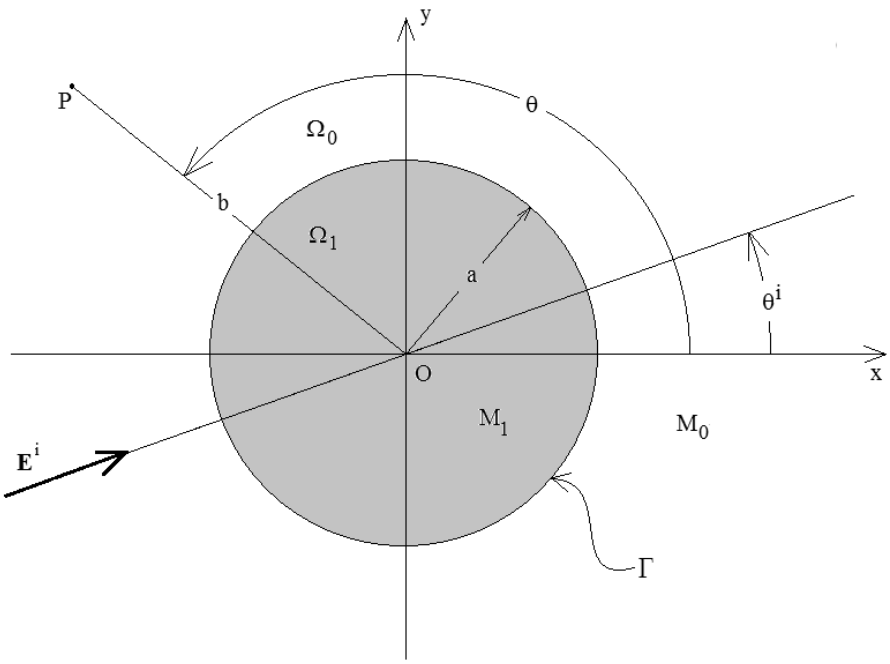

Figure 1: Problem configuration in the $x-y$ plane.

the $x-y$ plane) sensors are perfectly well-known in both the forward and inverse problem contexts.

In the second, main, part of this document, the objective will be: given the total potential fields registered at one or more sensors located at angular positions starting with $\theta = \theta^b$ on the circle $r = B$ (analogous to, but different from, b due to uncertainty of this parameter), as well as the set of parameters E^i, Θ^i, A and $\mathcal{E}_0$ (analogous to e^i, θ^i, a and ε_0, but integrating uncertainties), find $\mathcal{E}_1'$ (analogous to ε_1). Actually, the *exact* solution (to simulate measured data concerning the total field) obtained in the first part of this document will be employed as the data (the corresponding model is termed the *data simulation model*) to solve the inverse problem in the second part of the document. In addition, we appeal to a *parameter retrieval model*, also based on the aforementioned physical configuration, to recover the constitutive parameter of the cylinder.

Some of the fixed (during the inversion) parameters (the so-called *nuisance parameters*) of the retrieval models will be assumed to be not precisely known. The effect of various amounts of nuisance parameter uncertainty on the accuracy of the retrievals will be studied in depth in the sequel.

3 The forward problem

3.1 Boundary-value problem

The generic potential $\psi(\mathbf{x})$ is related to the generic vectorial electric field $\mathbf{E}(\mathbf{x})$ by $\mathbf{E}(\mathbf{x}) = -[\psi_{,r}(\mathbf{x})\mathbf{i}_r - r^{-1}\psi_{,\theta}(\mathbf{x})\mathbf{i}_\theta]$, with $\mathbf{i}_r$, $\mathbf{i}_\theta$ the unit vectors corresponding to r, θ. Furthermore, $\boldsymbol{\nu} = \mathbf{i}_r$, so that $\boldsymbol{\nu} \cdot \nabla\psi(\mathbf{x}) = \psi_{,r}(\mathbf{x})$.

The assumed primary electric potential which satisfies

$$\frac{1}{r}\frac{\partial}{\partial r}\Big(r\frac{\partial\psi^i(r,\theta)}{\partial r}\Big) + \frac{1}{r^2}\frac{\partial^2\psi^i(r,\theta)}{\partial\theta^2} = 0 \ ; \ \forall(r,\theta) \in \Omega_0 \ , \tag{26}$$

is

$$\psi^i(r,\theta) = -e^i r\cos(\theta - \theta^i) \ , \tag{27}$$

with e^i a constant amplitude term. Applied to our cylindrical geometry problem, the governing equations of sect. 1 become

$$\frac{1}{r}\frac{\partial}{\partial r}\Big(r\frac{\partial\psi_l^d(r,\theta)}{\partial r}\Big) + \frac{1}{r^2}\frac{\partial^2\psi_l^d(r,\theta)}{\partial\theta^2} = 0 \ ; \ \forall(r,\theta) \in \Omega_l \ \ ; \ \ l = 0,1 \ , \tag{28}$$

$$\psi_0(a,\theta) - \psi_1(a,\theta) = 0 \ ; \ \forall\theta \in [0, 2\pi[, \tag{29}$$

$$\varepsilon_0\psi_{0,r}(a,\theta) - \varepsilon_1\psi_{1,r}(a,\theta) = 0 \ ; \ \forall\theta \in [0, 2\pi[\ . \tag{30}$$

$$|\psi_l^d(r,\theta)| < \infty \ ; \ \forall\mathbf{r},\theta \in \Omega_l \ \ ; \ \ l = 0,1 \ , \tag{31}$$

3.2 Field representations and application of the boundary conditions

By separation of variables, we obtain the following electric potential field representations satisfying (27)-(31); note that a term such as $\ln r$ does not satisfy (31) either in Ω_0 (notably at $r \to \infty$) or Ω_1 (notably at $r = 0$):

$$\psi_0^d(\mathbf{x}) = \sum_{n=0}^{\infty} r^{-n}\left[\mathcal{A}_n\cos(n\theta) + \mathcal{A}'_n\sin(n\theta)\right] \ ; \ \forall\mathbf{x} \in \Omega_0 \ , \tag{32}$$

$$\psi_1^d(\mathbf{x}) = \sum_{n=0}^{\infty} r^{n}\left[\mathcal{B}_n\cos(n\theta) + \mathcal{B}'_n\sin(n\theta)\right] \ ; \ \forall\mathbf{x} \in \Omega_1 \ , \tag{33}$$

with the understanding that $\mathcal{A}'_0 = \mathcal{B}'_0 = 0$. This suggests writing ψ^i as:

$$\psi_1^i(\mathbf{x}) = \sum_{n=0}^{\infty} r^{n}\left[\mathcal{C}_n\cos(n\theta) + \mathcal{C}'_n\sin(n\theta)\right] \ , \tag{34}$$

wherein

$$\mathcal{C}_n = -e^i\cos(n\theta^i)\delta_{n1} \ \ , \ \ \mathcal{C}'_n = -e^i\sin(n\theta)\delta_{n1} \ , \tag{35}$$

and δ_{nm} is the Kronecker delta symbol.

Eqs. (29)-(30) lead to:

$$\mathcal{A}_m = e^i a^2 \Big(\frac{\varepsilon_1 - \varepsilon_0}{\varepsilon_1 + \varepsilon_0}\Big) \cos(\theta^i)\delta_{m1} \quad , \quad \mathcal{A}'_m = e^i a^2 \Big(\frac{\varepsilon_1 - \varepsilon_0}{\varepsilon_1 + \varepsilon_0}\Big) \sin(\theta^i)\delta_{m1} \ , \tag{36}$$

$$\mathcal{B}_m = -e^i \Big(\frac{2\varepsilon_0}{\varepsilon_1 + \varepsilon_0}\Big) \cos(\theta^i)\delta_{m1} \quad , \quad \mathcal{B}'_m = e^i \Big(\frac{2\varepsilon_0}{\varepsilon_1 + \varepsilon_0}\Big) \sin(\theta^i)\delta_{m1} \ , \tag{37}$$

whence, by virtue of (32)-(33), and taking, for convenience, $\mathcal{A}_0 = \mathcal{B}_0 = 0$:

$$\psi_0^d(\mathbf{x}) = e^i \frac{a^2}{r}\Big(\frac{\varepsilon_1 - \varepsilon_0}{\varepsilon_1 + \varepsilon_0}\Big) \cos(\theta - \theta^i) \ \Rightarrow \ \psi_0(\mathbf{x}) = e^i \Big[-r + \frac{a^2}{r}\Big(\frac{\varepsilon_1 - \varepsilon_0}{\varepsilon_1 + \varepsilon_0}\Big)\Big] \cos(\theta - \theta^i) \ , \tag{38}$$

$$\psi_1(\mathbf{x}) = \psi_1^d(\mathbf{x}) = -e^i r \Big(\frac{2\varepsilon_0}{\varepsilon_1 + \varepsilon_0}\Big) \cos(\theta - \theta^i) \ . \tag{39}$$

Note that these expressions are identical to those in [30], p. 1185 when $\theta^i = 0$.

4 Exact solution of the inverse problem

4.1 General considerations

The inversion consists in obtaining estimates $\mathcal{E}'_1,\ \mathcal{E}''_1$ of the sought-for constitutive parameters $\varepsilon'_1,\ \varepsilon''_1$ by minimizing a cost functional which expresses the discrepancy between the data simulation model (ψ_0) of the electric potential and the parameter retrieval model (Ψ_0) of the electric potential on the circle of radius b (which becomes B if it is uncertain) in the angular interval of observation $[0, 2\pi[$. This cost functional is:

$$\mathcal{K}(\mathcal{E}'_1, \mathcal{E}''_1) = \frac{\int_0^{2\pi} \Big\| \psi_0(b, \theta | e^i, \theta^i, a, \varepsilon_0, \varepsilon'_1, \varepsilon''_1) - \Psi_0(B, \theta | E^i, \Theta^i, A, \mathcal{E}_0, \mathcal{E}'_1, \mathcal{E}''_1) \Big\|^2 d\theta}{\int_0^{2\pi} \Big\| \psi_0(b, \theta | e^i, \theta^i, a, \varepsilon_0, \varepsilon_1) \Big\|^2 d\theta} \ . \tag{40}$$

$\mathcal{K}$ is actually replaced, in the numerical context, and to account for the discrete nature of the physical sensing process, by another cost functional obtained by adopting a simple quadrature rule for the integrals:

$$\mathcal{K} \approx \mathcal{K}^{(N)}(\mathcal{E}'_1, \mathcal{E}''_1) = \frac{\delta_\theta \sum_{n=1}^N \Big\| \psi_0(b, \theta_n | e^i, \theta^i, a, \varepsilon_0, \varepsilon'_1, \varepsilon''_1) - \Psi_0(B, \theta_n | E^i, \Theta^i, A, \mathcal{E}_0, \mathcal{E}'_1, \mathcal{E}''_1) \Big\|^2}{\delta_\theta \sum_{n=1}^N \Big\| \psi_0(b, \theta_n | e^i, \theta^i, a, \varepsilon_0, \varepsilon'_1, \varepsilon''_1) \Big\|^2} \ , \tag{41}$$

wherein $\delta_\theta = 2\pi/N$, and $\theta_n = \theta^b + \frac{\delta_\theta}{2} + (n-1)\delta_\theta$ are the actual angles (for $n = 1, 2, ..., N$; θ^b a chosen starting angle and θ^e a chosen ending angle) at which the electric potential is sensed.

Note that the set of parameters (lower case letters and symbols) is different in the simulated data model from the corresponding set (upper case letters and symbols) in the parameter retrieval model; this expresses the fact that the subset of nuisance parameters (all the parameters except ε_1) may be not well-known to us before, and during, the inversion.

We have

$$\psi_0(b,\theta) = e^i\Big[-b+\frac{a^2}{b}\Big(\frac{\varepsilon_1'+i\varepsilon_1''-\varepsilon_0}{\varepsilon_1'+i\varepsilon_1''+\varepsilon_0}\Big)\Big]\cos(\theta-\theta^i) = \mathfrak{f}(e^i,a,b,\varepsilon_0,\varepsilon_1',\varepsilon_1'')\cos(\theta-\theta^i)\ , \quad (42)$$

so that

$$\Psi_0(B,\theta) = E^i\Big[-B+\frac{A^2}{B}\Big(\frac{\mathcal{E}_1'+i\mathcal{E}_1''-\mathcal{E}_0}{\mathcal{E}_1'+i\mathcal{E}_1''+\mathcal{E}_0}\Big)\Big]\cos(\theta-\Theta^i) = \mathfrak{F}(E^i,A,B,\mathcal{E}_0,\mathcal{E}_1',\mathcal{E}_1'')\cos(\theta-\Theta^i)\ . \quad (43)$$

It ensues that:

$$\mathcal{K}(\mathcal{E}_1) = \frac{\int_0^{2\pi}\Big\|\mathfrak{f}\cos(\theta-\theta^i)-\mathfrak{F}\cos(\theta-\Theta^i)\Big\|^2 d\theta}{\int_0^{2\pi}\Big\|\mathfrak{f}\cos(\theta-\theta^i)\Big\|^2 d\theta}\ . \quad (44)$$

and

$$\mathcal{K}^{(N)}(\mathcal{E}_1) = \frac{\delta_\theta\sum_{n=1}^{N}\Big\|\mathfrak{f}\cos(\theta_n-\theta^i)-\mathfrak{F}\cos(\theta_n-\Theta^i)\Big\|^2 d\theta}{\delta_\theta\sum_{0}^{N}\Big\|\mathfrak{f}\cos(\theta_n-\theta^i)\Big\|^2 d\theta}\ . \quad (45)$$

4.2 Finding a constitutive parameter of the cylinder by minimizing $\mathcal{K}$

Let G be any one of the capital-letter parameters and $\kappa = \cos(\Theta^i-\theta^i)$. From (44) we obtain

$$\mathcal{K}(G) = \frac{\|\mathfrak{f}\|^2 - 2\kappa\Re(\mathfrak{f}^*\mathfrak{F})+\|\mathfrak{F}\|^2}{\|\mathfrak{f}\|^2}\ , \quad (46)$$

wherein the symbol * designates the complex conjugate operator. An extremum of the cost functional with respect to the variable G (henceforth, $\mathcal{E}'$ or $\mathcal{E}''$) is found for $\frac{\partial\mathcal{K}(G)}{\partial G}=0$ or

$$\Re\Big(\frac{\partial\mathfrak{F}^*}{\partial G}\Big)\Re(\mathfrak{F}-\kappa\mathfrak{f}) - \Im\Big(\frac{\partial\mathfrak{F}^*}{\partial G}\Big)\Im(\mathfrak{F}-\kappa\mathfrak{f}) = 0\ . \quad (47)$$

It is easily found that:

$$\Re(\mathfrak{F}-\kappa\mathfrak{f}) = E^i\Big[-B+\frac{A^2}{B}\Big(\frac{\mathcal{E}_1'^2+\mathcal{E}_1''^2-\mathcal{E}_0^2}{\|\mathcal{E}_1+\mathcal{E}_0\|^2}\Big)\Big] - e^i\kappa\Big[-b+\frac{a^2}{b}\Big(\frac{\varepsilon_1'^2+\varepsilon_1''^2-\varepsilon_0^2}{\|\varepsilon_1+\varepsilon_0\|^2}\Big)\Big]\ , \quad (48)$$

$$\Im(\mathfrak{F}-\mathfrak{f}\kappa) = E^i\frac{A^2}{B}\Big[\frac{2\mathcal{E}_1''\mathcal{E}_0}{\|\mathcal{E}_1+\mathcal{E}_0\|^2}\Big] - e^i\kappa\frac{a^2}{b}\Big[\frac{2\varepsilon_1''\varepsilon_0}{\|\varepsilon_1+\varepsilon_0\|^2}\Big]\ , \quad (49)$$

$$\frac{\partial\mathfrak{F}^*}{\partial\mathcal{E}_1'}=\frac{E^{i*}A^2 2\mathcal{E}_0^*}{B\|(\mathcal{E}_1+\mathcal{E}_0)^2\|^2}\Big[\big(\mathcal{E}_1'^2-\mathcal{E}_1''^2+2\mathcal{E}_0\mathcal{E}_1'+\mathcal{E}_0^2\big)+2i\big(\mathcal{E}_1'\mathcal{E}_1''+\mathcal{E}_0\mathcal{E}_1''\big)\Big]:=\mathcal{F}\frac{E^{i*}A^2 2\mathcal{E}_0^*}{B\|(\mathcal{E}_1+\mathcal{E}_0)^2\|^2}\ , \tag{50}$$

$$\frac{\partial\mathfrak{F}^*}{\partial\mathcal{E}_1''}=-i\frac{\partial\mathfrak{F}^*}{\partial\mathcal{E}'}:=-i\mathcal{F}\frac{E^{i*}A^2 2\mathcal{E}_0^*}{B\|(\mathcal{E}_1+\mathcal{E}_0)^2\|^2}\ . \tag{51}$$

Henceforth, we shall assume that E^i and $\mathcal{E}_0$ are positive real, so that dividing (47) by $\frac{E^{i*}A^2 2\mathcal{E}_0^*}{B\|(\mathcal{E}_1+\mathcal{E}_0)^2\|^2}\neq 0$ yields either

$$\Re(\mathcal{F})\Re(\mathfrak{F}-\kappa\mathfrak{f})-\Im(\mathcal{F})\Im(\mathfrak{F}-\kappa\mathfrak{f})=0\ , \tag{52}$$

(for the determination of $\mathcal{E}_1'$) or

$$\Re(-i\mathcal{F})\Re(\mathfrak{F}-\kappa\mathfrak{f})-\Im(-i\mathcal{F})\Im(\mathfrak{F}-\kappa\mathfrak{f})=0\ , \tag{53}$$

(for the determination of $\mathcal{E}_1''$) wherein

$$\mathcal{F}=\big(\mathcal{E}_1'^2-\mathcal{E}_1''^2+2\mathcal{E}_0\mathcal{E}_1'+\mathcal{E}_0^2\big)+2i\big(\mathcal{E}_1'\mathcal{E}_1''+\mathcal{E}_0\mathcal{E}_1''\big)\ , \tag{54}$$

4.3 Finding $\mathcal{E}_1'$ of the cylinder by minimizing $\mathcal{K}$

Eq.(54) tells us that

$$\Re(\mathcal{F})=\mathcal{E}_1'^2-\mathcal{E}_1''^2+2\mathcal{E}_0\mathcal{E}_1'+\mathcal{E}_0^2\ , \tag{55}$$

$$\Im(\mathcal{F})=2\big(\mathcal{E}_1'\mathcal{E}_1''+\mathcal{E}_0\mathcal{E}_1''\big)\ , \tag{56}$$

so that (52) becomes

$$\big(\mathcal{E}_1'^2-\mathcal{E}_1''^2+2\mathcal{E}_0\mathcal{E}_1'+\mathcal{E}_0^2\big)\Re(\mathfrak{F}-\kappa\mathfrak{f})-2\big(\mathcal{E}_1'\mathcal{E}_1''+\mathcal{E}_0\mathcal{E}_1''\big)\Im(\mathfrak{F}-\kappa\mathfrak{f})=0\ . \tag{57}$$

On the other hand, we can write (48) and (49) as:

$$\Re(\mathfrak{F}-\kappa\mathfrak{f})=F\Big[-B^2+A^2\Big(\frac{\mathcal{E}_1'^2+\mathcal{E}_1''^2-\mathcal{E}_0^2}{\|\mathcal{E}_1+\mathcal{E}_0\|^2}\Big)\Big]-fg\ , \tag{58}$$

$$\Im(\mathfrak{F}-\mathfrak{f}\kappa)=FA^2\Big(\frac{2\mathcal{E}_1''\mathcal{E}_0}{\|\mathcal{E}_1+\mathcal{E}_0\|^2}\Big)-fh\ , \tag{59}$$

wherein

$$F:=\frac{E^i}{B}\quad,\quad f:=\frac{e^i\kappa}{b}\quad,\quad g:=-b^2+a^2\Big(\frac{\varepsilon_1'^2+\varepsilon_1''^2-\varepsilon_0^2}{\|\varepsilon_1+\varepsilon_0\|^2}\Big)\quad,\quad h:=\frac{2a^2\varepsilon_1''\varepsilon_0}{\|\varepsilon_1+\varepsilon_0\|^2}\ , \tag{60}$$

so that (52) becomes

$$\Big[\mathcal{E}_1'^2-\mathcal{E}_1''^2+2\mathcal{E}_0\mathcal{E}_1'+\mathcal{E}_0^2\Big]\Big[-FB^2+FA^2\Big(\frac{\mathcal{E}_1'^2+\mathcal{E}_1''^2-\mathcal{E}_0^2}{\|\mathcal{E}_1+\mathcal{E}_0\|^2}\Big)-fg\Big]-$$
$$\Big[2\big(\mathcal{E}_1'\mathcal{E}_1''+\mathcal{E}_0\mathcal{E}_1''\big)\Big]\Big[FA^2\Big(\frac{2\mathcal{E}_1''\mathcal{E}_0}{\|\mathcal{E}_1+\mathcal{E}_0\|^2}\Big)-fh\Big]=0\ . \tag{61}$$

The product of this equation with $\|\mathcal{E}_1+\mathcal{E}_0\|^2=\mathcal{E}_1^{'2}+\mathcal{E}_1^{''2}+2\mathcal{E}_1'\mathcal{E}_0+\mathcal{E}_0^2\neq 0$ yields

$$\Big[\mathcal{E}_1^{'2}-\mathcal{E}_1^{''2}+2\mathcal{E}_0\mathcal{E}_1'+\mathcal{E}_0^2\Big]\Big[-(FB^2+fg)(\mathcal{E}_1^{'2}+\mathcal{E}_1^{''2}+2\mathcal{E}_1'\mathcal{E}_0+\mathcal{E}_0^2)+FA^2(\mathcal{E}_1^{'2}+\mathcal{E}_1^{''2}-\mathcal{E}_0^2)\Big]-$$
$$\Big[2\big(\mathcal{E}_1'\mathcal{E}_1''+\mathcal{E}_0\mathcal{E}_1''\big)\Big]\Big[FA^2\Big(2\mathcal{E}_1''\mathcal{E}_0\Big)-fh(\mathcal{E}_1^{'2}+\mathcal{E}_1^{''2}+2\mathcal{E}_1'\mathcal{E}_0+\mathcal{E}_0^2)\Big]=0\ , \quad (62)$$

which can be cast into the form of the *quartic* equation [4]

$$\mathfrak{C}_4\mathcal{E}_1^{'4}+\mathfrak{C}_3\mathcal{E}_1^{'3}+\mathfrak{C}_2\mathcal{E}_1^{'2}+\mathfrak{C}_1\mathcal{E}_1'+\mathfrak{C}_0=0\ , \quad (63)$$

whose coefficients are:

$$\mathfrak{C}_4=FA^2-(FB^2+fg)\ , \quad (64)$$
$$\mathfrak{C}_3=2\mathcal{E}_0FA^2-4\mathcal{E}_0(FB^2+fg)+2\mathcal{E}_1''fh\ , \quad (65)$$
$$\mathfrak{C}_2=-2\mathcal{E}_0^2(FB^2+fg)+6\mathcal{E}_0\mathcal{E}_1''fh\ , \quad (66)$$
$$\mathfrak{C}_1=-2\mathcal{E}_0k_+FA^2-2\mathcal{E}_0(k_++k_-)(FB^2+fg)+(2k_++4\mathcal{E}_0^2)\mathcal{E}_1''fh\ , \quad (67)$$
$$\mathfrak{C}_0=-k_+^2FA^2-k_+k_-(FB^2+fg)+2k_+\mathcal{E}_0\mathcal{E}_1''fh\ , \quad (68)$$

with

$$k_\pm:=\mathcal{E}_0^2\pm\mathcal{E}_1^{''2}\ . \quad (69)$$

It ensues from these formulae that:

$$\mathfrak{C}_1=\frac{2\mathcal{E}_0\mathfrak{C}_0}{k_+}+k_+(\mathfrak{C}_3-2\mathcal{E}_0\mathfrak{C}_4)\ , \quad (70)$$

$$\mathfrak{C}_2=\frac{\mathfrak{C}_0}{k_+}+2\mathcal{E}_0(\mathfrak{C}_3-2\mathcal{E}_0\mathfrak{C}_4)+k_+\mathfrak{C}_4\ , \quad (71)$$

so that the quartic equation can re-written as

$$\mathfrak{C}_4\mathcal{E}_1^{'4}+\mathfrak{C}_3\mathcal{E}_1^{'3}+\Big[\frac{\mathfrak{C}_0}{k_+}+2\mathcal{E}_0(\mathfrak{C}_3-2\mathcal{E}_0\mathfrak{C}_4)+k_+\mathfrak{C}_4\Big]\mathcal{E}_1^{'2}+\Big[\frac{2\mathcal{E}_0\mathfrak{C}_0}{k_+}+k_+(\mathfrak{C}_3-2\mathcal{E}_0\mathfrak{C}_4)\Big]\mathcal{E}_1'+\mathfrak{C}_0=0\ , \quad (72)$$

or

$$(\mathcal{E}_1^{'2}+2\mathcal{E}_0\mathcal{E}_1'+k_+)\Big[\mathcal{C}_4\mathcal{E}_1'(\mathcal{E}_1'-2\mathcal{E}_0)+\mathfrak{C}_3\mathcal{E}_1'+\frac{\mathfrak{C}_0}{k_+}\Big]=0\ . \quad (73)$$

Thus, the solutions of the quartic equation can be obtained from the solutions of the two quadratic equations:

$$\mathcal{E}_1^{'2}+2\mathcal{E}_0\mathcal{E}_1'+k_+=0\ . \quad (74)$$

$$\mathcal{C}_4\mathcal{E}_1'(\mathcal{E}_1'-2\mathcal{E}_0)+\mathfrak{C}_3\mathcal{E}_1'+\frac{\mathfrak{C}_0}{k_+}=0\ . \quad (75)$$

The two roots of (74) are:

$$\begin{aligned}\mathcal{E}_1^{'(1)}&=-\mathcal{E}_0-i\mathcal{E}_1''\\ \mathcal{E}_1^{'(2)}&=-\mathcal{E}_0+i\mathcal{E}_1''\end{aligned}\ , \quad (76)$$

whereas the two roots of (75) are:

$$\begin{array}{l} \mathcal{E}_1^{\prime(-)} = \frac{-k_+(\mathfrak{C}_3-2\mathcal{E}_0\mathfrak{C}_4)-\sqrt{k_+^2(\mathfrak{C}_3-2\mathcal{E}_0\mathfrak{C}_4)^2-4k_+\mathfrak{C}_4\mathfrak{C}_0}}{2k_+\mathfrak{C}_4} \\ \mathcal{E}_1^{\prime(+)} = \frac{-k_+(\mathfrak{C}_3-2\mathcal{E}_0\mathfrak{C}_4)+\sqrt{k_+^2(\mathfrak{C}_3-2\mathcal{E}_0\mathfrak{C}_4)^2-4k_+\mathfrak{C}_4\mathfrak{C}_0}}{2k_+\mathfrak{C}_4} \end{array} \quad . \tag{77}$$

Eqs. (76)-(77) represent the exact solutions of the inverse problem of the identification of the sole parameter $\mathcal{E}_1'$. Recall that it was assumed that $\mathcal{E}_0$, $\mathcal{E}_1'$ and $\mathcal{E}_1''$ (of the same nature as ε_0, ε_1', ε_1'' respectively) are positive real. Thus, $\mathcal{E}_1^{\prime(1)}$ and $\mathcal{E}_1^{\prime(2)}$ are not admissible solutions. Whether $\mathcal{E}_1^{\prime(\pm)}$ are admissible or not can be decided empirically, or by other means, using this same criterium (a solution is admissible if it is positive real).

4.3.1 Perturbation solutions of $\mathcal{E}_1^{\prime(\pm)}$ for small ε_1''

Let us return to (75) which can be written as

$$\sum_{j=0}^{2} U_j u_j = 0 \ , \tag{78}$$

wherein:

$$U_0 = \frac{\mathfrak{C}_0}{k_+} \ \ , \ U_1 = \mathfrak{C}_3 - 2\mathcal{E}_0\mathfrak{C}_4 \ \ , \ \ U_2 = \mathfrak{C}_4 \ , \tag{79}$$

and

$$u_0 = 1 \ \ , \ \ u_1 = \mathcal{E}_1' \ \ , \ \ u_2 = \mathcal{E}_1^{\prime 2} = u_1^2 \ . \tag{80}$$

We expand U_j and u_j in series of powers of the supposedly-small quantity

$$\delta := \varepsilon_1'' \ , \tag{81}$$

that is,

$$U_j = \sum_{k=0}^{\infty} U_j^{(k)} \delta^k \ \ , \ \ u_j = \sum_{l=0}^{\infty} u_j^{(l)} \delta^l \ , \tag{82}$$

with the understanding

$$u_0^{(l)} = \delta_{l0} \ , \tag{83}$$

(in which δ_{l0} is the Kronecker delta symbol) and

$$u_2^{(l)} = \sum_{l_1=0}^{\infty} u_1^{(l_1)} \delta^{l_1} \sum_{l_2=0}^{\infty} u_1^{(l_2)} \delta^{l_2} = \sum_{l=0}^{\infty} \sum_{l_1=0}^{l} u_1^{(l_1)} u_1^{(l-l_1)} \ . \tag{84}$$

whence

$$u_2^{(0)} = u_1^{(0)2} \ \ , \ \ u_2^{(1)} = 2u_1^{(0)}u_1^{(1)} \ \ , \ \ u_2^{(2)} = 2u_1^{(0)}u_1^{(2)} + u_1^{(1)2} \ , \tag{85}$$

and so on. The introduction of (82) into (78) gives rise to

$$\sum_{m=0}^{\infty}\sum_{j=0}^{2}\sum_{l=0}^{m} U_j^{(m-l)} u_j^{(l)} \delta^m = 0 \ , \tag{86}$$

whence

$$\sum_{j=0}^{2} U_j^{(0)} u_j^{(0)} = 0 \ , \tag{87}$$

$$\sum_{j=0}^{2} [U_j^{(0)} u_j^{(1)} + U_j^{(1)} u_j^{(0)}] = 0 \ , \tag{88}$$

$$\sum_{j=0}^{2} [U_j^{(0)} u_j^{(2)} + U_j^{(1)} u_j^{(1)} + + U_j^{(2)} u_j^{(0)}] = 0 \ , \tag{89}$$

and so on. More explicitly, we have:

$$U_0^{(0)} u_0^{(0)} + U_1^{(0)} u_1^{(0)} + U_2^{(0)} u_2^{(0)} = 0 \ , \tag{90}$$

$$U_0^{(0)} u_0^{(1)} + U_0^{(1)} u_0^{(0)} + U_1^{(0)} u_1^{(1)} + U_1^{(1)} u_1^{(0)} + U_2^{(0)} u_2^{(1)} + U_2^{(1)} u_2^{(0)} = 0 \ , \tag{91}$$

$$U_0^{(0)} u_0^{(2)} + U_0^{(1)} u_0^{(1)} + U_0^{(2)} u_0^{(0)} + U_1^{(0)} u_1^{(2)} + U_1^{(1)} u_1^{(1)} + U_1^{(2)} u_1^{(0)} + U_2^{(0)} u_2^{(2)} + U_2^{(1)} u_2^{(1)} + U_2^{(2)} u_2^{(0)} = 0 \ , \tag{92}$$

and so on.

Taking into account (83) and (85) enables (90)-(92) to be written as:

$$U_0^{(0)} + U_1^{(0)} u_1^{(0)} + U_2^{(0)} u_1^{(0)2} = 0 \ , \tag{93}$$

$$U_0^{(1)} + U_1^{(0)} u_1^{(1)} + U_1^{(1)} u_1^{(0)} + U_2^{(0)} 2 u_1^{(0)} u_1^{(1)} + U_2^{(1)} u_1^{(0)2} = 0 \ , \tag{94}$$

$$U_0^{(2)} + U_1^{(0)} u_1^{(2)} + U_1^{(1)} u_1^{(1)} + U_1^{(2)} u_1^{(0)} + U_2^{(0)} (2 u_1^{(0)} u_1^{(2)} + u_1^{(1)2}) + U_2^{(1)} 2 u_1^{(0)} u_1^{(1)} + U_2^{(2)} u_1^{(1)2} = 0 \ . \tag{95}$$

The first of these last three relations is a quadratic equation for the unknown $u_1^{(0)}$. The second relation is a linear equation (involving the previously-obtained $u_1^{(0)}$) for the unknown $u_1^{(1)}$. The third relation is a linear equation (involving the previously-obtained $u_1^{(0)}$ and $u_1^{(1)}$) for the unknown $u_1^{(2)}$. Thus, the perturbation method consititues an iterative scheme for the obtention of the $u_1^{(l)}$; $l = 0, 1, 2, ...$

We now address the problem of the $U_j^{(k)}$. To do this, we must first recall (79) and the expressions for $\mathfrak{C}_4$, $\mathfrak{C}_3$ and $\mathfrak{C}_0$:

$$\mathfrak{C}_4 = FA^2 - (FB^2 + fg) \ , \tag{96}$$

$$\mathfrak{C}_3 = 2\mathcal{E}_0 FA^2 - 4\mathcal{E}_0 (FB^2 + fg) + 2\mathcal{E}_1'' fh \ , \tag{97}$$

$$\mathfrak{C}_0 = -k_+^2 FA^2 - k_+ k_- (FB^2 + fg) + 2k_+ \mathcal{E}_0 \mathcal{E}_1'' fh \ , \tag{98}$$

so that:

$$U_0 = \frac{\mathfrak{C}_0}{k_+} = -k_+ FA^2 - k_-(FB^2 + fg) + 2\mathcal{E}_0\mathcal{E}_1'' fh \ , \tag{99}$$

$$U_1 = \mathfrak{C}_3 - 2\mathcal{E}_0\mathfrak{C}_4 = -2\mathcal{E}_0(FB^2 + fg) + 2\mathcal{E}_1'' fh \ , \tag{100}$$

$$U_2 = \mathfrak{C}_4 = FA^2 - (FB^2 + fg) \ . \tag{101}$$

Recall that:

$$g = -b^2 + a^2\left(\frac{\varepsilon_1^{'2} + \varepsilon_1^{''2} - \varepsilon_0^{'2}}{\|\varepsilon_1 + \varepsilon_0\|^2}\right) \quad , \quad h = 2a^2\left(\frac{\varepsilon_0\varepsilon_1^{''}}{\|\varepsilon_1 + \varepsilon_0\|^2}\right) \ , \tag{102}$$

which can be written as:

$$g = \frac{[-b^2(\varepsilon_1^{'2} + \varepsilon_0^2) + a^2(\varepsilon_1^{'2} - \varepsilon_0^2)] + (-b^2 + a^2)\varepsilon_1^{''2}}{(\varepsilon_1' + \varepsilon_0)^2 + \varepsilon_1^{''2}} \quad , \quad h = \left(\frac{2a^2\varepsilon_0}{(\varepsilon_1' + \varepsilon_0)^2 + \varepsilon_1^{''2}}\right)\varepsilon_1^{''} \ . \tag{103}$$

or (with the new condensed notations and $\delta := \varepsilon_1''$)

$$g = \frac{\mathcal{A} + \mathcal{B}\delta^2}{\mathcal{C} + \delta^2} \quad , \quad h = \frac{2a^2\varepsilon_0\delta}{\mathcal{C} + \delta^2} \tag{104}$$

Under the (small-δ) hypothesis (implicit in the perturbation method)

$$0 \leq \delta << 1 \ , \tag{105}$$

we find

$$g = \frac{\mathcal{A}}{\mathcal{C}} + \frac{1}{\mathcal{C}}\left(\mathcal{B} - \frac{\mathcal{A}}{\mathcal{C}}\right)\delta^2 + \mathcal{O}(\delta^4) := g^{(0)} + g^{(2)}\delta^2 + \mathcal{O}(\delta^4) \ , \tag{106}$$

$$h = \frac{2a^2\varepsilon_0}{\mathcal{C}}\delta - \frac{2a^2\varepsilon_0}{\mathcal{C}^2}\delta^3 + \mathcal{O}(\delta^5) := h^{(1)}\delta + h^{(3)}\delta^3 + \mathcal{O}(\delta^5) \ , \tag{107}$$

Consequently:

$$\begin{aligned} U_0 = [-k_+ FA^2 - k_- FB^2] - k_- f(g^{(0)} + g^{(2)}\delta^2) + 2\mathcal{E}_0\mathcal{E}_1'' f(h^{(1)}\delta + h^{(3)}\delta^3) + \mathcal{O}(\delta^4) = \\ [-k_+ FA^2 - k_- FB^2 - k_- fg^{(0)}] + [2\mathcal{E}_0\mathcal{E}_1'' fh^{(1)}]\delta + [-k_- f(g^{(0)}]\delta^2 + \mathcal{O}(\delta^3) \ , \end{aligned} \tag{108}$$

whence

$$\begin{aligned} U_0^{(0)} = [-k_+ FA^2 - k_- FB^2 - k_- fg^{(0)}] \ , \\ U_0^{(1)} = [2\mathcal{E}_0\mathcal{E}_1'' fh^{(1)}] \ , \\ U_0^{(2)} = [-k_- fg^{(2)}] \end{aligned} \tag{109}$$

$$\begin{aligned} U_1 = [-2\mathcal{E}_0 FB^2] + [-2\mathcal{E}_0 fg^{(0)} + g^{(2)}\delta^2)] + [2\mathcal{E}_1'' f(h^{(1)}\delta + h^{(3)}\delta^3)] + \mathcal{O}(\delta^4) = \\ [-2\mathcal{E}_0 FB^2 - 2\mathcal{E}_0 fg^{(0)}] + [2\mathcal{E}_1'' fh^{(1)}]\delta + [-2\mathcal{E}_0 fg^{(2)}]\delta^2 + \mathcal{O}(\delta^3) \ , \end{aligned} \tag{110}$$

whence

$$\begin{array}{c} U_1^{(0)} = [-2\mathcal{E}_0 FB^2 - 2\mathcal{E}_0 f g^{(0)}] \ , \\ U_1^{(1)} = [2\mathcal{E}_1'' f h^{(1)}] \ , \\ U_1^{(2)} = [-2\mathcal{E}_0 f g^{(2)}] \ , \end{array} \tag{111}$$

$$U_2 = [FA^2 - FB^2] - f(g^{(0)} + g^{(2)}\delta^2) + \mathcal{O}(\delta^4) = [FA^2 - FB^2 - fg^{(0)}] + [-fg^{(2)}]\delta^2 + \mathcal{O}(\delta^4) \ , \tag{112}$$

whence

$$\begin{array}{c} U_2^{(0)} = [FA^2 - FB^2 - fg^{(0)}] \ , \\ U_2^{(1)} = 0 \ , \\ U_2^{(2)} = [-fg^{(2)}] \ . \end{array} \tag{113}$$

The solution of (93) is

$$u_1^{(0)} = \frac{-U_1^{(0)} \pm \sqrt{U_1^{(0)2} - 4U_2^{(0)}U_0^{(0)}}}{2U_2^{(0)}} \ , \tag{114}$$

or

$$u_1^{(0)} = \frac{\mathcal{E}_0(FB^2 + fg^{(0)}) \pm \sqrt{\mathcal{E}_0^2(FA^2)^2 + \mathcal{E}_1''^2(FA^2 - FB^2 - fg^{(0)})^2}}{FA^2 - FB^2 - fg^{(0)}} \ , \tag{115}$$

Since we assumed ε_1'' to be small, it is not illogical to assume $\mathcal{E}_1''$ also to be small, i.e.,

$$0 < \mathcal{E}_1'' << 1 \ . \tag{116}$$

With the change of variables

$$\alpha = FA^2 \quad , \quad \beta = FB^2 + fg^{(0)} \ , \tag{117}$$

and recalling that $k_\pm = \mathcal{E}_0^2 \pm \mathcal{E}_1''^2$, it is easily shown that

$$\sqrt{U_1^{(0)2} - 4U_2^{(0)}U_0^{(0)}} = 2\sqrt{\mathcal{E}_0^2\alpha^2 + \mathcal{E}_1''^2(\alpha - \beta)^2} = 2\left[\mathcal{E}_0\alpha + \frac{(\alpha - \beta)^2}{2\mathcal{E}_0\alpha}\mathcal{E}_1''^2 + \mathcal{O}(\mathcal{E}_1''^4)\right] \ , \tag{118}$$

so that

$$u_1^{(0)} = u_1^{(0)\pm} := \frac{\mathcal{E}_0(\beta \pm \alpha)}{\alpha - \beta} \pm \frac{\mathcal{E}_1''^2}{2(\alpha - \beta)\mathcal{E}_0\alpha} + \mathcal{O}(\mathcal{E}_1''^4) \ , \tag{119}$$

or

$$u_1^{(0)-} = -\mathcal{E}_0 - \frac{\mathcal{E}_1''^2}{2(\alpha - \beta)\mathcal{E}_0\alpha} + \mathcal{O}(\mathcal{E}_1''^4) \ , \tag{120}$$

$$u_1^{(0)+} = \frac{\mathcal{E}_0(\alpha + \beta)}{\alpha - \beta} + \frac{\mathcal{E}_1''^2}{2(\alpha - \beta)\mathcal{E}_0\alpha} + \mathcal{O}(\mathcal{E}_1''^4) \ , \tag{121}$$

The negative nature of $u_1^{(0)-}$ makes this solution inadmissible, so that only $u_1^{(0)+}$ is admissible. This finding translates to the choice of sign in (115), so that the unique, exact solution for $u_1^{(0)}$ is

$$u_1^{(0)} = \frac{\mathcal{E}_0(FB^2 + fg^{(0)}) + \sqrt{\mathcal{E}_0^2(FA^2)^2 + \mathcal{E}_1''^2(FA^2 - FB^2 - fg^{(0)})^2}}{FA^2 - FB^2 - fg^{(0)}} \ , \tag{122}$$

or, after integrating the small nature of $\mathcal{E}_1''$

$$u_1^{(0)} = \mathcal{E}_0 \left(\frac{FA^2 + FB^2 + fg^{(0)}}{FA^2 - FB^2 - fg^{(0)}} \right) + \mathcal{O}(\mathcal{E}_1''^2) \ . \tag{123}$$

The next step in the perturbation procedure is to obtain $u_1^{(1)}$ from $u_1^{(0)}$. This is done via (94) from which we obtain

$$u_1^{(1)} = - \left(\frac{U_0^{(1)} + U_1^{(1)} u_1^{(0)} + U_2^{(1)} u_1^{(0)2}}{U_1^{(0)} + U_2^{(0)} 2u_1^{(0)}} \right) \ , \tag{124}$$

But, instead of writing the explicit expression for $u_1^{(1)}$, we recall that here u_1 stands for $\mathcal{E}_1'$, and to first order in ε''

$$u_1 = \mathcal{E}_1' \approx u_1^{(0)} + u_1^{(1)} \varepsilon_1'' \ , \tag{125}$$

or, neglecting terms of order $\mathcal{E}_1''$ *and* ε_1'' (due to the assumed smallness of $\mathcal{E}_1''$ and ε_1''), the approximate solution for $\mathcal{E}_1'$ is

$$\mathcal{E}_1' \approx \mathcal{E}_0 \left(\frac{FA^2 + FB^2 + fg^{(0)}}{FA^2 - FB^2 - fg^{(0)}} \right) \ , \tag{126}$$

with the understanding that, on account of the what the perturbation analysis showed concerning the admissible solution, the exact solution for $\mathcal{E}_1'$ is

$$\mathcal{E}_1' = \frac{-k_+(\mathfrak{C}_3 - 2\mathcal{E}_0\mathfrak{C}_4) + \sqrt{k_+^2(\mathfrak{C}_3 - 2\mathcal{E}_0\mathfrak{C}_4)^2 - 4k_+\mathfrak{C}_4\mathfrak{C}_0}}{2k_+\mathfrak{C}_4} \ . \tag{127}$$

4.3.2 Comments on the exact and approximate solutions for $\mathcal{E}_1'$

The result embodied in (127) calls for the following comments:

1- It shows that the solution to the inverse problem of the identification of the sole parameter $\mathcal{E}_1'$ *exists*, even in the presence of nuisance parameter uncertainties;
2- it shows that it is possible to obtain the *mathematically-explicit and exact solution* to the given inverse problem, even in the presence of nuisance parameter uncertainties;
3- it shows that this solution is *unique* for a given set of parameters ε_1', ε_1'', ε_0, a, e^i, θ^i, b, $\mathcal{E}_1''$, $\mathcal{E}_0$, A, E^i, Θ^i, B, subject to the assumed physical constraint (i.e., the real part of the permittivity should be positive real);
4- it shows that the accuracy of the retrieval of the real part of the permittivity ($\mathcal{E}_1'$) is conditioned, albeit in a complex manner, by the uncertainty of the nuisance parameters $\mathcal{E}_0$, A, E^i, Θ^i, B;

The result embodied in (126)

5- shows that the accuracy of the retrieval of $\mathcal{E}_1'$ is weakly-conditioned by ε_1'' and $\mathcal{E}_1''$ since the dependence of $\mathcal{E}_1'$ on these parameters is at least of order $\mathcal{E}_1''$ or ε_1'' (and therefore small due to ε_1'' and $\mathcal{E}_1''$ having been assumed to be small).

4.3.3 Preliminaries concerning the dependence of the retrieval error of $\mathcal{E}_1'$ on the nuisance parameter uncertainties

Due to the fifth comment in sect. 4.3.2 it is no longer necessary to delve on the issue of the dependence of the retrieval error of $\mathcal{E}_1'$ on the (assumed-small) nuisance parameter $\mathcal{E}_1''$. Thus, from now on, we deal with (126)

$$\mathcal{E}_1' = \mathcal{E}_0 \left(\frac{FA^2 + FB^2 + fg^{(0)}}{FA^2 - FB^2 - fg^{(0)}} \right) := \mathcal{E}_0 \Big[\frac{\varepsilon_1' X_+ + \varepsilon_0 Y_+}{\varepsilon_1' Y_- + \varepsilon_0 X_-} \Big] \ . \tag{128}$$

wherein

$$X_\pm = (FA^2 + fa^2) \pm (FB^2 - fb^2) \ \ , \ \ Y_\pm = (FA^2 - fa^2) \pm (FB^2 - fb^2) \ . \tag{129}$$

To unravel the complexity alluded to in the fourth comment in sect. 4.3.2, first suppose that the nuisance parameters $A,\ B,\ E^i,\ \Theta^i$ are known precisely, i.e., $E^i = e^i,\ A = a,\ B = b,\ \Theta^i = \theta^i$, whence $X_+ = X^-$ and $Y_\pm = 0$, so that

$$\mathcal{E}_1' = \check{\mathcal{E}}_1' = \mathcal{E}_0 \frac{\varepsilon_1'}{\varepsilon_0} \ , \tag{130}$$

which shows that the the relative error of the retrieved parameter, i.e.,

$$\varepsilon_{\varepsilon_1'} = \frac{\mathcal{E}_1' - \varepsilon_1}{\varepsilon_1} = \frac{\mathcal{E}_1'}{\varepsilon_1} - 1 \ , \tag{131}$$

depends linearly on the ratio $\frac{\mathcal{E}_0}{\varepsilon_0}$, or, equivalently, the relative error of the retrieved constitutive parameter of the cylinder equals the relative uncertainty of the nuisance parameter concerning the constitutive parameter of the host

$$\delta_{\varepsilon_0} = \frac{\mathcal{E}_0 - \varepsilon_0}{\varepsilon_0} = \frac{\mathcal{E}_0}{\varepsilon_0} - 1 \ , \tag{132}$$

which fact translates to

$$\varepsilon_{\varepsilon_1'} = \delta_{\varepsilon_0} \ . \tag{133}$$

Returning to (128), which can now be written as

$$\mathcal{E}_1' = \check{\mathcal{E}}_1' + \frac{\mathcal{E}_0}{\varepsilon_0} \Big[\frac{\varepsilon_0 \varepsilon_1' (X_+ - X_-) + (\varepsilon_1'^2 Y_+ - \varepsilon_0^2 Y_-)}{\varepsilon_1' Y_- + \varepsilon_0 X_-} \Big] \ , \tag{134}$$

we find that

$$\mathcal{E}_1' \approx \check{\mathcal{E}}_1' \ , \tag{135}$$

for small uncertainties of the nuisance parameters $E^i,\ A,\ B,\ \Theta^i$.

4.3.4 Properties of $\mathcal{E}_1'$ as a function of B

We can write

$$\mathcal{E}_1'(B) = \mathcal{E}_0 \left[\frac{E^i b(B^2 + A^2) - e^i BM}{-E^i b(B^2 - A^2) - e^i BM} \right] = -\mathcal{E}_0 \left[\frac{B^2 - \frac{e^i M}{E^i b} B + A^2}{B^2 - \frac{e^i M}{E^i b} B - A^2} \right] := -\mathcal{E}_0 \frac{\mathcal{N}}{\mathcal{D}} \ . \tag{136}$$

wherein

$$M := -\kappa g^{(0)} = \kappa \left[\frac{(\varepsilon_1' + \varepsilon_0) b^2 - (\varepsilon_1' - \varepsilon_0) a^2}{\varepsilon_1' + \varepsilon_0} \right] \ . \tag{137}$$

Since we assume a relatively-small uncertainty on the nuisance parameter Θ^i, it follows that $|\Theta^i - \theta^i| < \pi/2$, whence $\kappa > 0$. Also, since we assumed that $\varepsilon_0 > 0$, $\varepsilon_1' > 0$, $b^2 > a^2$, it follows that

$$M > 0 \ . \tag{138}$$

Finally, recall that we assume $\mathcal{E}_0 > 0$.

Now, assume that $\delta > 0$ and consider $\mathcal{E}_1'(B_0 \pm \delta)$. It is easy to show that

$$\mathcal{E}_1'(B_0 + \delta) = \mathcal{E}_1'(B_0 - \delta) \ , \tag{139}$$

entails

$$B_0 = \frac{e^i M}{2E^i b} > 0 \ , \tag{140}$$

so that

$$\mathcal{E}_1'(B) = -\mathcal{E}_0 \left[\frac{B^2 - 2B_0 B + A^2}{B^2 - 2B_0 B - A^2} \right] \ . \tag{141}$$

whence

$$\mathcal{E}_1'(B_0) = \mathcal{E}_0 \ . \tag{142}$$

Differentiating gives

$$\frac{d\mathcal{E}_1'(B)}{dB} = \frac{4\mathcal{E}_0 (B - B_0) A^2}{B^2 - 2B_0 B - A^2} \ , \tag{143}$$

whence

$$\frac{d\mathcal{E}_1'(B_0)}{dB} = 0 \ . \tag{144}$$

The equation $\mathcal{D} = 0$ has two solutions

$$B_\pm = \frac{\frac{e^i M}{E^i b} \pm \sqrt{\left(\frac{e^i M}{E^i b}\right)^2 + 4A^2}}{2} = B_0 \pm \sqrt{B_0^2 + A^2} \ . \tag{145}$$

at which $\mathcal{E}_1'$ blows up.

It is generally admitted that nonlinear inverse problems are ill posed ([18], [8], [23]) which means that the solution either does not exist, or is not unique (our particular inverse solution was shown to be unique when certain physical constraints are satisfied) and is unstable in

the case of existence. *Instability* is usually defined ([7]) by retrievals not being continuously-dependent on variations of the data. We, on the other hand, find that the function $\mathcal{E}_1'(B)$ *diverges* at B_- and B_+, which suggests a new form of instability, first observed, but not explained, in [27].

Borrowing a notion first expressed in [38], we define *retrieval instability induced by nuisance parameter uncertainty* as that which occurs when a very small variation of a nuisance parameter B (and perhaps other nuisance parameters) produces a very large variation of a retrieved parameter (at present, $\mathcal{E}_1'$).

Now consider $\mathcal{E}_1'(B_+ \pm \delta)$, with $0 < \delta << 1$ defined as previously. We find

$$\mathcal{E}_1'(B_+ \pm \delta) = -\mathcal{E}_0 \left[\frac{A^2 \pm \delta\sqrt{B_0^2 + A^2}}{\pm\delta\sqrt{B_0^2 + A^2}} \right] \approx \mp\mathcal{E}_0 \frac{A^2}{\delta\sqrt{B_0^2 + A^2}} \ , \tag{146}$$

which shows that for small positive δ,

$$\mathcal{E}_1'(B_+ - \delta) > 0 \ \ , \quad \mathcal{E}_1'(B_+ + \delta) < 0. \ . \tag{147}$$

Similarly, for $\varepsilon >> 1$,

$$\mathcal{E}_1'(B_+ \pm \varepsilon) \sim -\mathcal{E}_0 \ ; \ \varepsilon \to \infty \ , \tag{148}$$

which shows that $\mathcal{E}_1'(B)$ tends to the negative value $-\mathcal{E}_0$ for $B \to \pm\infty$. This result, which at first appears to be surprising since it was assumed at the outset that $\mathcal{E}_1' > 0$, actually means that no physically-meaningful result can be obtained for large uncertainty of $|B|$. In other words, *the solutions obtained for $B > B_+$ and $B < B_+$ must be rejected.*

The analytical properties (symmetries, behavior in the neighborhoods of B_0, B_- and B_+) of the function $\mathcal{E}_1'(B)$, deduced from the preceding formulae, are exhibited in fig. **??**.

It should be noted, in this figure, that it is possible to retrieve a physically-meaningful $\mathcal{E}_1'$ (i.e., that is positive real) only for $B_+ > B \geq 0$.

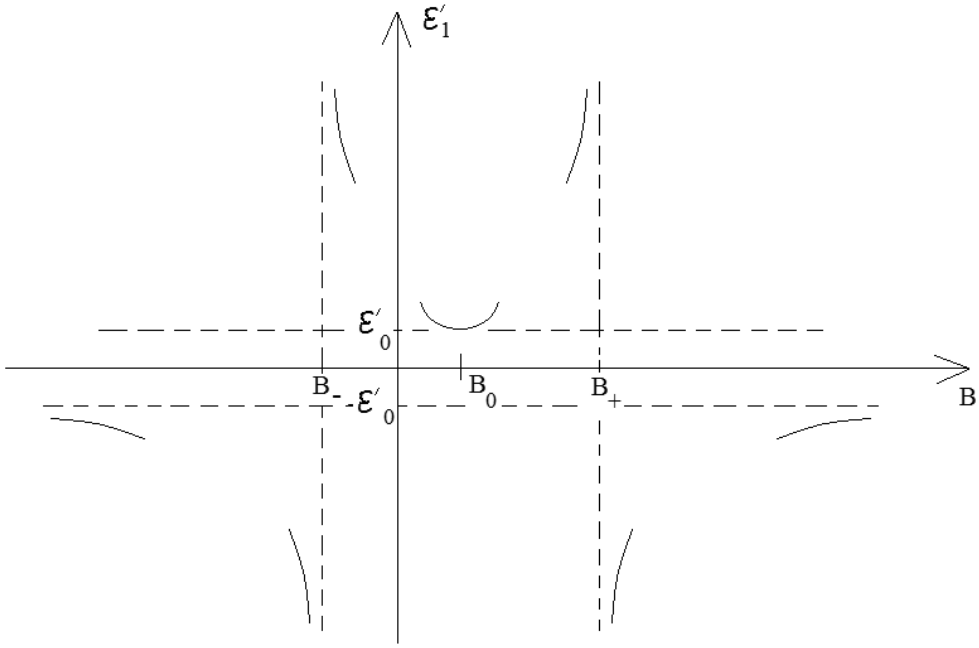

Figure 2: Graphical representation of the analytical properties of $\mathcal{E}_1'(B)$.

4.3.5 Properties of $\mathcal{E}_1'$ as a function of A

We can write

$$\mathcal{E}_1'(A) = \mathcal{E}_0 \left[\frac{A^2 - \frac{e^i BM}{E^i b} + B^2}{A^2 - \frac{e^i BM}{E^i b} - B^2} \right] = \mathcal{E}_0 \left[\frac{A^2 - C^2 + B^2}{A^2 - C^2 - B^2} \right] := \mathcal{E}_0 \frac{\mathcal{N}}{\mathcal{D}} \ , \tag{149}$$

wherein

$$C^2 := \frac{e^i BM}{E^i b} \tag{150}$$

It is immediately apparent that $\mathcal{E}_1'(A)$ is symmetrical with respect to $A = 0$, i.e.,

$$\mathcal{E}_1'(-A) = \mathcal{E}_1'(A) \ . \tag{151}$$

The equation $\mathcal{D} = 0$ has two solutions

$$A_\pm = \pm\sqrt{B^2 - C^2} \ . \tag{152}$$

at which $\mathcal{E}_1'$ blows up. We can write

$$\mathcal{E}_1'(A) = \mathcal{E}_0 \left[\frac{A^2 + A_+^2}{A^2 - A_+^2} \right] \ , \tag{153}$$

whence the result

$$\mathcal{E}_1'(0) = -\mathcal{E}_0 \ . \tag{154}$$

It also follows (for $0 < \delta << 1$) that

$$\mathcal{E}_1'(A_+ \pm \delta) = \mathcal{E}_0 \left[\frac{2A_+^2 \pm 2A_+\delta + \delta^2}{\pm 2A_+\delta + \delta^2} \right] \ , \tag{155}$$

whence

$$\mathcal{E}_1'(A_+ \pm \delta) \sim \pm\mathcal{E}_0 \frac{A_+}{\delta} \ ; \ \delta \to 0 \ , \tag{156}$$

which means that $\mathcal{E}_1' > 0$ for $A \gtrsim A_+$, $\mathcal{E}_1' < 0$ for $A \lesssim A_+$ and $\lim_{A \to A_+ - \delta} = -\infty$.

Next, consider $d\mathcal{E}_1'(A)/dA$:

$$\frac{d\mathcal{E}_1'(A)}{dA} = \frac{-4\mathcal{E}_0 A_+^2 A}{(A^2 - A_+^2)^2} \ , \tag{157}$$

from which it follows that $d\mathcal{E}_1'(A)/dA = 0$ for $A = 0$, $d\mathcal{E}_1'(A)/dA < 0$ for $A > 0$ and $d\mathcal{E}_1'(A)/dA > 0$ for $A < 0$.

The analytical properties (symmetries, behavior in the neighborhoods of $A = 0$, A_- and A_+) of the function $\mathcal{E}_1'(A)$, deduced from the preceding formulae, are exhibited in fig. 3 in which one should note that all negative solutions for $\mathcal{E}_1'$ are forbidden. It should be noted, in this figure, that it is possible to retrieve a physically-meaningful $\mathcal{E}_1'$ (i.e., that is positive real) only for $\infty > A > A_+$.

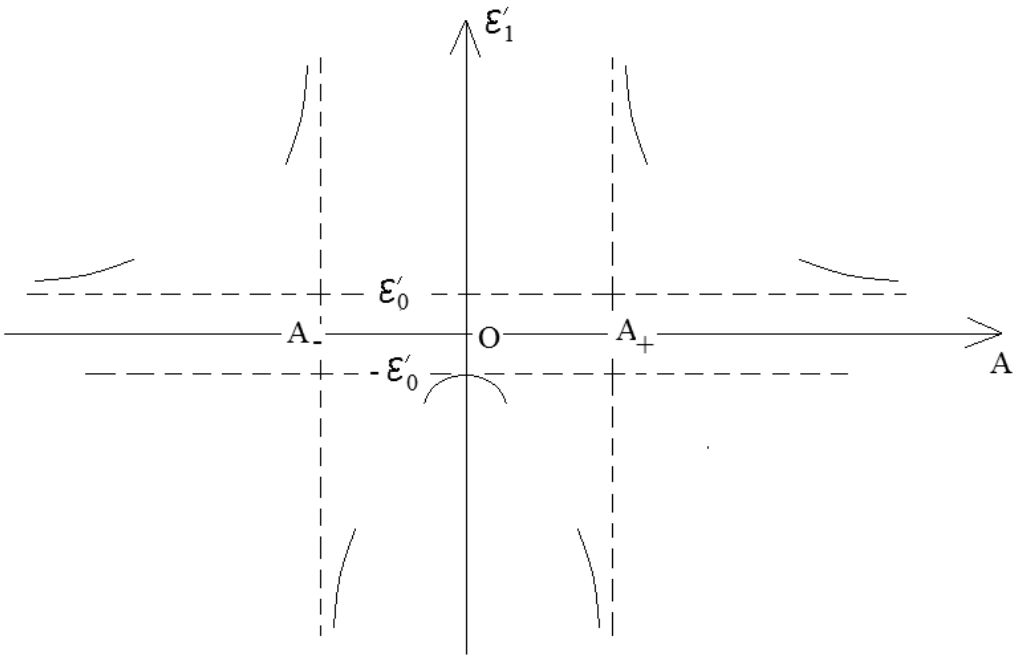

Figure 3: Graphical representation of the analytical properties of $\mathcal{E}'_1(A)$.

4.3.6 Properties of $\mathcal{E}_1'$ as a function of E^i

We can write

$$\mathcal{E}_1'(E^i) = -\mathcal{E}_0 \left(\frac{B^2+A^2}{B^2-A^2}\right)\left[\frac{E^i-E_0^i}{E^i-E_+^i}\right] \ , \tag{158}$$

wherein:

$$E_0^i = \frac{e^i BM}{b(B^2+A^2)} \ \ , \ \ E_+^i = \frac{e^i BM}{b(B^2-A^2)} > E_0^i \ . \tag{159}$$

It ensues that:

$$\mathcal{E}_1'(E_0^i) = 0 \ , \tag{160}$$

Moreover, $\mathcal{E}_1'(E^i)$ blows up at $E^i = E_+^i$, and from the fact that

$$\mathcal{E}_1'(E^i) \sim -\mathcal{E}_0 \left(\frac{B^2+A^2}{B^2-A^2}\right) := \mathcal{E}_1'^{\infty} \ ; \ E^i \to \pm\infty \ , \tag{161}$$

we find that $\mathcal{E}_1'^{\infty} < 0$ (because, by hypothesis, $b > a$).

Now we seek the behavior of $\mathcal{E}_1'(E^i)$ in the neighborhood of E_0^i. Assume that $\delta > 0$, so that

$$\mathcal{E}_1'(E_0^i \pm \delta) = \mp\mathcal{E}_0 \left(\frac{B^2+A^2}{B^2-A^2}\right)\left[\frac{\delta}{E_0^i - E_+^i \pm \delta}\right] \ , \tag{162}$$

whence the asymptotic behavior, for small positive δ

$$\mathcal{E}_1'(E_0^i \pm \delta) = \pm\mathcal{E}_0 \left(\frac{B^2+A^2}{B^2-A^2}\right)\left[\frac{\delta}{E_+^i - E_0^i}\right] \ ; \ \delta \to 0 \ , \tag{163}$$

and the result that, for small positive δ, $\mathcal{E}_1'(E^i) > 0$ at points $E^i = E_0^i + \delta$, and $\mathcal{E}_1'(E^i) < 0$ at points $E_0^i = E_0^i - \delta$.

Similarly,

$$\mathcal{E}_1'(E_+^i \pm \delta) = \mp\mathcal{E}_0 \left(\frac{B^2+A^2}{B^2-A^2}\right)\left[\frac{E_+^i - E_0^i \pm \delta}{\delta}\right] \sim \mp\mathcal{E}_0 \left(\frac{B^2+A^2}{B^2-A^2}\right)\left[\frac{E_+^i - E_0^i}{\delta}\right] \ ; \ \delta \to 0 \ , \tag{164}$$

whence the result that, for small positive δ, $\mathcal{E}_1'(E^i) < 0$ at points $E^i = E_+^i + \delta$, and $\mathcal{E}_1'(E^i) > 0$ at points $E_0^i = E_+^i - \delta$.

Finally,

$$\frac{d\mathcal{E}_1'(E^i)}{dE^i} = \mathcal{E}_0 \left(\frac{B^2+A^2}{B^2-A^2}\right)\left[\frac{E_+^i - E_0^i}{(E^i - E_+^i)^2}\right] \ , \tag{165}$$

which means that $\frac{d\mathcal{E}_1'(E^i)}{dE^i} > 0$ for all finite E^i and $\frac{d\mathcal{E}_1'(E^i)}{dE^i} \to 0$ for $E^i \to \pm\infty$.

The analytical properties (behavior in the neighborhoods of E_0^i, E_+^i of the function $\mathcal{E}_1'(E^i)$, deduced from the preceding formulae, are exhibited in fig. 4 in which one should note that all negative solutions for $\mathcal{E}_1'$ are forbidden.

It should be noted, in this figure, that it is possible to retrieve a physically-meaningful $\mathcal{E}_1'$ (i.e., that is positive real) only for $E_+^i > B > E_0^i$.

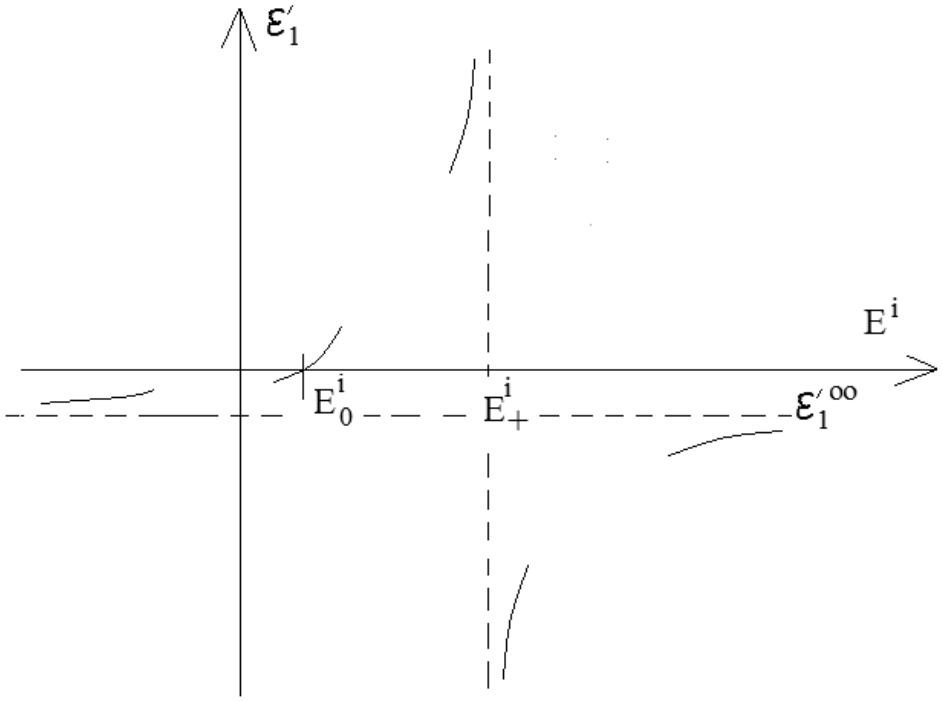

Figure 4: Graphical representation of the analytical properties of $\mathcal{E}_1'(E^i)$.

4.3.7 Comments on the analytical properties of $\mathcal{E}_1'(A)$, $\mathcal{E}_1'(E^i)$, $\mathcal{E}_1'(B)$

In sect 4.3.2, it was stated that the explicit formula for $\mathcal{E}_1'$ demonstrates the existence of a solution of the inverse problem, even in the presence of nuisance parameter uncertainties. We now see that this statement must be interpreted in the following sense: a physically-admissible solution (i.e., positive and not infinite) for $\mathcal{E}_1'$ exists only for a *range* of nuisance parameter uncertainties (i.e., those for which $\mathcal{E}_1'$ is positive and not infinite).

Furthermore, it was stated in sect 4.3.2 that the explicit formula for $\mathcal{E}_1'$ constitutes a *unique* solution for a given set of parameters ε_1', ε_1'', ε_0, a, e^i, θ^i, b, θ^b, $\mathcal{E}_1''$, $\mathcal{E}_0$, A, E^i, Θ^i, B. However, this does not mean that a physically-admissible $\mathcal{E}_1'$ cannot arise from more than one sets of nuisance parameters, as is illustrated in fig. 2 for B in the neighborhood of B_0 (i.e., the two values $B_0 \pm \delta$ give rise to the same $\mathcal{E}_1'$).

4.4 Finding the real part of the permittivity of the cylinder by minimizing $\mathcal{K}^{(N)}$

The method of obtaining the real part of the permittivity of the cylinder outlined in sect. 4.2 is somewhat unrealistic in that it supposes that the data is registered at a continuum of points on the sensing circle $r = b$. *In reality, the data is registered at discrete locations on this circle and the number N of these locations is finite.* Of course, N *will have an influence on the accuracy of the retrieval* and it is this influence that we shall now examine.

From (45) we obtain

$$\mathcal{K}^{(N)}(\mathcal{E}_1') = \left(\frac{1}{\|\mathfrak{f}\|^2 \delta_\theta \sum_{n=1}^{N} \cos^2(\alpha + (n-1)\delta_\theta)} \right) \times$$
$$\delta_\theta \sum_{n=1}^{N} \Big(\|\mathfrak{f}\|^2 \cos^2(\alpha + (n-1)\delta_\theta) - 2\Re(\mathfrak{f}^* \mathfrak{F}) \cos(\alpha + (n-1)\delta_\theta) \cos(\beta + (n-1)\delta_\theta) +$$
$$\|\mathfrak{F}\|^2 \cos^2(\beta + (n-1)\delta_\theta) \Big) \ , \quad (166)$$

wherein $\alpha = \theta^b + \frac{\delta_\theta}{2} - \theta^i$ and $\beta = \theta^b + \frac{\delta_\theta}{2} - \Theta^i$, $\delta_\theta = \frac{\theta^e - \theta^b}{N}$, $\theta_n = \theta^b + \frac{\delta_\theta}{2} + (n-1)\delta_\theta$. Note that since δ_θ depends on N, α and β also depend on N. Also note that, contrary to what is assumed in $\mathcal{K}$, i.e., $\theta^e - \theta^e = 2\pi$, here we admit arbitrary θ^b and θ^b, with the only restriction that $\theta^e > \theta^b$.

Consider

$$\sigma^{(N)}(\alpha, \beta) = \delta_\theta \sum_{n=1}^{N} \cos\big(\alpha + (n-1)\delta_\theta\big) \cos\big(\beta + (n-1)\delta_\theta\big) \ , \quad (167)$$

It is straightforward to show that

$$\sigma^{(N)}(\alpha, \beta) = \frac{\delta_\theta}{2} \left[N \cos(\alpha - \beta) + \cos\big(\alpha + \beta + (N-1)\delta_\theta\big) \left(\frac{\sin(N\delta_\theta)}{\sin(\delta_\theta)} \right) \right] \ . \quad (168)$$

and, on account of (166)

$$\mathcal{K}^{(N)}(\mathcal{E}_1') = \frac{\|\mathfrak{f}\|^2\sigma^{(N)}(\alpha,\alpha) - 2\Re(\mathfrak{f}^*\mathfrak{F})\sigma^{(N)}(\alpha,\beta) + \|\mathfrak{F}\|^2\sigma^{(N)}(\beta,\beta)}{\|\mathfrak{f}\|^2\sigma^{(N)}(\alpha,\alpha)} \ . \tag{169}$$

For $\theta^e - \theta^b = 2\pi$, the fact that

$$\lim_{N\to\infty} \sigma^{(N)}(\alpha,\beta) = \pi\cos(\alpha-\beta) = \pi\cos(\theta^i - \Theta^i) = \pi\kappa \ , \tag{170}$$

gives rise to the expected result

$$\lim_{N\to\infty} \mathcal{K}^{(N)}(\mathcal{E}_1') = \mathcal{K}(\mathcal{E}_1') \ , \tag{171}$$

Recall that our goal was to obtain an estimation of $\mathcal{E}_1'$ by minimizing $\mathcal{K}^{(N))}(\mathcal{E}_1')$. The procedure is the same as in sect. 4.2 and yields the exact (mathematical) solution

$$\mathcal{E}_1^{\prime(N)} = \frac{-k_+(\mathfrak{C}_3^{(N)} - 2\mathcal{E}_0\mathfrak{C}_4^{(N)}) + \sqrt{k_+^2(\mathfrak{C}_3^{(N)} - 2\mathcal{E}_0\mathfrak{C}_4^{(N)})^2 - 4k_+\mathfrak{C}_4^{(N)}\mathfrak{C}_0^{(N)}}}{2k_+\mathfrak{C}_4^{(N)}} \ , \tag{172}$$

and the approximate solution

$$\mathcal{E}_1^{\prime(N)} \approx \mathcal{E}_0\left(\frac{FA^2 + FB^2 + f^{(N)}g^{(0)}}{FA^2 - FB^2 - f^{(N)}g^{(0)}}\right) \ , \tag{173}$$

wherein:

$$\mathfrak{C}_4 = FA^2 - (FB^2 + f^{(N)}g) \ , \tag{174}$$

$$\mathfrak{C}_3 = 2\mathcal{E}_0FA^2 - 4\mathcal{E}_0(FB^2 + f^{(N)}g) + 2\mathcal{E}_1''f^{(N)}h \ , \tag{175}$$

$$\mathfrak{C}_0 = -k_+^2FA^2 - k_+k_-(FB^2 + f^{(N)}g) + 2k_+\mathcal{E}_0\mathcal{E}_1''f^{(N)}h \ , \tag{176}$$

$$f^{(N)} = \frac{e^i\kappa^{(N)}}{b} \ , \tag{177}$$

$$\kappa^{(N)} = \frac{\sigma^{(N)}(\alpha,\beta)}{\sigma^{(N)}(\beta,\beta)} \ . \tag{178}$$

Eqs. (172)-(173) are the (mathematically) exact and approximate solutions respectively to the inverse problem for discrete data in the interval $[\theta^b + \frac{\delta_\theta}{2}, \theta^e - \frac{\delta_\theta}{2}]$.

Eqs. (174)-(178)) show that the accuracy of the retrieval of ε_1' is conditioned, not only by the uncertainty of the nuisance parameters $\mathcal{E}_1''$, $\mathcal{E}_0$, A, E^i, B, Θ^i, but also by the number N of data samples.

It is of some interest to see how the choice of N influences the retrieval of ε_1', either via the explicit formula (172) or via minimization of the cost functional $\mathcal{K}^{(N)}$ in (173). To do

this, we consider solely the case $\theta^e - \theta^b = 2\pi$, keeping in mind the reference solution obtained by minimization of the cost functional $\mathcal{K}$. From (168) it ensues that

$$\kappa^{(N)}(\alpha,\beta) = \frac{\cos\alpha}{\cos\beta}\ ;\ N = 1,2\ . \tag{179}$$

$$\kappa^{(N)}(\alpha,\beta) = \cos(\alpha-\beta)\ ;\ N \geq 3\ . \tag{180}$$

wherein

$$\alpha = \frac{\pi}{N} - \theta^i\ \ ,\ \ \beta = \frac{\pi}{N} - \Theta^i\ . \tag{181}$$

Consequently,

$$\kappa^{(1)} = \frac{\cos\theta^i}{\cos\Theta^i}\ \ ,\ \ \kappa^{(2)} = \frac{\sin\theta^i}{\sin\Theta^i}\ \ ,\ \ \kappa^{(N\geq 3)} = \cos(\theta^i - \Theta^i) = \kappa\ . \tag{182}$$

This result tells us that, in the case $\theta^e - \theta_b = 2\pi$, the retrieval depends on N for small N $(= 1, 2)$, but no longer depends on N for $N \geq 3$, which suggests that *the optimal number N of sensors is $N = 3$* separated (in terms of angle θ) by $2\pi/3$, on the sensing circle of radius $b \geq a$. Note also that owing to the result $\kappa^{(N\geq 3)} = \kappa$, it ensues that

$$\mathcal{K}^{(N\geq 3)} = \mathcal{K}\ , \tag{183}$$

which means that the employment of the term 'optimal', is all the more justified that the $N = 3$ inversion gives rise to the reference retrieval (obtained by minimization of $\mathcal{K}$).

4.5 Finding $\mathcal{E}''$ of the cylinder by minimizing $\mathcal{K}$

Eq.(54) tells us that

$$\Re(-i\mathcal{F}) = \Im(\mathcal{F}) = 2\big(\mathcal{E}_1'\mathcal{E}_1'' + \mathcal{E}_0\mathcal{E}_1''\big)\ , \tag{184}$$

$$\Im(-i\mathcal{F}) = -\Re(\mathcal{F}) = -\big(\mathcal{E}_1'^2 - \mathcal{E}_1''^2 + 2\mathcal{E}_0\mathcal{E}_1' + \mathcal{E}_0^2\big)\ , \tag{185}$$

so that (53) becomes

$$2\big(\mathcal{E}_1'\mathcal{E}_1'' + \mathcal{E}_0\mathcal{E}_1''\big)\Re(\mathfrak{F} - \kappa\mathfrak{f}) + \big(\mathcal{E}_1'^2 - \mathcal{E}_1''^2 + 2\mathcal{E}_0\mathcal{E}_1' + \mathcal{E}_0^2\big)\Im(\mathfrak{F} - \kappa\mathfrak{f}) = 0\ , \tag{186}$$

or, more explicitly:

$$\Big(\frac{FA^2 4\mathcal{E}_0\mathcal{E}_1''\mathcal{E}_+}{\|\mathcal{E}_1 + \mathcal{E}_0\|^4}\Big)\Big\{F\Big[-B^2 + A^2\Big(\frac{\mathcal{E}_1''^2 + \mathcal{E}_+\mathcal{E}_-}{\|\mathcal{E}_1 + \mathcal{E}_0\|^2}\Big)\Big] - fg\Big\} + \Big(\frac{FA^2 2\mathcal{E}_0(\mathcal{E}_+^2 - \mathcal{E}_1''^2)}{\|\mathcal{E}_1 + \mathcal{E}_0\|^4}\Big)\Big\{FA^2\frac{2\mathcal{E}_0\mathcal{E}_1''}{\|\mathcal{E}_1 + \mathcal{E}_0\|^2}\Big) - fh\Big\} = 0\ , \tag{187}$$

wherein

$$\mathcal{E}_\pm := \mathcal{E}_1' \pm \mathcal{E}_0\ \ ,\ \ \varepsilon_\pm := \varepsilon_1' \pm \varepsilon_0\ . \tag{188}$$

After division by $\frac{FA^2 2\mathcal{E}_0}{\|\mathcal{E}_1+\mathcal{E}_0\|^6} \neq 0$, (187) becomes

$$(2\mathcal{E}_1''\mathcal{E}_+)\big\{-[FB^2+fg]\|\mathcal{E}_1+\mathcal{E}_0\|^2+FA^2(\mathcal{E}_1''^2+\mathcal{E}_+\mathcal{E}_-)\big\}+ \\ \big(\mathcal{E}_+^2-\mathcal{E}_1'^2\big)\big\{FA^2 2\mathcal{E}_0\mathcal{E}_1''-fh\|\mathcal{E}_1+\mathcal{E}_0\|^2\big\}=0\ , \quad (189)$$

This relation can be cast into the form of the fourth-order (in terms of $\mathcal{E}''$) (quartic) algebraic equation

$$\mathfrak{O}_4\mathcal{E}_1''^4+\mathfrak{O}_3\mathcal{E}_1''^3+\mathfrak{O}_2\mathcal{E}_1''^2+\mathfrak{O}_1\mathcal{E}_1''+\mathfrak{O}_0=0\ , \quad (190)$$

wherein

$$\begin{array}{c} \mathfrak{O}_4=fh\ , \\ \mathfrak{O}_3=2\left[FA^2(\mathcal{E}_+-\mathcal{E}_0)-(FB^2+fg)\mathcal{E}_+\right]\ , \\ \mathfrak{O}_2=0\ , \\ \mathfrak{O}_1=2\mathcal{E}_+^2\left\{[FA^2\mathcal{E}_- -(FB^2+fg)\mathcal{E}_+]+FA^2\mathcal{E}_0\right\}\ , \\ \mathfrak{O}_0=-fh\mathcal{E}_+^4 \end{array} \quad . \quad (191)$$

It ensues from these formulae that:

$$\mathfrak{O}_1=\mathcal{E}_+^2\mathfrak{O}_3\ \ ,\ \ \mathfrak{O}_0=-\mathfrak{O}_4\mathcal{E}_+^4\ , \quad (192)$$

so that the roots of the quartic equation can be found from those of the two quadratic equations

$$\mathcal{E}_1''^2+\mathcal{E}_+^2=0\ , \quad (193)$$

$$\mathfrak{O}_4\left(\mathcal{E}_1''^2-\mathcal{E}_+^2\right)+\mathfrak{O}_3\mathcal{E}_1''=0\ , \quad (194)$$

The two roots of the first quadratic equation are:

$$\begin{array}{c} \mathcal{E}_1''^{(1)}=-i\mathcal{E}_+\ , \\ \mathcal{E}_1''^{(2)}=i\mathcal{E}_+ \end{array} \quad , \quad (195)$$

and the two roots of the second quadratic equation are:

$$\begin{array}{c} \mathcal{E}_1''^{(-)}=\frac{-\mathfrak{O}_3-\sqrt{\mathfrak{O}_3^2+4\mathfrak{O}_4^2\mathcal{E}_+^2}}{2\mathfrak{O}_4}\ , \\ \mathcal{E}_1''^{(+)}=\frac{-\mathfrak{O}_3+\sqrt{\mathfrak{O}_3^2+4\mathfrak{O}_4^2\mathcal{E}_+^2}}{2\mathfrak{O}_4} \end{array} \quad . \quad (196)$$

Eqs. (195)-(196) represent the exact solutions of the inverse problem of the identification of the sole parameter $\mathcal{E}_1''$. Recall that it was assumed that $\mathcal{E}_0$, $\mathcal{E}_1'$ and $\mathcal{E}_1''$ (of the same nature as ε_0, ε_1', ε_1'' respectively) are positive real. Thus, $\mathcal{E}_1''^{(1)}$ and $\mathcal{E}_1''^{(2)}$ are not admissible solutions. Whether $\mathcal{E}_1''^{(\pm)}$ are admissible or not can be decided empirically, or by other means, using this same criterium (a solution is admissible if it is positive real).

4.5.1 Perturbation solutions of $\mathcal{E}_1^{''(\pm)}$ for small ε_1''

Let us return to (194) which can be written as

$$\sum_{j=0}^{2} U_j u_j = 0 \ , \tag{197}$$

wherein:

$$U_0 = -\mathfrak{O}_4 \mathcal{E}_+^2 \ \ , \ U_1 = \mathfrak{O}_3 \ \ , \ \ U_2 = \mathfrak{O}_4 \ , \tag{198}$$

and

$$u_0 = 1 \ \ , \ \ u_1 = \mathcal{E}_1'' \ \ , \ \ u_2 = \mathcal{E}_1''^2 = u_1^2 \ . \tag{199}$$

We expand U_j and u_j in series of powers of the supposedly-small quantity

$$\delta := \varepsilon_1'' \ , \tag{200}$$

to find, as in sect. 4.3.1,

$$U_0^{(0)} + U_1^{(0)} u_1^{(0)} + U_2^{(0)} u_1^{(0)2} = 0 \ , \tag{201}$$

$$U_0^{(1)} + U_1^{(0)} u_1^{(1)} + U_1^{(1)} u_1^{(0)} + U_2^{(0)} 2 u_1^{(0)} u_1^{(1)} + U_2^{(1)} u_1^{(0)2} = 0 \ , \tag{202}$$

$$U_0^{(2)} + U_1^{(0)} u_1^{(2)} + U_1^{(1)} u_1^{(1)} + U_1^{(2)} u_1^{(0)} + U_2^{(0)} (2 u_1^{(0)} u_1^{(2)} + u_1^{(1)2}) + U_2^{(1)} 2 u_1^{(0)} u_1^{(1)} + U_2^{(2)} u_1^{(1)2} = 0 \ . \tag{203}$$

We now address the problem of the $U_j^{(k)}$. To do this, we employ the expressions for $\mathfrak{O}_4$ and $\mathfrak{O}_3$ in (191):

$$\mathfrak{O}_4 = fh \ , \tag{204}$$

$$\mathfrak{O}_3 = 2\mathcal{E}_0 F A^2 - 4\mathcal{E}_0 (FB^2 + fg) \ , \tag{205}$$

so that:

$$U_0 = -\mathcal{E}_+^2 fh \ , \tag{206}$$

$$U_1 = 2\mathcal{E}_0 F A^2 - 4\mathcal{E}_0 (FB^2 + fg) \ , \tag{207}$$

$$U_2 = fh \ . \tag{208}$$

Under the (small-δ) hypothesis (implicit in the perturbation method)

$$0 \leq \delta << 1 \ , \tag{209}$$

we found in sect. 4.3.1:

$$g = g^{(0)} + g^{(2)} \delta^2 + \mathcal{O}(\delta^4) \ , \tag{210}$$

$$h = h^{(1)} \delta + h^{(3)} \delta^3 + \mathcal{O}(\delta^5) \ , \tag{211}$$

Consequently:

$$U_0 = -\mathcal{E}_+^2 fh \ , \tag{212}$$

whence

$$\left.\begin{array}{c} U_0^{(0)} = 0 \ , \\ U_0^{(1)} = -\mathcal{E}_+^2 f h^{(1)} \ , \\ U_0^{(2)} = 0 \end{array}\right. \ . \tag{213}$$

$$U_1 = 2\mathcal{E}_0 F A^2 - 4\mathcal{E}_0 F B^2 - 4\mathcal{E}_0 f g^{(0)} - 4\mathcal{E}_0 f g^{(2)} \delta^2 + \mathcal{O}(\delta^4) \ , \tag{214}$$

$$\left.\begin{array}{c} U_1^{(0)} = 2\mathcal{E}_0 F A^2 - 4\mathcal{E}_0 F B^2 - 4\mathcal{E}_0 f g^{(0)} \ , \\ U_1^{(1)} = 0 \ , \\ U_1^{(2)} = -4\mathcal{E}_0 f g^{(2)} \ , \end{array}\right. \tag{215}$$

$$U_2 = f h^{(1)} \delta + f h^{(3)} \delta^3 + \mathcal{O}(\delta^5) \ , \tag{216}$$

$$\left.\begin{array}{c} U_2^{(0)} = 0 \ , \\ U_2^{(1)} = f h^{(1)} \ , \\ U_2^{(2)} = 0 \ . \end{array}\right. \tag{217}$$

The solution of (201) is

$$u_1^{(0)} = \frac{-U_0^{(0)}}{U_1^{(0)}} = 0 \ . \tag{218}$$

The next step in the perturbation procedure is to obtain $u_1^{(1)}$ from $u_1^{(0)}$. This is done via (202) from which we obtain

$$u_1^{(1)} = u_1^{(1)} = -\left(\frac{U_0^{(1)} + U_1^{(1)} u_1^{(0)} + U_2^{(1)} u_1^{(0)2}}{U_1^{(0)} + U_2^{(0)} 2 u_1^{(0)}} \right) \ , \tag{219}$$

or, on account of (218),

$$u_1^{(1)} = -\left(\frac{U_0^{(1)}}{U_1^{(0)}} \right) = \frac{\mathcal{E}_+^2 f h^{(1)}}{2\mathcal{E}_0 [F A^2 - 2(F B^2 + f g^{(0)})]} \ . \tag{220}$$

The next step in the perturbation procedure is to obtain $u_1^{(2)}$ from $u_1^{(0)}$ and $u_1^{(1)}$. This is done via (203). But, instead of writing the explicit expression for $u_1^{(2)}$, we recall that here u_1 stands for $\mathcal{E}_1''$, and to second order in ε''

$$u_1 = \mathcal{E}_1'' \approx u_1^{(0)} + u_1^{(1)} \varepsilon_1'' + u_1^{(2)} \varepsilon''^2 \ , \tag{221}$$

or, on account of (218) and neglecting terms of order ε''^2 (due to the assumed smallness of ε_1'', the approximate solution for $\mathcal{E}_1''$ is

$$\mathcal{E}_1'' \approx \left(\frac{\mathcal{E}_+^2 f h^{(1)}}{F A^2 - F B^2 - f g^{(0)}} \right) \varepsilon'' \ , \tag{222}$$

with the understanding that, on account of what the same type of perturbation analysis as in sect. 4.3.1 can show, the (only-admissible) exact solution for ε_1'' is

$$\mathcal{E}_1'' = \frac{-\mathfrak{O}_3 + \sqrt{\mathfrak{O}_3^2 + 4\mathfrak{O}_4^2 \mathcal{E}_+^2}}{2\mathfrak{O}_4} \ . \tag{223}$$

4.5.2 Comments on the exact and approximate solutions for $\mathcal{E}_1''$

The result embodied in (223) calls for the following comments:

1- It shows that the solution to the inverse problem of the identification of the sole parameter $\mathcal{E}_1''$ *exists*, even in the presence of nuisance parameter uncertainties;
2- it shows that it is possible to obtain the *mathematically-explicit and exact solution* to the given inverse problem, even in the presence of nuisance parameter uncertainties;
3- it shows that this solution is *unique* for a given set of parameters; ε_1', ε_1'', ε_0, a, e^i, θ^i, b, $\mathcal{E}_1''$, $\mathcal{E}_0$, A, E^i, Θ^i, B, provided a physical constraint (i.e., that $\mathcal{E}_1''$ be positive real) is satisfied;
4- it shows that the accuracy of the retrieval of the imaginary part of the permittivity ($\mathcal{E}_1''$) is conditioned, albeit in a complex manner, by the uncertainty of the nuisance parameters $\mathcal{E}_1', \mathcal{E}_0$, A, E^i, Θ^i, B;

The result embodied in (222)

5- shows that the accuracy of the retrieval of $\mathcal{E}_1''$ is strongly-conditioned by ε_1'' and $\mathcal{E}_1'$ since the dependence of $\mathcal{E}_1''$ on ε_1'' is linear and that on $\mathcal{E}_1'$ is quadratic,
6- shows nevertheless that $\mathcal{E}_1''$ is usually small due to ε_1'' having been assumed to be small,
7- shows that, due to the possibility of vanishing denominator in (222)), the retrieval of $\mathcal{E}_1''$, like that of $\mathcal{E}_1'$, can be unstable with respect to certain nuisance parameters.

4.6 Finding the imaginary part of the permittivity ($\mathcal{E}''$) of the cylinder by minimizing $\mathcal{K}^{(N)}$

The method of obtaining the imaginary part of the permittivity of the cylinder outlined in sect. 4.5 is somewhat unrealistic in that it supposes that the data is registered at a continuum of points on the sensing circle $r = b$. *In reality, the data is registered at discrete locations on this circle and the number N of these locations is finite.* Of course, N *will have an influence on the accuracy of the retrieval* and it is this influence that we shall now examine.

From (45) we obtain

$$\mathcal{K}^{(N)}(\mathcal{E}_1'') = \left(\frac{1}{\|\mathfrak{f}\|^2 \delta_\theta \sum_{n=1}^{N} \cos^2(\alpha + (n-1)\delta_\theta)} \right) \times$$
$$\delta_\theta \sum_{n=1}^{N} \Big(\|\mathfrak{f}\|^2 \cos^2(\alpha + (n-1)\delta_\theta) - 2\Re(\mathfrak{f}^* \mathfrak{F}) \cos(\alpha + (n-1)\delta_\theta) \cos(\beta + (n-1)\delta_\theta) +$$
$$\|\mathfrak{F}\|^2 \cos^2(\beta + (n-1)\delta_\theta) \Big) , \quad (224)$$

wherein all quantities are as in sect. 4.4, and find, as in sect. 4.4,

$$\mathcal{K}^{(N)}(\mathcal{E}_1'') = \frac{\|\mathfrak{f}\|^2\sigma^{(N)}(\alpha,\alpha) - 2\Re(\mathfrak{f}^*\mathfrak{F})\sigma^{(N)}(\alpha,\beta) + \|\mathfrak{F}\|^2\sigma^{(N)}(\beta,\beta)}{\|\mathfrak{f}\|^2\sigma^{(N)}(\alpha,\alpha)} \ . \tag{225}$$

For $\theta^e - \theta^b = 2\pi$, the fact that

$$\lim_{N\to\infty} \sigma^{(N)}(\alpha,\beta) = \pi\cos(\alpha-\beta) = \pi\cos(\theta^i - \Theta^i) = \pi\kappa \ , \tag{226}$$

gives rise to the expected result

$$\lim_{N\to\infty} \mathcal{K}^{(N)}(\mathcal{E}_1'') = \mathcal{K}(\mathcal{E}_1'') \ , \tag{227}$$

Recall that our goal was to obtain an estimation of $\mathcal{E}_1''$ by minimizing $\mathcal{K}^{(N))}(\mathcal{E}_1'')$. The procedure is the same as in sect. 4.5 and yields the exact solution

$$\mathcal{E}_1^{''(N)} = \frac{-\mathfrak{O}_3^{(N)} + \sqrt{\mathfrak{O}_3^{(N)2} + 4\mathfrak{O}_4^{(N)2}\mathcal{E}_+^2}}{2\mathfrak{O}_4^{(N)}} \ . \tag{228}$$

and the approximate solution

$$\mathcal{E}_1^{''(N)} \approx \left(\frac{\mathcal{E}_+^2 f^{(N)} h^{(1)}}{FA^2 - FB^2 - f^{(N)}g^{(0)}}\right)\varepsilon'' \ , \tag{229}$$

wherein:

$$\mathfrak{O}_4^{(N)} = f^{(N)}h \ , \tag{230}$$

$$\mathfrak{O}_3^{(N)} = 2\mathcal{E}_0 FA^2 - 4\mathcal{E}_0(FB^2 + f^{(N)}g) \ , \tag{231}$$

$$f^{(N)} = \frac{e^i\kappa^{(N)}}{b} \ , \tag{232}$$

$$\kappa^{(N)} = \frac{\sigma^{(N)}(\alpha,\beta)}{\sigma^{(N)}(\beta,\beta)} \ . \tag{233}$$

Eqs. (228) and (228) are the (mathematically) exact and approximate solutions to the inverse problem for discrete data in the interval $[\theta^b + \frac{\delta_\theta}{2}, \theta^e - \frac{\delta_\theta}{2}]$. These relations, as well as (230)-(233), show that the accuracy of the retrieval of $\mathcal{E}_1''$ is conditioned, not only by the uncertainty of the nuisance parameters $\mathcal{E}_1'$, $\mathcal{E}_0$, A, E^i, B, Θ^i, but also by the number N of data samples.

As in sect. 4.4, we can show that, in the case $\theta^e - \theta_b = 2\pi$, the retrieval depends on N for small N $(= 1, 2)$, but no longer depends on N for $N \geq 3$, which suggests that *the optimal number N of sensors is $N = 3$* separated (in terms of angle θ) by $2\pi/3$, on the sensing circle of radius $b \geq a$. Moreover, the term 'optimal', is all the more justified that the $N = 3$ inversion gives rise to the reference retrieval (obtained by minimization of $\mathcal{K}$).

5 Inversion by solving numerically the quartic equations

We saw in sects. 4.3, 4.5, 4.4, 4.6, that the next-to-final step of the inverse problem boiled down to the resolution of either the quartic equations

$$\mathfrak{C}_4^{(N)}\mathcal{E}_1'^4+\mathfrak{C}_3^{(N)}\mathcal{E}_1'^3+\mathfrak{C}_2^{(N)}\mathcal{E}_1'^2+\mathfrak{C}_1^{(N)}\mathcal{E}_1'+\mathfrak{C}_0^{(N)}=0\ , \tag{234}$$

or the quartic equation

$$\mathfrak{O}_4^{(N)}\mathcal{E}_1''^4+\mathfrak{O}_3^{(N)}\mathcal{E}_1''^3+\mathfrak{O}_2^{(N)}\mathcal{E}_1''^2+\mathfrak{O}_1^{(N)}\mathcal{E}_1''+\mathfrak{O}_0^{(N)}=0\ , \tag{235}$$

with $N=\infty$ or $N\geq 3$.

Consider the general problem of finding the n (an integer) complex roots $(z_1,z_2,...z_n)$ of the n-th order polynomical equation

$$\sum_{j=1}^{n}a_n z^n=0\ . \tag{236}$$

By employing the Viète formulae for the product of the roots one is led to the formation of the companion matrix

$$\begin{pmatrix} -\frac{a_1}{a_0} & -\frac{a_2}{a_0} & . & . & . & . & -\frac{a_n}{a_0} \\ 1 & 0 & 0 & . & . & 0 & 0 \\ 0 & 1 & 0 & . & . & . & . \\ . & . & . & . & . & . & . \\ . & . & . & . & . & . & . \\ . & . & . & . & 1 & 0 & . \\ 0 & 0 & . & . & . & 1 & 0 \end{pmatrix}\ . \tag{237}$$

so that finding the eigenvalues $\lambda_j=\frac{1}{z_j}\ ;\ j=1,2,...,n$ of this matrix is equivalent to finding the solutions $\lambda_j=\frac{1}{z_j}\ ;\ j=1,2,...,n$ to the equation

$$det\begin{pmatrix} -\frac{a_1}{a_0}-\lambda & -\frac{a_2}{a_0} & . & . & . & . & -\frac{a_n}{a_0} \\ 1 & -\lambda & 0 & . & . & 0 & 0 \\ 0 & 1 & 0 & . & . & . & . \\ . & . & . & . & . & . & . \\ . & . & . & . & . & . & . \\ . & . & . & . & 1 & 0 & . \\ 0 & 0 & . & . & . & 1 & -\lambda \end{pmatrix}=0\ , \tag{238}$$

so that the determination of the roots of the polynomial equation reduces to the determination of the eigenvalues of the companion matrix. This can be done by any standard (such as the QR) technique [47].

In fact, we employed the MATLAB function *roots*, which is based on the companion matrix and eigenvalue evaluation algorithm, to find the roots of our two quartic equations. It turned out that these roots are identical to the mathematically-exact roots we found previously in sects. 4.3 and 4.5 (for $N = \infty$), the same applying to the case $N \geq 3$. As in these two sections, we choose the "right" root (one $\mathcal{E}_1'$ and one for $\mathcal{E}_1''$) by imposing the physical constraints:

$$\Im\mathcal{E}_1' = 0 \quad , \quad \Re\mathcal{E}_1' \geq 0 \ , \tag{239}$$

$$\Im\mathcal{E}_1'' = 0 \quad , \quad \Re\mathcal{E}_1'' \geq 0 \ , \tag{240}$$

6 Inversion by a numerical scheme for finding the minimum of the cost functional

6.1 Basic retrieval scheme

The direct problem model, by which the data is generated, involves the (true) parameter set $\mathbf{p} = \{p_1, p_2, ...\}$, a subset $\mathbf{r}$ of which is to be retrieved in the inverse problem context. At present, $\mathbf{r}$ reduces to the single parameter $r_1 = \varepsilon_1'$ (so that $\mathbf{r} = \{r_1\}$) or $r_2 = \varepsilon_1''$ (so that $\mathbf{r} = \{r_2\}$). The remaining parameters of $\mathbf{p}$ form the set of nuisance parameters $\mathbf{g}$.

Although we saw previously that an exact, explicit solution to our inverse problem could be found, at present we want to solve this problem in a *numerical manner* (as is usually the case in inverse problems) and see to what extent the so-obtained solution coincides with the exact solution.

The numerical inversion is carried out by means of a (retrieval) model involving the parameter set $\mathbf{P}$ whose components are qualitatively the same as the corresponding components of $\mathbf{p}$. During the inversion, the real (or imaginary) part of the permittivity takes on (variable) trial values $\mathbf{R} = \{R_1\} = \{\mathcal{E}_1'\}$ (or $\mathbf{R} = \{R_2\} = \{\mathcal{E}_1''\}$), while the remaining parameters of the retrieval model, forming the set $\mathbf{G}$, are fixed, but (as explained earlier) not necessarily equal to the corresponding parameters of the set $\mathbf{g}$.

Now, the basic inversion scheme consists in searching, in iterative, *numerical* manner, for the real $\mathbf{R} = \tilde{\mathbf{r}}$ that minimizes the discrepancy (the measure of which is a cost functional $\mathcal{K}^{(N)}$) between trial electric potential fields (resulting from the trial parameter R_1 and the nuisance parameter set $\mathbf{G}$) and the true electric potential field (resulting from the true parameter r_1 and the nuisance parameter set $\mathbf{g}$).

Note that if, as will be assumed in the examples presented hereafter, there exists some uncertainty in the nuisance parameters, $\mathbf{G}$ will not be identical to $\mathbf{g}$. In fact, this possible (model) *discordance* will affect the accuracy of the retrieval.

6.2 Simplex minimization of the cost functional

Most inverse problems are solved by numerical minimization of a cost functional for the simple reason that these inverse problems cannot be solved in a mathematical, explicit, exact

manner. On the contrary, our inverse problem was shown to possess mathematical, explicit, exact solutions. Thus by confronting the two types (i.e., numerical and mathematical) of solutions enables us to test the quality of the numerical solutions.

The numerical minimization of the cost functional $\mathcal{K}^{(N)}$ can be carried out by a large variety of schemes; our choice was that of the Nelder-Mead Simplex algorithm [32] implemented in MATLAB by the function *fminsearch*. This algorithm is a geometrical, rather than gradient-based, optimization manner of finding the parameter (or parameters if more than one parameters are to be retrieved) which corresponds to the minimum of a (cost) function. Few theoretical results have been proved explicitly concerning this algorithm, and then essentially in one and two dimensions [25]. Nevertheless, the Simplex algorithm has been frequently employed, particularly in parameter estimation problems [16], [24], [39], [11], [51], and even in problems involving noisy data [46], [38]. Like other optimization schemes, the Simplex algorithm is iterative by nature, with each iteration requiring a certain number of (cost) functional computations. The number of iterations and function computations increases with: a) the precision with which one wants to locate the minimum of the (cost) functional, b) the distance of the initial values of the parameters to their target values, and depends on the topological nature of the cost functional. In the present study, the dimension of the search space (of real variables) is one and the function to be minimized appears (by the previously-evoked theoretical considerations) to be convex (i.e., such as to admit only one minimum). In $fminsearch$, the maximum number of function evaluations and maximum number of iterations can be chosen, via the parameters $MaxFunEvals$ and $MaxIter$ (designated by MFE and MI in the following respectively, by the user. This appears to us to be a better strategy than choosing the precision, because aiming at a high precision may require a prohibitive amount of function evaluations and/or iterations. Each call to this function returns a value called $exitflag$ that describes the exit condition of $fminsearch$. $exitflag = 1$ when $fminsearch$ converged to a solution, $exitflag = 0$ when MFE or MI was reached and no further computations are made during this call, $exitflag = -1$ when the algorithm is terminated by the output function. Consequently, it is important to choose MFE and MI large enough for $fminsearch$ to converge to a bona fide solution (corresponding to an authentic minimum of the cost functional as indicated by $exitflag = 1$) for each call to $fminseach$.

The minimum of the cost functional (in the real parameter space explored by the Simplex scheme, anchored at the user-defined starting value of the to-be-retrieved parameter), is found for $\mathbf{R} = \tilde{\mathbf{r}}$. $\tilde{\mathbf{r}}$ can depend on the starting value, so that it is advisable to carry out the inversion in N_s stages, each of which involves a different starting value. Thus, if $R_1^{(n)}$ is the n-th starting value, then the N_s-stage Simplex scheme generates N_s candidate retrievals $\tilde{r}_1^{(n)}$; $n = 1, 2, ..., N_s$. The question is then how to select the most appropriate solution (this procedure is hereafter termed *regularization*) among the multitude of (N_s-stage) retrievals. Let $\min \mathcal{K}^{(N)(n)}$ be the value of the minimum of the cost function found by the Simplex scheme at the n-th stage. The *first step* in the regularization procedure consists in rejecting solutions that are not admissible i.e., a solution that is negative, since it was assumed that $\varepsilon_1' > 0$ (or $\varepsilon_1'' > 0$). Very large positive retrievals are not rejected on the grounds that they

are indicative of retrieval instability and therefore of some use. At this point, the values of n corresponding to admissible retrievals form the set $\mathbf{N}_a \subset \mathbf{N}_s$. The *second step* stems from the observation that the result of the multistage Simplex minimization scheme can lead to one or more $r_1^{(n)}$ that are not within the initial search interval $[R_1^b, R_1^e]$; a logical option is to reject such retrievals (otherwise, why impose initial search intervals other than to constrain the retrievals?), by assigning a large value of $\min \mathcal{K}^{(N)(n)}$ to them. Note that this action furnishes a means for telling us to enlarge $[R_1^b, R_1^e]$. The *last step* in the regularization proceeds as follows: the final retrieved value of r_1 is designated by $\tilde{r}_1$ and is *chosen*, amongst the remaining candidate retrievals $\{\tilde{r}_1^{(n)} \ ; \ n \in \mathbf{N}_a\}$, to be the one corresponding to the minimum of the set $\{\min \mathcal{K}^{(N)(n)} \ ; \ n \in \mathbf{N}_a\}$. This regularization procedure is incorporated into our MATLAB code to numerically solve the inverse problem.

We found that the Simplex scheme gives rise to exactly the same results as the companion matrix-eigenvalue scheme outlined in sect. 5. Moreover, it gives rise to exactly the same results as the mathematical solutions presented in sects. 4.3, 4.5, 4.4, 4.6 in a great variety of test cases. Thus, the numerical minimization of a cost function via the Simplex scheme is a robust, sound method for solving an inverse parameter-retrieval problem such as ours.

7 Results concerning the retrieval error as a function of nuisance parameter uncertainties

7.1 Overview of the evaluation of retrieval error for variable nuisance parameter uncertainty

All the following numerical results pertain to the choice (the true parameters of which are): $\varepsilon_1' = 2$, $\varepsilon_1'' = 0.1$, $\varepsilon_0 = 1$, $a = 0.1$, $e^i = 1$, $\theta^i = 2°$, $b = 0.2$, $MFE = MI = 1000$ (when the Simplex scheme is employed). Moreover, $\theta^b = 0°$, $\theta^e = 360°$, and $N = 3$ unless indicated otherwise.

Six general cases of nuisance parameter uncertainty are possible:

1) one nuisance parameter is uncertain, the five others are equal to their true values;
2) two nuisance parameters are uncertain, the four others are equal to their true values;
3) three nuisance parameters are uncertain, the three others are equal to their true values;
4) four nuisance parameters are uncertain, the two others are equal to their true value;
5) five nuisance parameters are uncertain, the one other is equal to their true value;
6) all six nuisance parameters are uncertain.

Due to the large number of possibilities, we consider representative samples of cases 1), 2) and 5) only. The offered graphs are composed of three panels, the left-hand one of which relates $\tilde{\mathcal{E}}_1'$ or $\tilde{\mathcal{E}}_1''$ to a variable nuisance parameter G, the central one of which relates $\varepsilon_{\varepsilon_1'} = \frac{\tilde{\mathcal{E}}_1' - \varepsilon_1'}{\varepsilon_1'}$ or $\varepsilon_{\varepsilon_1''} = \frac{\tilde{\mathcal{E}}_1'' - \varepsilon_1''}{\varepsilon_1''}$ to $\delta_g = \frac{G-g}{g}$, and the right-hand one of which relates $\mathcal{K}^{(3)}$ (for the retrieved parameter) to δ_g. Moreover, the circles refer to the retrievals obtained by the

MATHLAB function *roots* (see sect. 5).

7.2 Retrieval of $\mathcal{E}_1'$: variable uncertainty of one nuisance parameter, all other nuisance parameters are certain

Fig. 5 concerns the effect of variable uncertainty of the nuisance parameter $G = G_1 = \mathcal{E}_1''$.

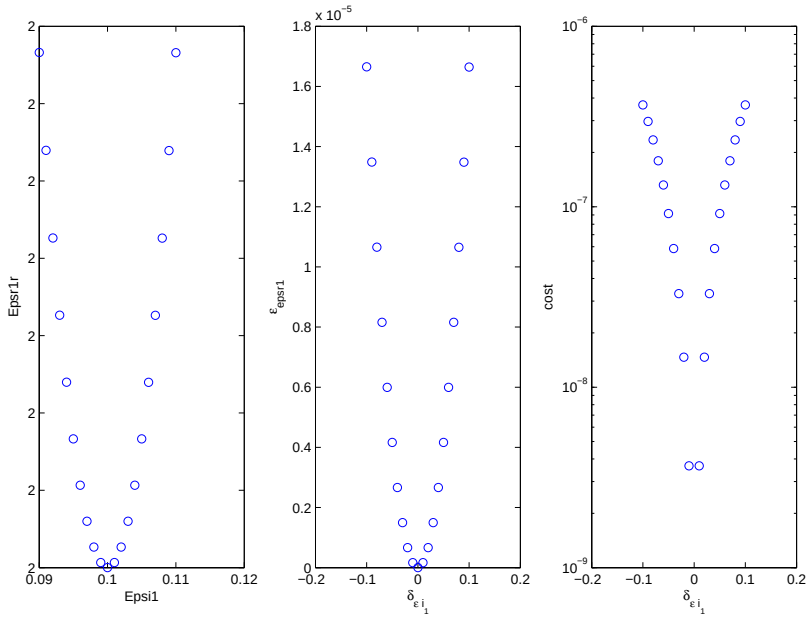

Figure 5: The abscissas in the left-hand panel represent $\mathcal{E}_1''$. The abscissas in the central and right-hand panels represent $\delta_{\varepsilon_1''}$. The ordinates represent the retrieved $\mathcal{E}_1'$ in the left-hand panel, $\varepsilon_{\varepsilon_1'}$ in the central panel, and $\mathcal{K}^{(3)}$ (for the retrieved parameter) in the right-hand panel. The circles refer to the retrieval obtained by resolution of the quartic equation via the MATHLAB function *roots*.

This figure shows that $|\varepsilon_{\varepsilon_1'}|$ is very small, which means that the retrieval of ε_1' is insensitive to uncertainty of the nuisance parameter $\mathcal{E}_1''$.

Fig. 6 concerns the effect of variable uncertainty of the nuisance parameter $G = G_4 = \mathcal{E}_0$.

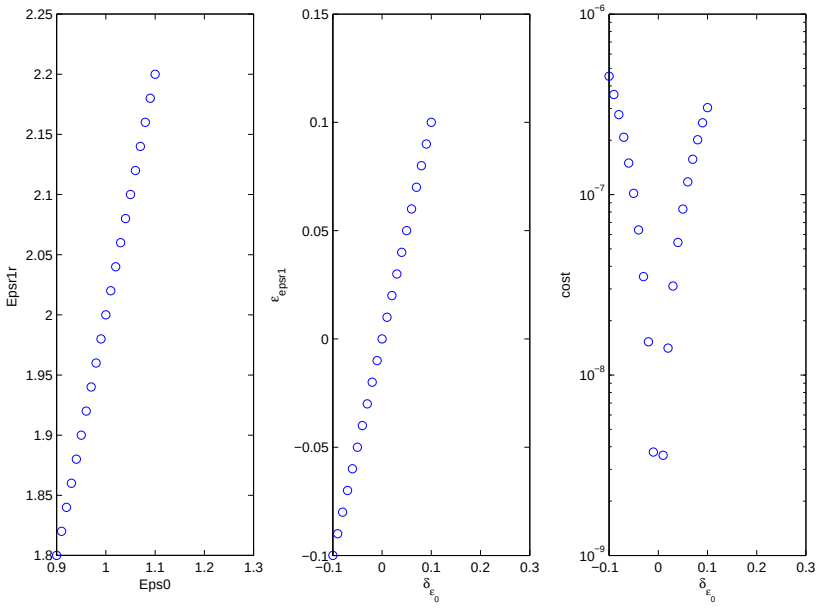

Figure 6: The abscissas in the left-hand panel represent $\mathcal{E}_0$. The abscissas in the central and right-hand panels represent δ_{ε_0}. The ordinates represent the retrieved $\mathcal{E}_1'$ in the left-hand panel, $\varepsilon_{\varepsilon_1'}$ in the central panel, and $\mathcal{K}^{(3)}$ in the right-hand panel. The circles have the same signification as in the previous figure.

This figure shows that $|\varepsilon_{\varepsilon_1'}| = |\delta_{\varepsilon_0}|$, in conformity with the prediction of the exact mathematical solution (133).

The left-hand panel of Fig. 7, relative to variable uncertainty of the nuisance parameter $G = G_2 = A$, is the numerical equivalent of the portion $A \in [A_+, \infty[$, $\mathcal{E}'_1 \in [\mathcal{E}_0, \infty[$ in fig. 3 translating the analytic properties of the exact mathematical solution of the inverse problem.

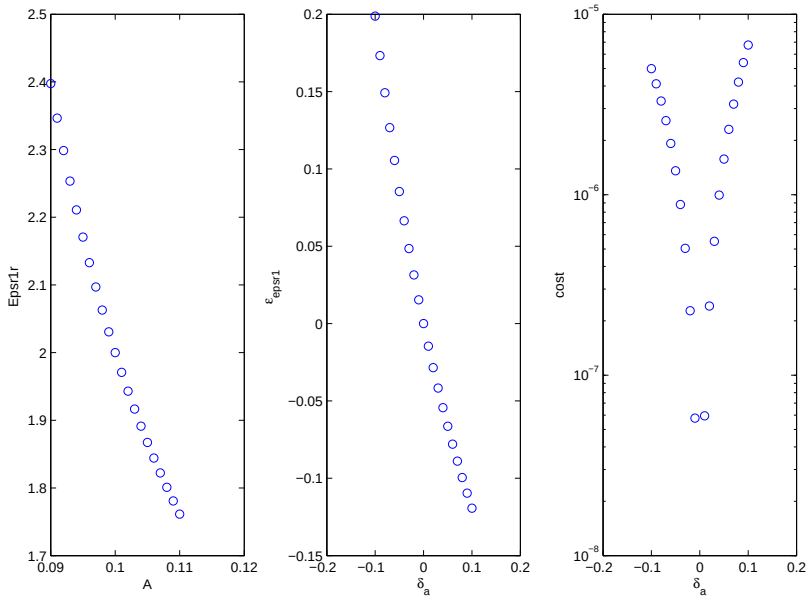

Figure 7: The abscissas in the left-hand panel represent A. The abscissas in the central and right-hand panels represent δ_a. The ordinates represent the retrieved $\mathcal{E}'_1$ in the left-hand panel, $\varepsilon_{\mathcal{E}'_1}$ in the central panel, and $\mathcal{K}^{(3)}$ in the right-hand panel. The circles have the same signification as in the previous figure.

This figure shows that, at $A = .09$ and $.11$, the retrieval error is of the same order as the nuisance parameter uncertainty since $|\varepsilon_{\mathcal{E}'_1}| \gtrsim |\delta_a|$.

The left-hand panel of Fig. 8, relative to variable uncertainty of the nuisance parameter $G = G_3 = E^i$, is the numerical equivalent of the portion $E^i \in [E^i_0, E^i_+[$, $\mathcal{E}'_1 \in [0, \infty[$ in fig. 4 translating the analytic properties of the exact mathematical solution of the inverse problem.

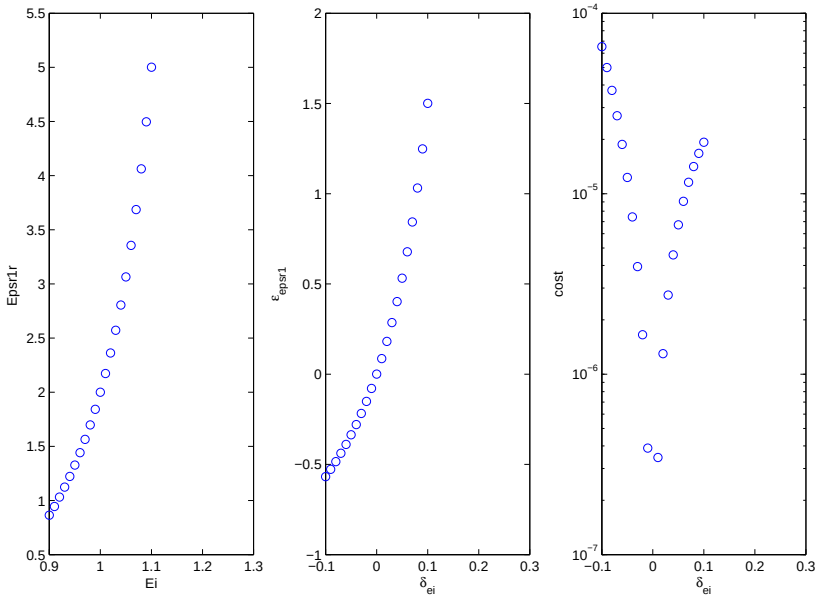

Figure 8: The abscissas in the left-hand panel represent E^i. The abscissas in the central and right-hand panels represent δ_{e^i}. The ordinates represent the retrieved $\mathcal{E}'_1$ in the left-hand panel, $\varepsilon_{\mathcal{E}'_1}$ in the central panel, and $\mathcal{K}^{(3)}$ in the right-hand panel. The circles have the same signification as in the previous figure.

This figure shows that, at $E^i = .9$ and 1.1, the retrieval error far exceeds the nuisance parameter uncertainty since $|\varepsilon_{\mathcal{E}'_1}| >> |\delta_{e^i}| = .1$, this being (in the neighborhood of $\delta_{e^i} = .1$) a manifestation of nuisance parameter uncertainty-induced retrieval instability.

Fig. 9 concerns the effect of variable uncertainty of the nuisance parameter $G = G_1 = \Theta^i$.

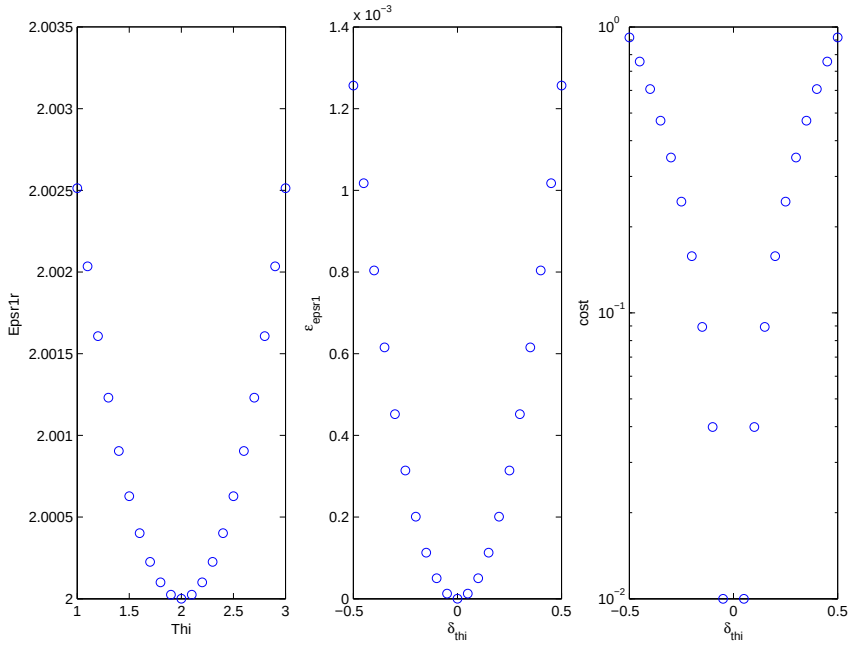

Figure 9: The abscissas in the left-hand panel represent Θ^i. The abscissas in the central and right-hand panels represent δ_{θ^i}. The ordinates represent the retrieved $\mathcal{E}_1'$ in the left-hand panel, $\varepsilon_{\varepsilon_1'}$ in the central panel, and $\mathcal{K}^{(3)}$ in the right-hand panel. The circles have the same signification as in the previous figure.

This figure shows that the retrieval error is quite small with respect to Θ^i uncertainty since $\varepsilon_{\varepsilon_1'} \leq 1.26 \times 10^{-3}$ over the whole Θ^i interval $[1°, 3°]$.

The left-hand panel of Fig. 10, relative to variable uncertainty of the nuisance parameter $G = G_5 = B$, is the numerical equivalent of the portion $B \in [B_0, B_+[$, $\mathcal{E}'_1 \in [\mathcal{E}'_0, \infty[$ in fig.2 translating the analytic properties of the exact mathematical solution of the inverse problem.

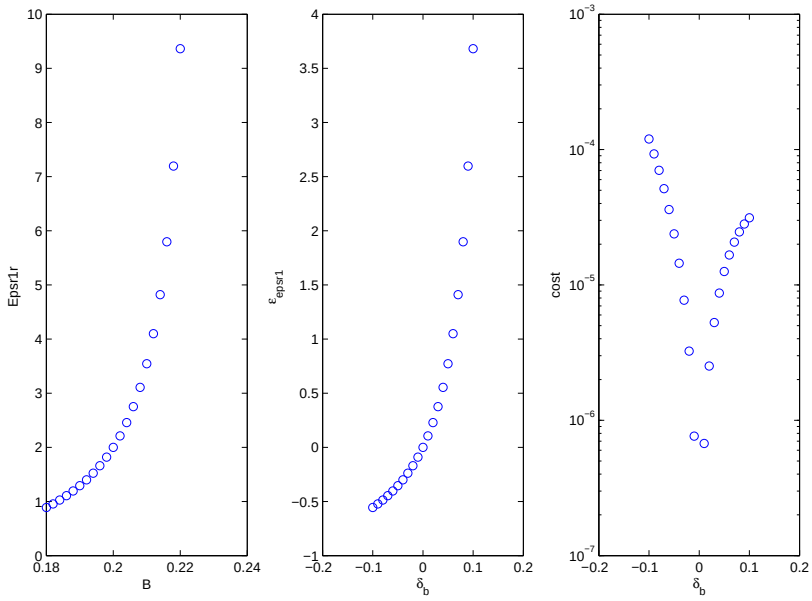

Figure 10: The abscissas in the left-hand panel represent B. The abscissas in the central and right-hand panels represent δ_b. The ordinates represent the retrieved $\mathcal{E}'_1$ in the left-hand panel, $\varepsilon_{\mathcal{E}'_1}$ in the central panel, and $\mathcal{K}^{(3)}$ in the right-hand panel. The circles have the same signification as in the previous figure.

This figure shows that, at $B = .18$ and $.22$, the retrieval error far exceeds the nuisance parameter uncertainty since $|\varepsilon_{\mathcal{E}'_1}| >> |\delta_b| = .1$, this being (in the neighborhood of $\delta_b = .1$) a manifestation of nuisance parameter uncertainty-induced retrieval instability.

7.3 Retrieval of $\mathcal{E}_1''$: variable uncertainty of one nuisance parameter, all other nuisance parameters are certain

Fig. 11 concerns the effect of variable uncertainty of the nuisance parameter $G = G_1 = \mathcal{E}_1'$.

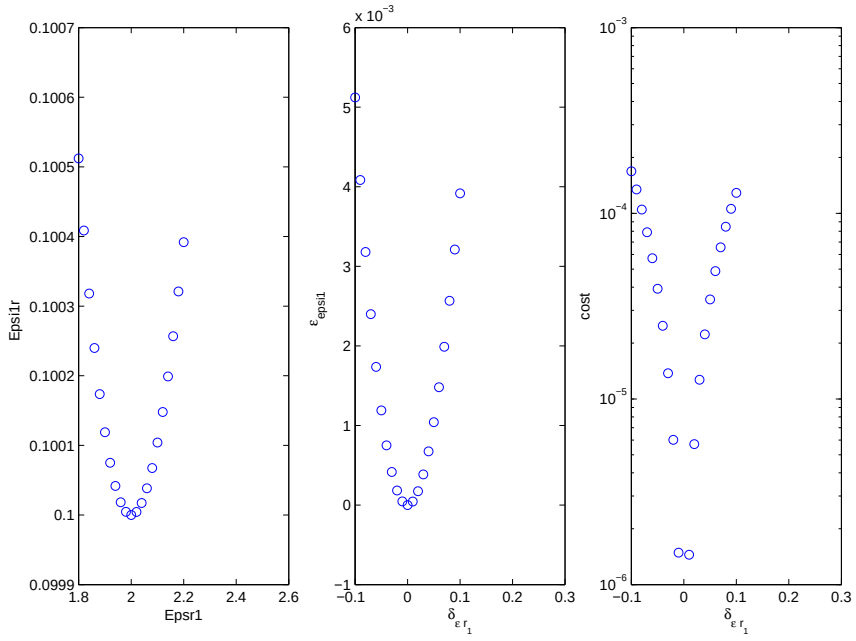

Figure 11: The abscissas in the left-hand panel represent $\mathcal{E}_1'$. The abscissas in the central and right-hand panels represent $\delta_{\varepsilon_1'}$. The ordinates represent the retrieved $\mathcal{E}_1''$ in the left-hand panel, $\varepsilon_{\varepsilon_1''}$ in the central panel, and $\mathcal{K}^{(3)}$ in the right-hand panel. The circles refer to the retrieval obtained by resolution of the quartic equation via the mathlab function *roots*.

This figure shows that $|\varepsilon_{\varepsilon_1''}|$ is very small, which means that the retrieval of ε_1'' is insensitive to uncertainty of the nuisance parameter ε_1'.

Fig. 12 concerns the effect of variable uncertainty of the nuisance parameter $G = G_4 = \mathcal{E}_0$.

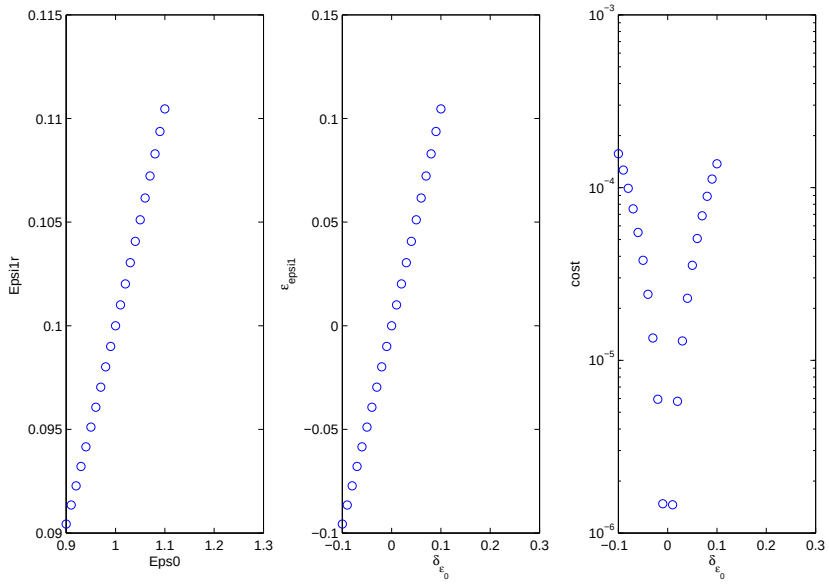

Figure 12: The abscissas in the left-hand panel represent $\mathcal{E}_0$. The abscissas in the central and right-hand panels represent δ_{ε_0}. The ordinates represent the retrieved $\mathcal{E}_1''$ in the left-hand panel, $\varepsilon_{\varepsilon_1''}$ in the central panel, and $\mathcal{K}^{(3)}$ in the right-hand panel. The circles have the same signification as in the previous figure.

This figure shows that $|\varepsilon_{\varepsilon_1''}| \approx |\delta_{\varepsilon_0}|$.

Fig. 13 concerns the effect of variable uncertainty of the nuisance parameter $G = G_2 = A$.

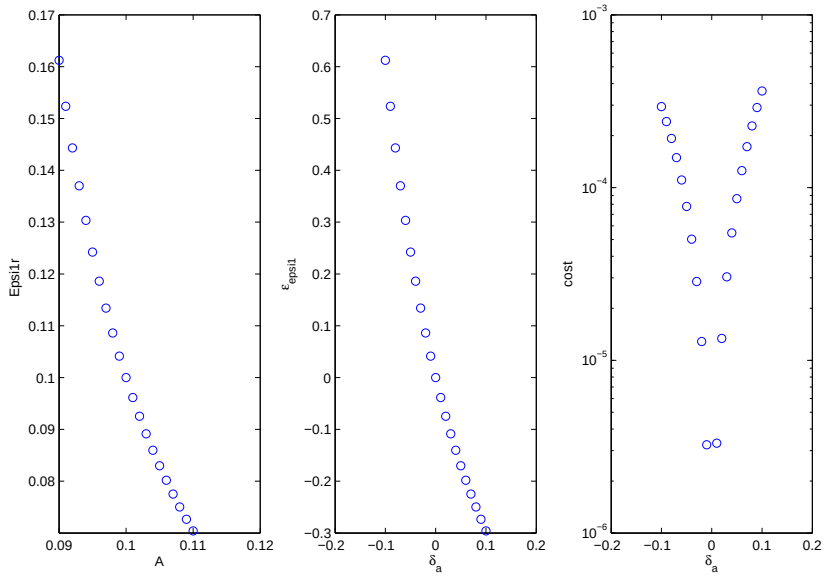

Figure 13: The abscissas in the left-hand panel represent A. The abscissas in the central and right-hand panels represent δ_a. The ordinates represent the retrieved $\mathcal{E}_1''$ in the left-hand panel, $\varepsilon_{\varepsilon_1''}$ in the central panel, and $\mathcal{K}^{(3)}$ in the right-hand panel. The circles have the same signification as in the previous figure.

This figure shows that, at $A = .09$ and $.11$, the retrieval error is of the same order as the nuisance parameter uncertainty since $|\varepsilon_{\varepsilon_1''}| \gtrsim |\delta_a|$, but with the manifestation of an instability in the neighborhood of $\delta_a = -0.1$.

Fig. 14 concerns the effect of variable uncertainty of the nuisance parameter $G = G_4 = \mathcal{E}^i$.

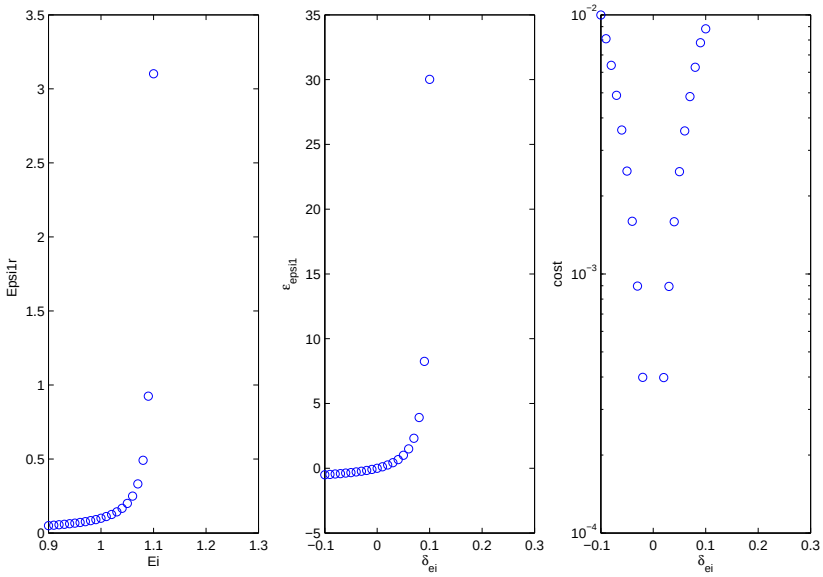

Figure 14: The abscissas in the left-hand panel represent E^i. The abscissas in the central and right-hand panels represent δ_{e^i}. The ordinates represent the retrieved $\mathcal{E}_1''$ in the left-hand panel, $\varepsilon_{\varepsilon_1''}$ in the central panel, and $\mathcal{K}^{(3)}$ in the right-hand panel. The circles have the same signification as in the previous figure.

This figure shows that, at $E^i = .9$, the retrieval error is of the same order as the nuisance parameter uncertainty since $|\varepsilon_{\varepsilon_1''}| \gtrsim |\delta_{e^i}|$, whereas, at $E^i = 1.1$, the retrieval error far exceeds the nuisance parameter uncertainty since $|\varepsilon_{\varepsilon_1''}| >> |\delta_{e^i}| = .1$, this being a manifestation of severe instability in the neighborhood of $\delta_{e^i} = .1$.

Fig. 15 concerns the effect of variable uncertainty of the nuisance parameter $G = G_1 = \Theta^i$.

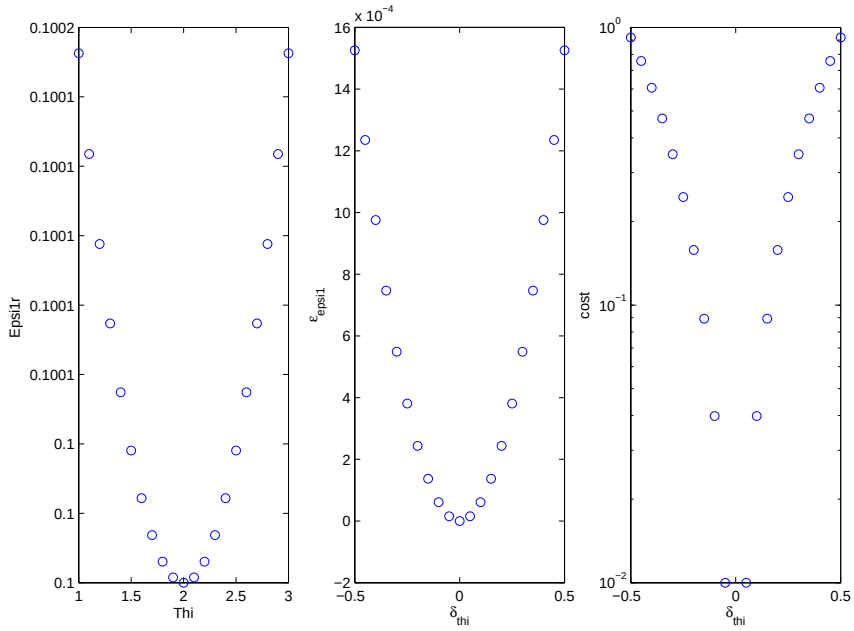

Figure 15: The abscissas in the left-hand panel represent Θ^i. The abscissas in the central and right-hand panels represent δ_{θ^i}. The ordinates represent the retrieved $\mathcal{E}_1''$ in the left-hand panel, $\varepsilon_{\varepsilon_1''}$ in the central panel, and $\mathcal{K}^{(3)}$ in the right-hand panel. The circles have the same signification as in the previous figure.

This figure shows that the retrieval error is quite small with respect to Θ^i uncertainty since $\varepsilon_{\varepsilon_1''} \leq 1.53 \times 10^{-3}$ over the whole Θ^i interval $[1°, 3°]$.

Fig. 16 concerns the effect of variable uncertainty of the nuisance parameter $G = G_5 = B$.

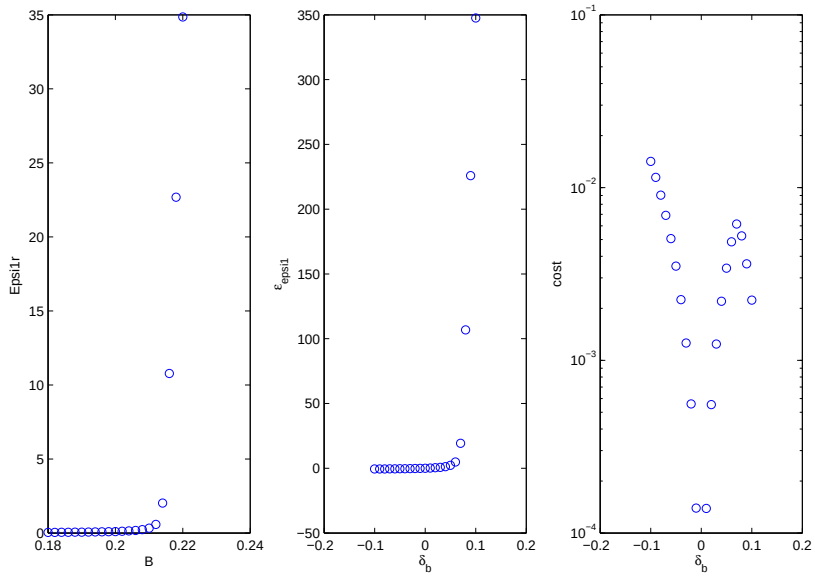

Figure 16: The abscissas in the left-hand panel represent B. The abscissas in the central and right-hand panels represent δ_b. The ordinates represent the retrieved $\mathcal{E}_1''$ in the left-hand panel, $\varepsilon_{\varepsilon_1''}$ in the central panel, and $\mathcal{K}^{(3)}$ in the right-hand panel. The circles have the same signification as in the previous figure.

This figure shows that, at $B = .18$, the retrieval error is of the same order as the nuisance parameter uncertainty since $|\varepsilon_{\varepsilon_1''}| \gtrsim |\delta_b|$, whereas, at $B = .22$, the retrieval error far exceeds the nuisance parameter uncertainty since $|\varepsilon_{\varepsilon_1''}| >> |\delta_b| = .1$, this being a manifestation of severe nuisance parameter uncertainty-induced instability in the neighborhood of $\delta_b = 0.1$.

7.4 Retrieval of $\mathcal{E}_1'$: Variable uncertainty of one nuisance parameter, fixed uncertainty of another nuisance parameter, all other nuisance parameters are certain

Figs. 17, 18 concern the effect of variable uncertainty of the nuisance parameter $G = G_1 = \mathcal{E}_0$ when E^i is -10% and $+10\%$ uncertain respectively. These two figures should be compared to fig. 6 relative to the case when E^i is certain.

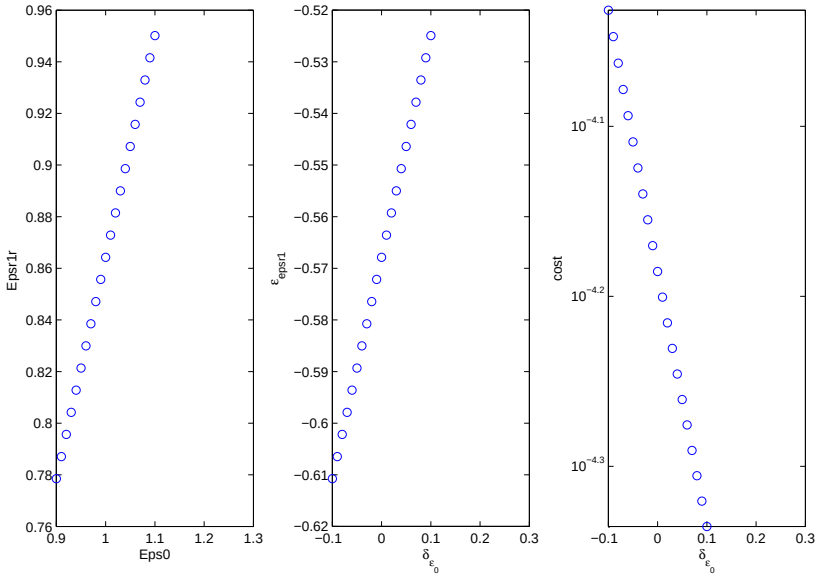

Figure 17: $E^i = .9$ ($\delta_{e^i} = -.1$). The abscissas in the left-hand panel represent $\mathcal{E}_0$. The abscissas in the central and right-hand panels represent δ_{ε_0}. The ordinates represent the retrieved $\mathcal{E}_1'$ in the left-hand panel, $\varepsilon_{\varepsilon_1'}$ in the central panel, and $\mathcal{K}^{(3)}$ in the right-hand panel. circles refer to the retrieval obtained by resolution of the quartic equation via the mathlab function *roots*.

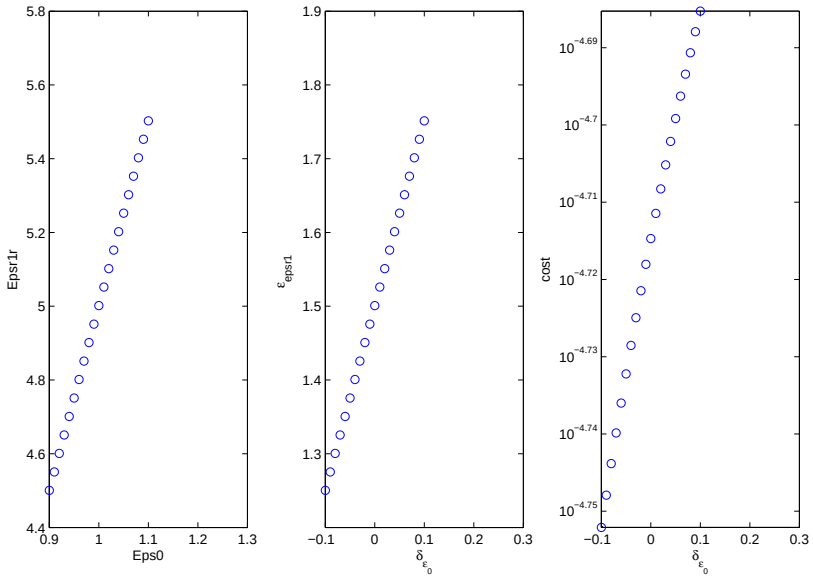

Figure 18: $E^i = 1.1$ ($\delta_{e^i} = .1$). The abscissas in the left-hand panel represent $\mathcal{E}_0$. The abscissas in the central and right-hand panels represent δ_{ε_0}. The ordinates represent the retrieved $\mathcal{E}'_1$ in the left-hand panel, $\varepsilon_{\varepsilon'_1}$ in the central panel, and $\mathcal{K}^{(3)}$ in the right-hand panel. The circles have the same signification as in the previous figure.

These figures show that $|\varepsilon_{\varepsilon'_1}| >> |\delta_{e^i}| = .1$ over the whole range $\delta_{\varepsilon_0} \in [-.1, .1]$.

Figs. 19, 20 concern the effect of variable uncertainty of the nuisance parameter $G = G_4 = \Theta^i$ when B is -10% and $+10\%$ uncertain respectively. These two figures should be compared to fig. 9 relative to the case when B is certain.

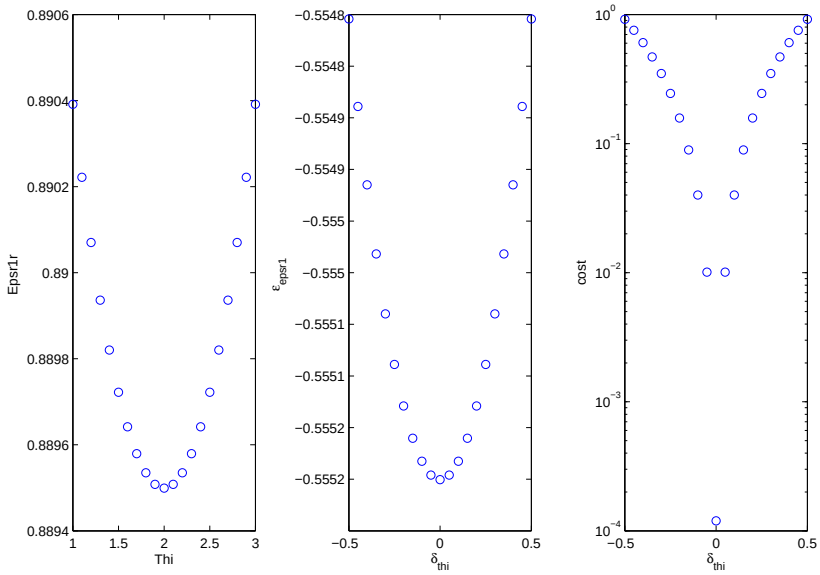

Figure 19: $B = .18$ ($\delta_b = -.1$). The abscissas in the left-hand panel represent Θ^i. The abscissas in the central and right-hand panels represent δ_{θ^i}. The ordinates represent the retrieved $\mathcal{E}'_1$ in the left-hand panel, $\varepsilon_{\varepsilon'_1}$ in the central panel, and $\mathcal{K}^{(3)}$ in the right-hand panel. The circles refer to the retrieval obtained by resolution of the quartic equation via the mathlab function *roots*.

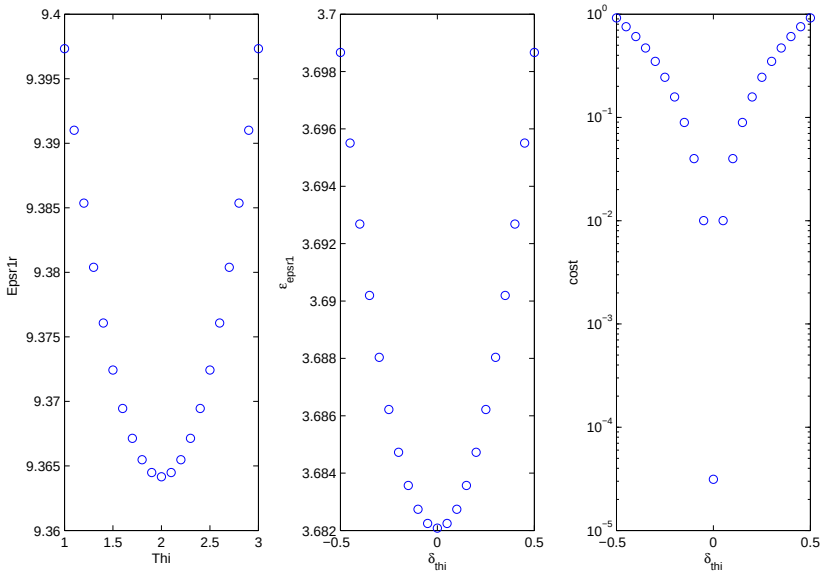

Figure 20: $B = .22$ ($\delta_b = .1$). The abscissas in the left-hand panel represent Θ^i. The abscissas in the central and right-hand panels represent δ_{θ^i}. The ordinates represent the retrieved $\mathcal{E}_1'$ in the left-hand panel, $\varepsilon_{\varepsilon_1'}$ in the central panel, and $\mathcal{K}^{(3)}$ in the right-hand panel. The circles have the same signification as in the previous figure.

These figures show that: 1) $|\varepsilon_{\varepsilon_1'}| >> |\delta_b| = .1$ over the whole range $\Theta^i \in [1°, 3°]$ and 2) $|\varepsilon_{\varepsilon_1'}|$ is much larger for $\delta_b = .1$ than for $\delta_b = -.1$.

Figs. 21, 22 concern the effect of variable uncertainty of the nuisance parameter $G = G_2 = A$ when $\mathcal{E}_0$ is $\pm 10\%$ uncertain. These two figures should be compared to fig. 7 relative to the case when $\mathcal{E}_0$ is certain.

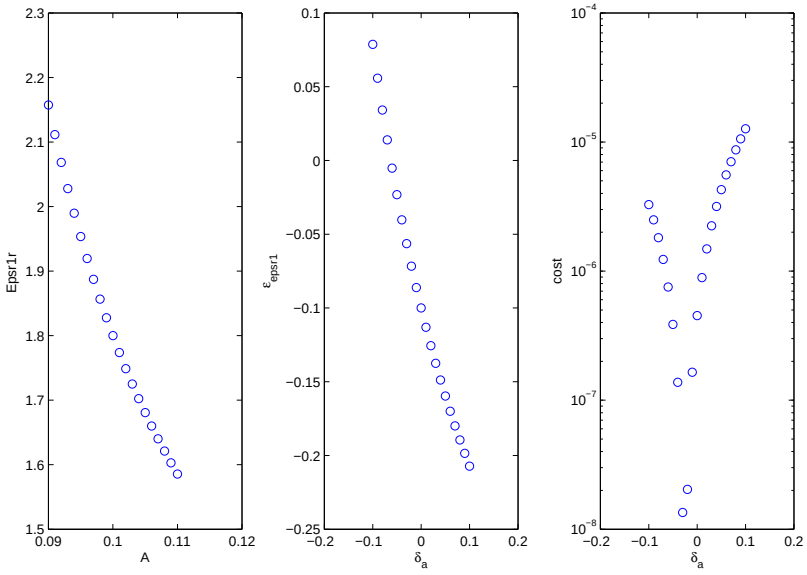

Figure 21: $\mathcal{E}_0 = .9$ ($\delta_{\varepsilon_0} = -.1$). The abscissas in the left-hand panel represent A. The abscissas in the central and right-hand panels represent δ_a. The ordinates represent the retrieved $\mathcal{E}_1'$ in the left-hand panel, $\varepsilon_{\varepsilon_1'}$ in the central panel, and $\mathcal{K}^{(3)}$ in the right-hand panel. The circles refer to the retrieval obtained by resolution of the quartic equation via the mathlab function *roots*.

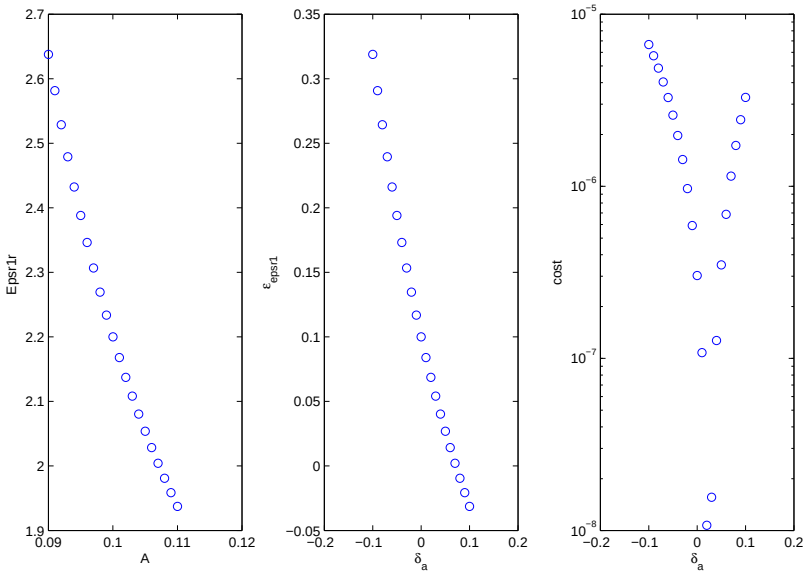

Figure 22: $\mathcal{E}_0 = 1.1$ ($\delta_{\varepsilon_0} = .1$). The abscissas in the left-hand panel represent A. The abscissas in the central and right-hand panels represent δ_a. The ordinates represent the retrieved $\mathcal{E}_1'$ in the left-hand panel, $\varepsilon_{\varepsilon_1'}$ in the central panel, and $\mathcal{K}^{(3)}$ in the right-hand panel. The circles have the same signification as in the previous figure.

These figures show that $|\varepsilon_{\varepsilon_1'}| > .2$, in the neighborhoods: $\delta_a = .1$ when $\delta_{\varepsilon_0} = -.1$, and $\delta_a = -.1$ when $\delta_{\varepsilon_0} = .1$.

Figs. 23, 24 concern the effect of variable uncertainty of the nuisance parameter $G = G_3 = E^i$ when A is $\pm 10\%$ uncertain. These two figures should be compared to fig. 8 relative to the case when A is certain.

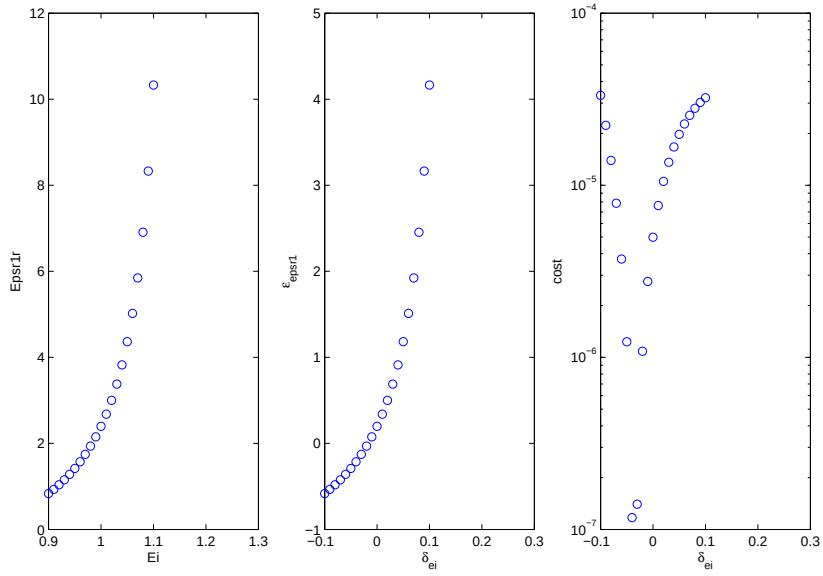

Figure 23: $A = .09$ ($\delta_a = -.1$). The abscissas in the left-hand panel represent E^i. The abscissas in the central and right-hand panels represent δ_{e^i}. The ordinates represent the retrieved $\mathcal{E}_1'$ in the left-hand panel, $\varepsilon_{\varepsilon_1'}$ in the central panel, and $\mathcal{K}^{(3)}$ in the right-hand panel. The circles refer to the retrieval obtained by resolution of the quartic equation via the mathlab function *roots*.

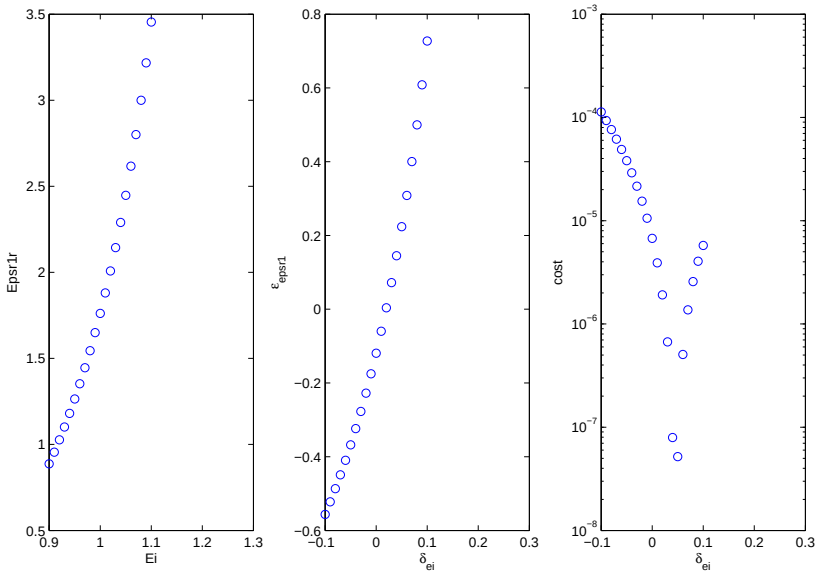

Figure 24: $A = .11$ ($\delta_a = .1$). The abscissas in the left-hand panel represent E^i. The abscissas in the central and right-hand panels represent δ_{e^i}. The ordinates represent the retrieved $\mathcal{E}'_1$ in the left-hand panel, $\varepsilon_{\mathcal{E}'_1}$ in the central panel, and $\mathcal{K}^{(3)}$ in the right-hand panel. The circles have the same signification as in the previous figure.

The retrieval errors in these figures are seen to be very large since: $|\varepsilon_{\mathcal{E}'_1}| > 4$ in the neighborhood $\delta_{e^i} = .1$ when $\delta_a = -.1$ and $|\varepsilon_{\mathcal{E}'_1}| > .5$ in the neighborhoods $\delta_{e^i} = \pm.1$ when $\delta_a = .1$.

Figs. 25, 26 concern the effect of variable uncertainty of the nuisance parameter $G = G_5 = B$ when E^i is -10% and $+10\%$ uncertain respectively. These two figures should be compared to fig. 10 relative to the case when E^i is certain.

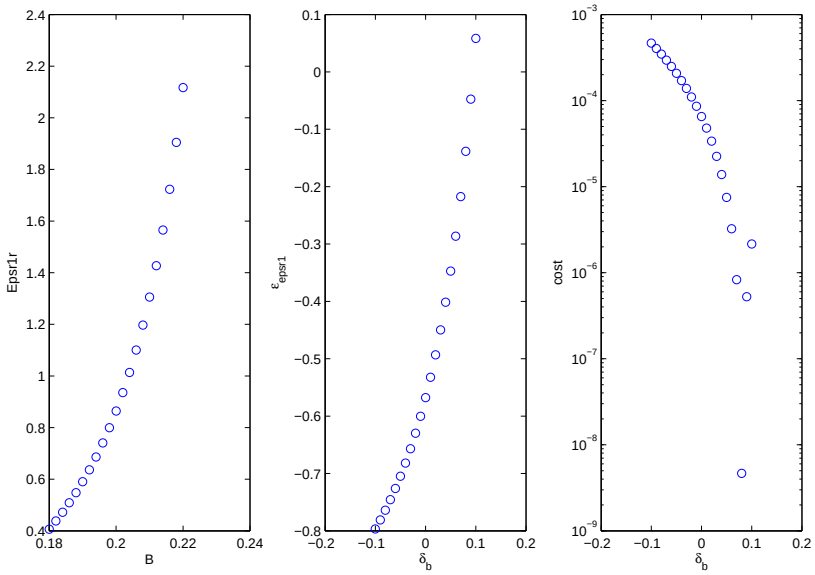

Figure 25: $E^i = .9$ ($\delta_{e^i} = -.1$). The abscissas in the left-hand panel represent B. The abscissas in the central and right-hand panels represent δ_b. The ordinates represent the retrieved $\mathcal{E}'_1$ in the left-hand panel, $\varepsilon_{\varepsilon'_1}$ in the central panel, and $\mathcal{K}^{(3)}$ in the right-hand panel. The circles refer to the retrieval obtained by resolution of the quartic equation via the mathlab function *roots*.

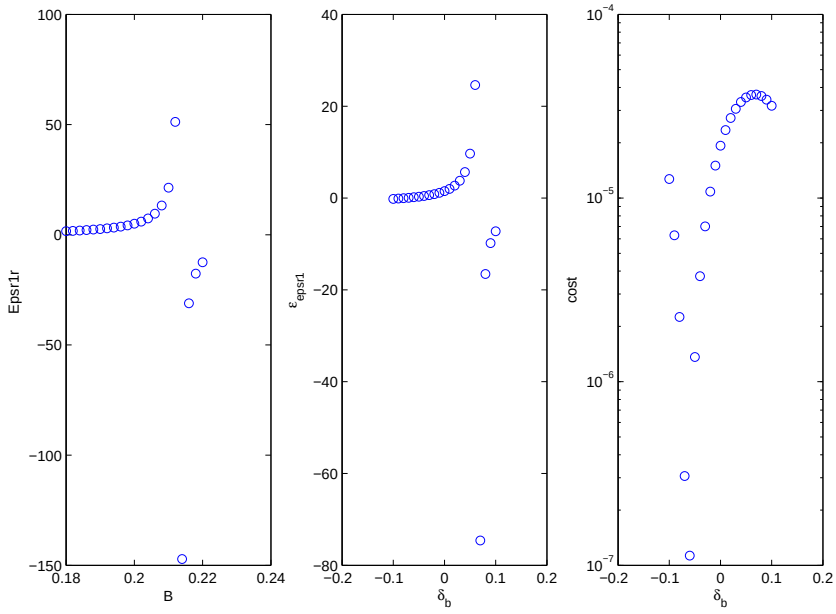

Figure 26: $E^i = 1.1$ ($\delta_{e^i} = .1$). The abscissas in the left-hand panel represent B. The abscissas in the central and right-hand panels represent δ_b. The ordinates represent the retrieved $\mathcal{E}_1'$ in the left-hand panel, $\varepsilon_{\varepsilon_1'}$ in the central panel, and $\mathcal{K}^{(3)}$ in the right-hand panel. The circles have the same signification as in the previous figure. Note that some negative solutions for $\mathcal{E}_1'$ have been shown in this figure even though they are not physical in order to illustrate more completely the nature of the nuisance parameter uncertainty-induced retrieval instability.

The retrieval errors in these figures are seen to be very large since: $|\varepsilon_{\varepsilon_1'}| > 7$ in the neighborhood $\delta_b = -.1$ when $\delta_{e^i} = -.1$ and $|\varepsilon_{\varepsilon_1'}| > 25$ in the neighborhoods $\delta_b = .05$ when $\delta_{e^i} = .1$.

Figs. 27 and 28 concern the effect of variable uncertainty of the nuisance parameter $G = G_5 = \mathcal{E}_1''$ when B is -10% and $+10\%$ uncertain respectively. These two figures should be compared to fig. 5 relative to the case when B is certain.

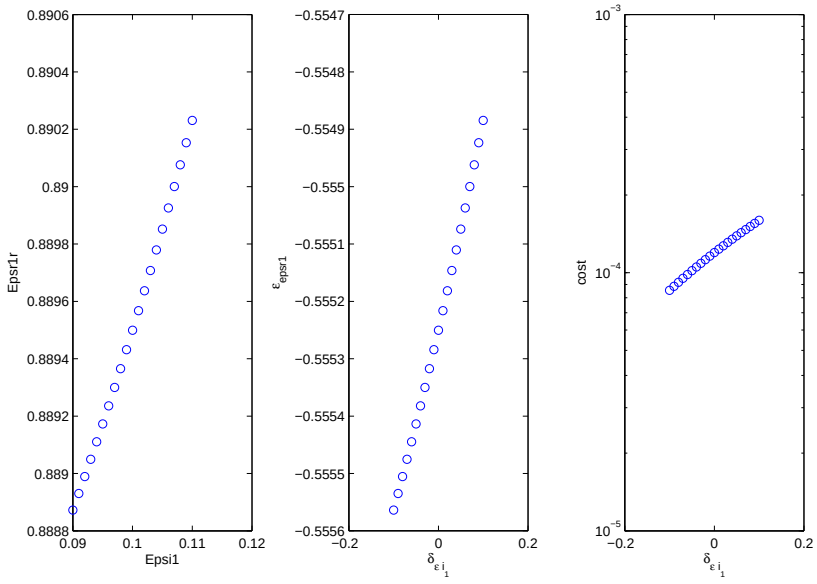

Figure 27: $B = .18$ ($\delta_b = -.1$). The abscissas in the left-hand panel represent $\mathcal{E}_1''$. The abscissas in the central and right-hand panels represent $\delta_{\mathcal{E}_1''}$. The ordinates represent the retrieved $\mathcal{E}_1'$ in the left-hand panel, $\varepsilon_{\mathcal{E}_1'}$ in the central panel, and $\mathcal{K}^{(3)}$ in the right-hand panel. The circles refer to the retrieval obtained by resolution of the quartic equation via the mathlab function *roots*.

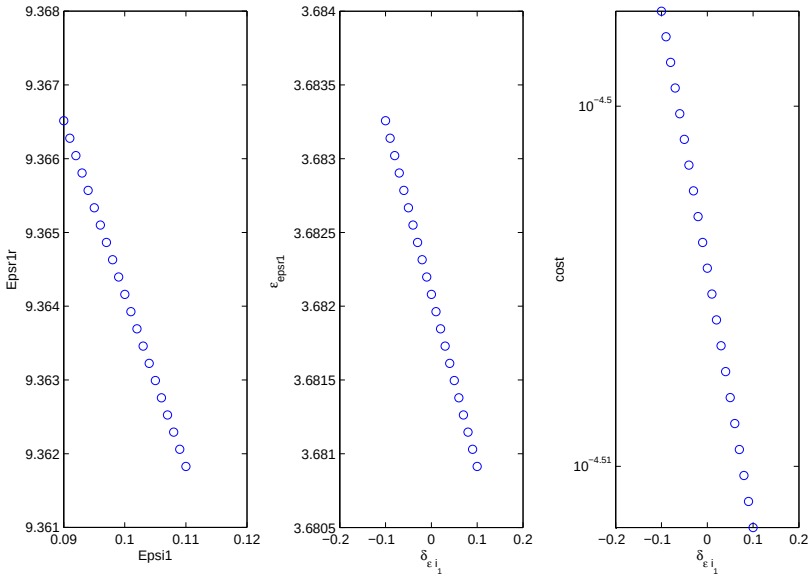

Figure 28: $B = .22$ ($\delta_b = .1$). The abscissas in the left-hand panel represent $\mathcal{E}_1''$. The abscissas in the central and right-hand panels represent $\delta_{\varepsilon_1''}$. The ordinates represent the retrieved $\mathcal{E}_1'$ in the left-hand panel, $\varepsilon_{\varepsilon_1'}$ in the central panel, and $\mathcal{K}^{(3)}$ in the right-hand panel. The circles have the same signification as in the previous figure.

The retrieval errors in these figures are seen to be large to very large since: $|\varepsilon_{\varepsilon_1'}| > .55$ when $\delta_b = -.1$ and $|\varepsilon_{\varepsilon_1'}| > 3.68$ when $\delta_b = .1$.

7.5 Retrieval of $\mathcal{E}_1''$: Variable uncertainty of one nuisance parameter, fixed uncertainty of another nuisance parameter, all other nuisance parameters are certain

Figs. 29, 30 concern the effect of variable uncertainty of the nuisance parameter $G = G_1 = \mathcal{E}_0$ when E^i is -10% and $+10\%$ uncertain respectively. These two figures should be compared to fig. 12 relative to the case when E^i is certain.

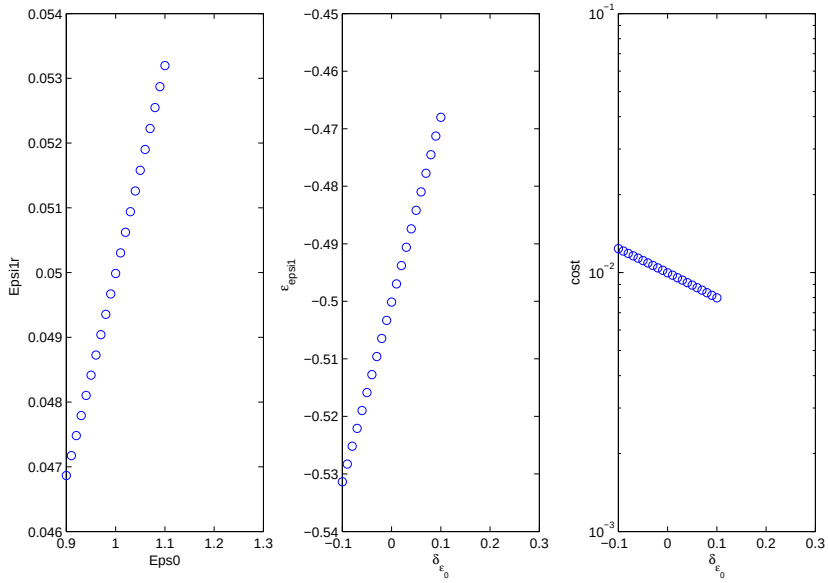

Figure 29: $E^i = .9$ ($\delta_{e^i} = -.1$). The abscissas in the left-hand panel represent $\mathcal{E}_0$. The abscissas in the central and right-hand panels represent δ_{ε_0}. The ordinates represent the retrieved $\mathcal{E}_1''$ in the left-hand panel, $\varepsilon_{\varepsilon_1''}$ in the central panel, and $\mathcal{K}^{(3)}$ in the right-hand panel. The circles refer to the retrieval obtained by resolution of the quartic equation via the mathlab function *roots*.

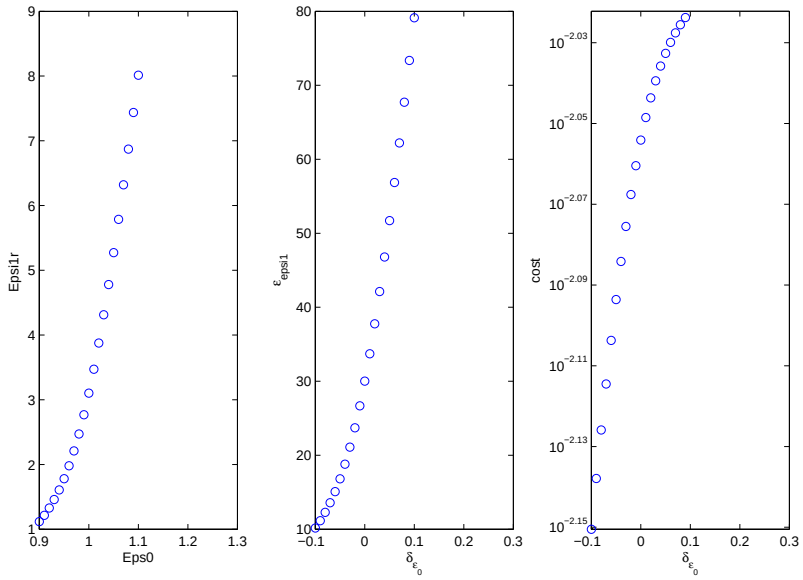

Figure 30: $E^i = 1.1$ ($\delta_{e^i} = .1$). The abscissas in the left-hand panel represent $\mathcal{E}_0$. The abscissas in the central and right-hand panels represent δ_{ε_0}. The ordinates represent the retrieved $\mathcal{E}_1''$ in the left-hand panel, $\varepsilon_{\varepsilon_1''}$ in the central panel, and $\mathcal{K}^{(3)}$ in the right-hand panel. The circles have the same signification as in the previous figure.

These figures show that: 1) $|\varepsilon_{\varepsilon_1''}| >> |\delta_{e^i}| = .1$ over the whole range $\delta_{\varepsilon_0} \in [-.1, .1]$ and 2) $|\varepsilon_{\varepsilon_1''}|$ is much larger for $\delta_{e^i} = .1$ than for $\delta_{e^i} = -.1$.

Figs. 31, 32 concern the effect of variable uncertainty of the nuisance parameter $G = G_4 = \Theta^i$ when B is -10% and $+10\%$ uncertain respectively. These two figures should be compared to fig. 15 relative to the case when B is certain.

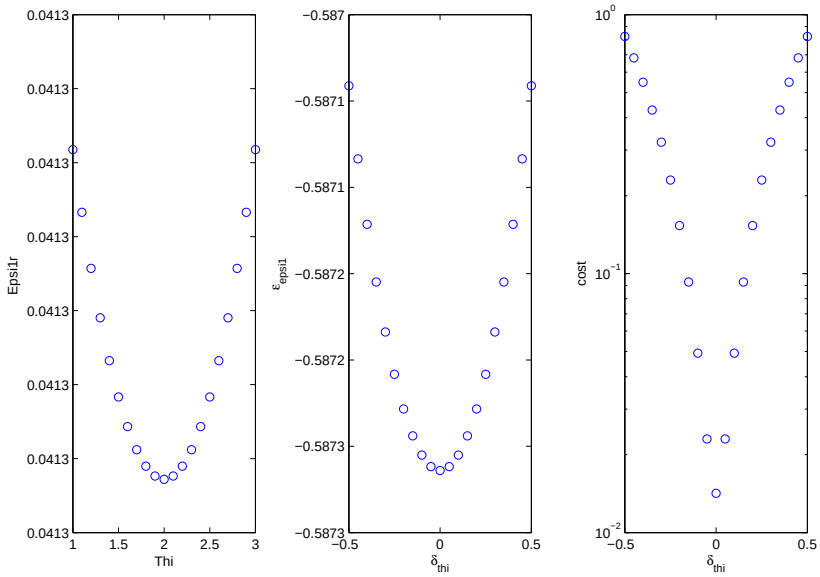

Figure 31: $B = .18$ ($\delta_b = -.1$). The abscissas in the left-hand panel represent Θ^i. The abscissas in the central and right-hand panels represent δ_{θ^i}. The ordinates represent the retrieved $\mathcal{E}_1''$ in the left-hand panel, $\varepsilon_{\varepsilon_1''}$ in the central panel, and $\mathcal{K}^{(3)}$ in the right-hand panel. The circles refer to the retrieval obtained by resolution of the quartic equation via the mathlab function *roots*.

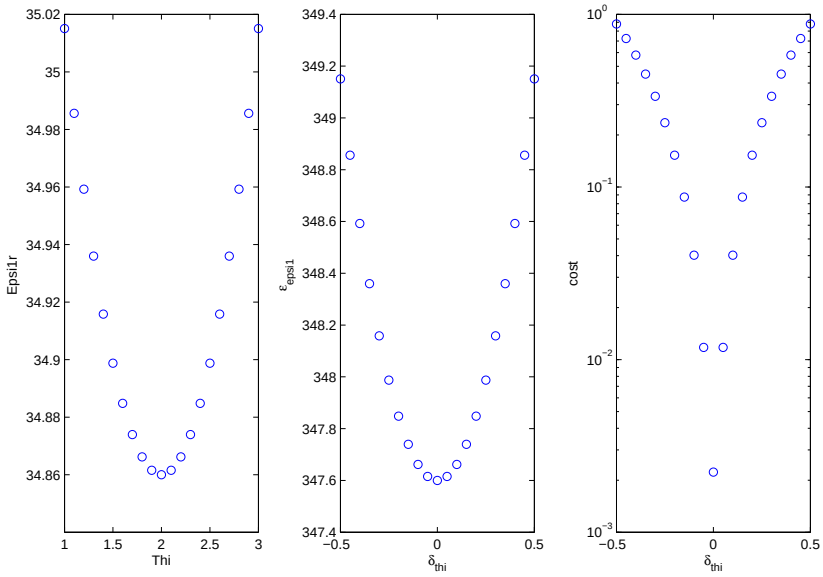

Figure 32: $B = .22$ ($\delta_b = .1$). The abscissas in the left-hand panel represent Θ^i. The abscissas in the central and right-hand panels represent δ_{θ^i}. The ordinates represent the retrieved $\mathcal{E}_1''$ in the left-hand panel, $\varepsilon_{\varepsilon_1''}$ in the central panel, and $\mathcal{K}^{(3)}$ in the right-hand panel. The circles have the same signification as in the previous figure.

These figures show that: 1) $|\varepsilon_{\varepsilon_1''}| >> |\delta_b| = .1$ over the whole range $\Theta^i \in [1°, 3°]$ and 2) $|\varepsilon_{\varepsilon_1''}|$ is much larger for $\delta_b = .1$ than for $\delta_b = -.1$, the large value of $|\varepsilon_{\varepsilon_1''}|$ being essentially due to the instability in the neighborhood of $\delta_b = .1$.

Figs. 33, 34 concern the effect of variable uncertainty of the nuisance parameter $G = G_2 = A$ when $\mathcal{E}_0$ is $\pm 10\%$ uncertain. These two figures should be compared to fig. 13 relative to the case when $\mathcal{E}_0$ is certain.

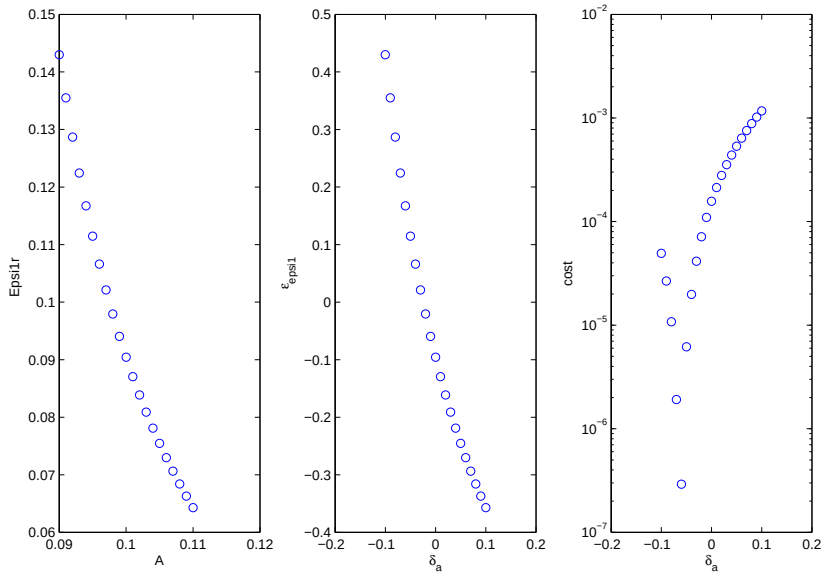

Figure 33: $\mathcal{E}_0 = .9$ ($\delta_{\varepsilon_0} = -.1$). The abscissas in the left-hand panel represent A. The abscissas in the central and right-hand panels represent δ_a. The ordinates represent the retrieved $\mathcal{E}_1''$ in the left-hand panel, $\varepsilon_{\varepsilon_1''}$ in the central panel, and $\mathcal{K}^{(3)}$ in the right-hand panel. The circles refer to the retrieval obtained by resolution of the quartic equation via the mathlab function *roots*.

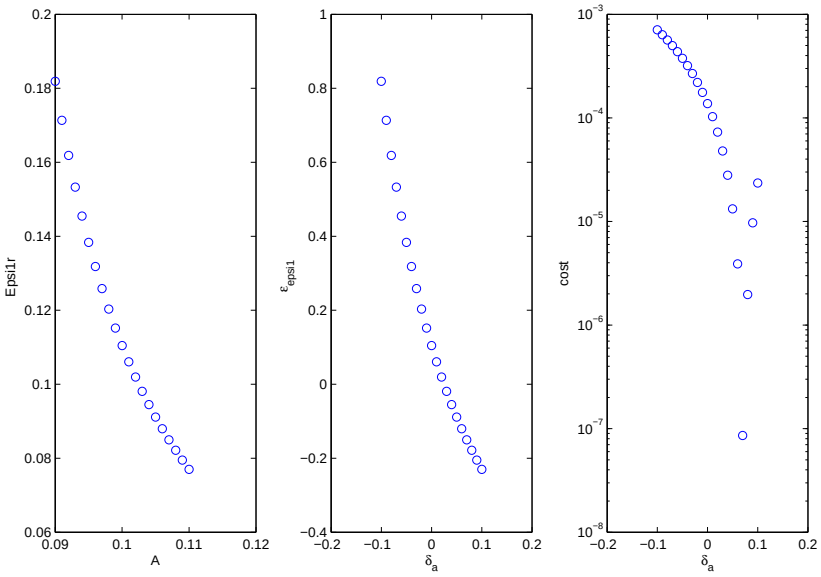

Figure 34: $\mathcal{E}_0 = 1.1$ ($\delta_{\varepsilon_0} = .1$). The abscissas in the left-hand panel represent A. The abscissas in the central and right-hand panels represent δ_a. The ordinates represent the retrieved $\mathcal{E}_1''$ in the left-hand panel, $\varepsilon_{\varepsilon_1''}$ in the central panel, and $\mathcal{K}^{(3)}$ in the right-hand panel. The circles have the same signification as in the previous figure.

These figures show that $|\varepsilon_{\varepsilon_1''}| > .2$, in the neighborhoods: $\delta_a = \pm.1$ when $\delta_{\varepsilon_0} = -.1$, and $\delta_a = \pm.1$ when $\delta_{\varepsilon_0} = .1$.

Figs. 35, 36 concern the effect of variable uncertainty of the nuisance parameter $G = G_3 = E^i$ when A is $\pm 10\%$ uncertain. These two figures should be compared to fig. 14 relative to the case when A is certain.

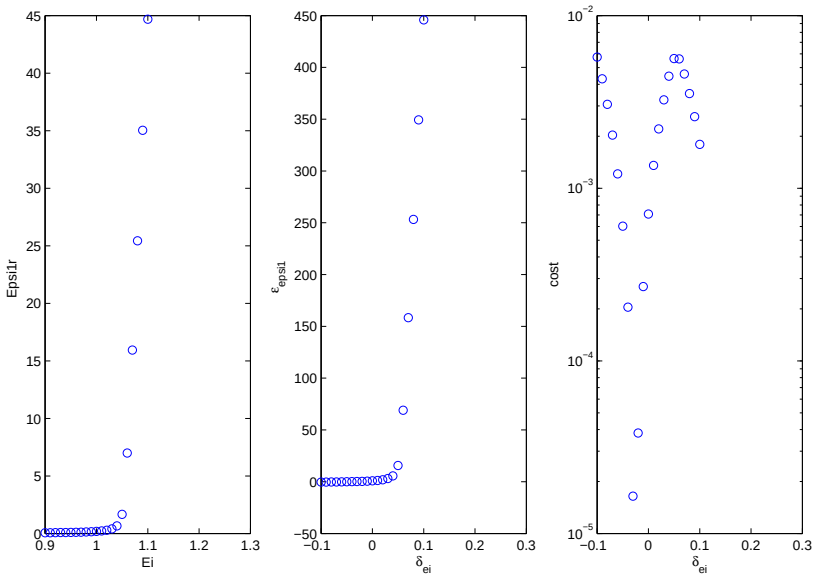

Figure 35: $A = .09$ ($\delta_a = -.1$). The abscissas in the left-hand panel represent E^i. The abscissas in the central and right-hand panels represent δ_{e^i}. The ordinates represent the retrieved $\mathcal{E}_1''$ in the left-hand panel, $\varepsilon_{\varepsilon_1''}$ in the central panel, and $\mathcal{K}^{(3)}$ in the right-hand panel. The circles refer to the retrieval obtained by resolution of the quartic equation via the mathlab function *roots*.

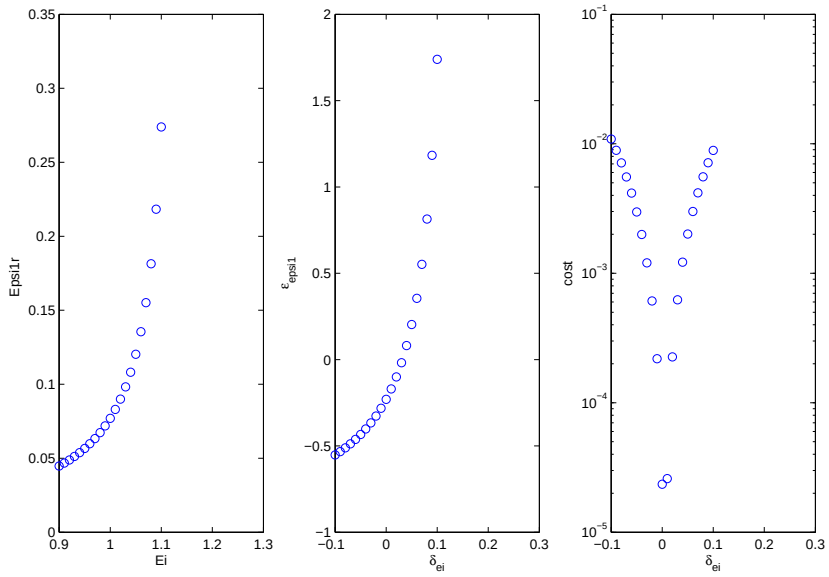

Figure 36: $A = .11$ ($\delta_a = .1$). The abscissas in the left-hand panel represent E^i. The abscissas in the central and right-hand panels represent δ_{e^i}. The ordinates represent the retrieved $\mathcal{E}_1''$ in the left-hand panel, $\varepsilon_{\varepsilon_1''}$ in the central panel, and $\mathcal{K}^{(3)}$ in the right-hand panel. The circles have the same signification as in the previous figure.

The retrieval errors in these figures are seen to be very large even for relatively-small δ_{e^i} since: $\varepsilon_{\varepsilon_1''}$ diverges in the neighborhood $\delta_{e^i} = 0.05$ when $\delta_a = -.1$ and $\varepsilon_{\varepsilon_1''}|$ diverges in the neighborhood of $\delta_{e^i} = .1$ when $\delta_a = .1$. The very sharp uprise of the left-hand and central curves of figs. 35 and 36 translates the instabilities induced by the combined uncertainties of A and E^i.

Figs. 37, 38 concern the effect of variable uncertainty of the nuisance parameter $G = G_5 = B$ when E^i is -10% and $+10\%$ uncertain respectively. These two figures should be compared to fig. 16 relative to the case when E^i is certain.

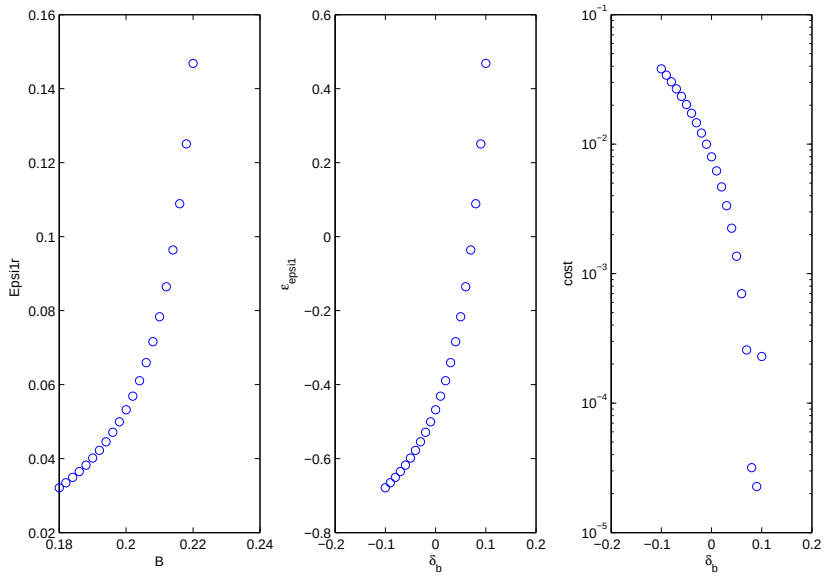

Figure 37: $E^i = .9$ ($\delta_{e^i} = -.1$). The abscissas in the left-hand panel represent B. The abscissas in the central and right-hand panels represent δ_b. The ordinates represent the retrieved $\mathcal{E}_1''$ in the left-hand panel, $\varepsilon_{\varepsilon_1''}$ in the central panel, and $\mathcal{K}^{(3)}$ in the right-hand panel. The circles refer to the retrieval obtained by resolution of the quartic equation via the mathlab function *roots*.

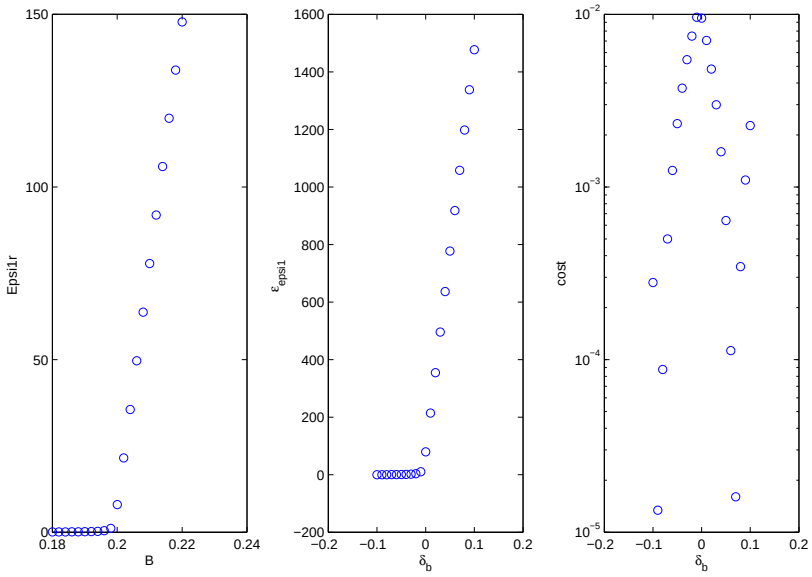

Figure 38: $E^i = 1.1$ ($\delta_{e^i} = .1$). The abscissas in the left-hand panel represent B. The abscissas in the central and right-hand panels represent δ_b. The ordinates represent the retrieved $\mathcal{E}_1''$ in the left-hand panel, $\varepsilon_{\varepsilon_1''}$ in the central panel, and $\mathcal{K}^{(3)}$ in the right-hand panel. The circles have the same signification as in the previous figure.

The retrieval errors in these figures are seen to be large since: $|\varepsilon_{\varepsilon_1''}| > 0.5$ in the neighborhood of $\delta_b = \pm.1$ when $\delta_{e^i} = -.1$ and $|\varepsilon_{\varepsilon_1''}| > 1400$ in the neighborhood of $\delta_b = .1$ when $\delta_{e^i} = .1$.

Figs. 39, 40 concern the effect of variable uncertainty of the nuisance parameter $G = G_5 = \mathcal{E}_1'$ when B is -10% and $+10\%$ uncertain respectively. These two figures should be compared to fig. 11 relative to the case when B is certain.

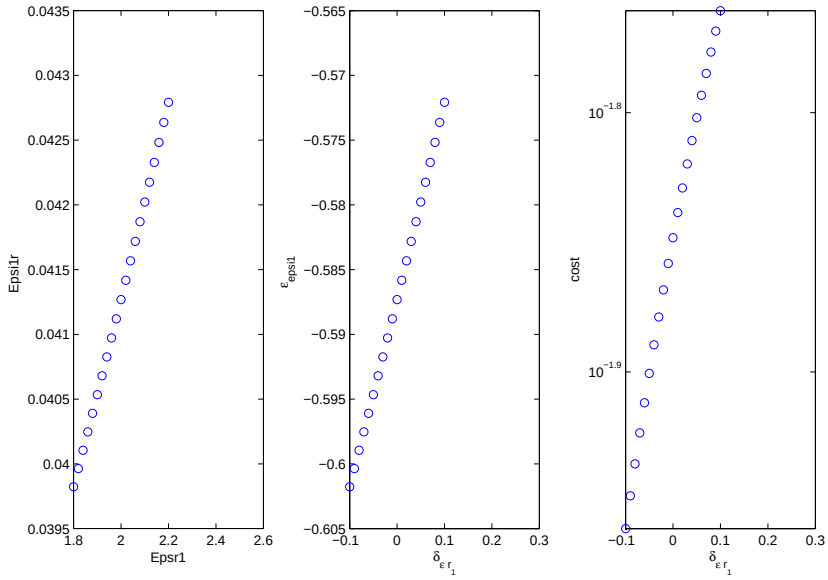

Figure 39: $B = .18$ ($\delta_b = -.1$). The abscissas in the left-hand panel represent $\mathcal{E}_1'$. The abscissas in the central and right-hand panels represent $\delta_{\varepsilon_1'}$. The ordinates represent the retrieved $\mathcal{E}_1''$ in the left-hand panel, $\varepsilon_{\varepsilon_1''}$ in the central panel, and $\mathcal{K}^{(3)}$ in the right-hand panel. The circles refer to the retrieval obtained by resolution of the quartic equation via the mathlab function *roots*.

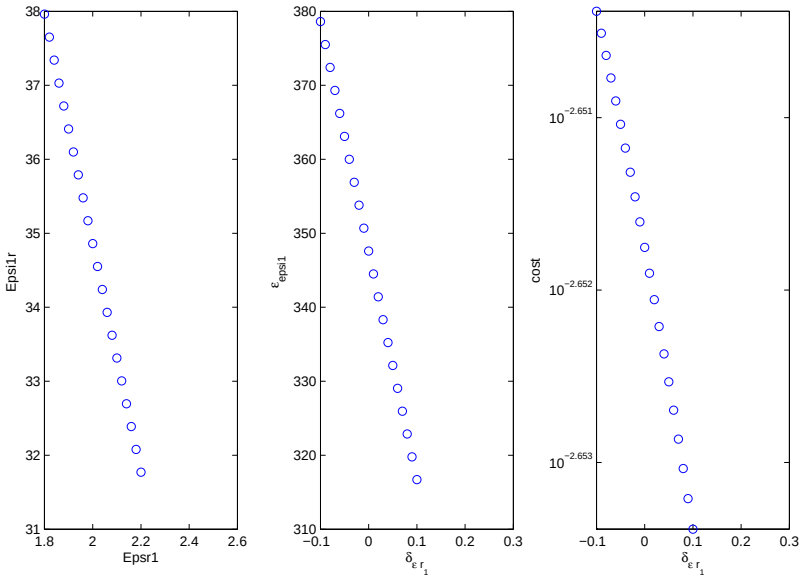

Figure 40: $B = .22$ ($\delta_b = .1$). The abscissas in the left-hand panel represent $\mathcal{E}'_1$. The abscissas in the central and right-hand panels represent $\delta_{\varepsilon'_1}$. The ordinates represent the retrieved $\mathcal{E}''_1$ in the left-hand panel, $\varepsilon_{\varepsilon''_1}$ in the central panel, and $\mathcal{K}^{(3)}$ in the right-hand panel. The circles have the same signification as in the previous figure.

The retrieval errors in these figures are seen to be large to very large since: $|\varepsilon_{\varepsilon''_1}| > .572$ when $\delta_b = -.1$ and $|\varepsilon_{\varepsilon''_1}| > 315$ when $\delta_b = .1$.

7.6 Table of the influence of uncertainty regarding one nuisance parameter, all other nuisance parameters being certain, on the accuracy of the retrieval of ε_1'

In table 1 we give the numerical values of $\tilde{\mathcal{E}}_1'$ and $\varepsilon_{\varepsilon_1'}$ (obtained by numerical minimization, via the Simplex scheme, of $\mathcal{K}^{(3)}$) in all of the 12 possible cases in which only one nuisance parameter is $\delta = \pm 10\%$ uncertain at a time.

$\delta_{\varepsilon_1''}$	δ_{ε_0}	δ_a	δ_{e^i}	$\Theta^i(^\circ)$	δ_b	$\tilde{\mathcal{E}}_1'$	$\varepsilon_{\varepsilon_1'}$
-.1	0	0	0	2	0	2.000	0.0000
.1	0	0	0	2	0	2.000	0.0000
0	-.1	0	0	2	0	1.800	-0.1000
0	-.1	0	0	2	0	2.200	0.1000
0	0	-.1	0	2	0	2.398	0.1988
0	0	.1	0	2	0	1.761	-0.1193
0	0	0	-.1	2	0	0.864	-0.5679
0	0	0	.1	2	0	5.002	1.5008
0	0	0	0	1	0	2.003	0.0013
0	0	0	0	3	0	2.003	0.0013
0	0	0	0	2	-.1	0.889	-0.5553
0	0	0	0	2	.1	9.364	3.6821

Table 1: Retrieval of ε_1' when one nuisance parameter is $\delta = \pm 10\%$ uncertain (except Θ^i, which when uncertain, deviates from its true value by $\pm 1^\circ$).

This table reveals that in six of these cases, $|\varepsilon_{\varepsilon_1'}| > |\delta|$, and in four of these cases, $|\varepsilon_{\varepsilon_1'}| >> |\delta|$ (due to nuisance parameter uncertainty-induced instability).

7.7 Table of the influence of uncertainty regarding one nuisance parameter, all other nuisance parameters being certain, on the accuracy of the retrieval of ε_1''

In table 2 we give the numerical values of $\tilde{\mathcal{E}}_1''$ and $\varepsilon_{\varepsilon_1''}$ (obtained by numerical minimization, via the Simplex scheme, of $\mathcal{K}^{(3)}$) in all of the 12 possible cases in which only one nuisance parameter is $\delta = \pm 10\%$ uncertain at a time.

$\delta_{\varepsilon_1'}$	δ_{ε_0}	δ_a	δ_{e^i}	$\Theta^i(^\circ)$	δ_b	$\tilde{\mathcal{E}}_1''$	$\varepsilon_{\varepsilon_1''}$
-.1	0	0	0	2	0	0.101	0.0052
.1	0	0	0	2	0	0.100	0.0039
0	-.1	0	0	2	0	0.090	-0.0957
0	-.1	0	0	2	0	0.110	0.1048
0	0	-.1	0	2	0	0.161	0.6122
0	0	.1	0	2	0	0.070	-0.2960
0	0	0	-.1	2	0	0.050	-0.5001
0	0	0	.1	2	0	3.102	30.0165
0	0	0	0	1	0	0.100	0.0016
0	0	0	0	3	0	0.100	0.0016
0	0	0	0	2	-.1	0.041	-0.5873
0	0	0	0	2	.1	34.86	347.60

Table 2: Retrieval of ε_1'' when one nuisance parameter is $\delta = \pm 10\%$ uncertain (except Θ^i, which when uncertain, deviates from its true value by $\pm 1^\circ$).

This table reveals that in eight of these cases, $|\varepsilon_{\varepsilon_1'}| > |\delta|$, and in seven of these cases, $|\varepsilon_{\varepsilon_1'}| >> |\delta|$ (due to nuisance parameter uncertainty-induced instability). The comparison of table 2 with table 1 shows that the pattern of retrieval error of $\mathcal{E}_1''$ is substantially the same as that of $\mathcal{E}_1'$, as predicted in theoretical manner previously.

7.8 Table of the influence of uncertainty regarding five nuisance parameters, the sixth nuisance parameter being certain, on the accuracy of the retrieval of ε_1'

In table 3 we give the numerical values of $\tilde{\mathcal{E}}_1'$ and $\varepsilon_{\varepsilon_1'}$ (obtained by numerical minimization, via the Simplex scheme, of $\mathcal{K}^{(3)}$) in all of the 32 possible cases in which five nuisance parameter are $\delta = \pm 10\%$ uncertain at a time. This table reveals that in sixteen of these cases, $|\varepsilon_{\varepsilon_1'}| > 5|\delta|$, and in eight of these cases, $|\varepsilon_{\varepsilon_1'}| >> |\delta|$ (due to combined nuisance parameter uncertainty-induced instability).

$\delta_{\varepsilon_1''}$	δ_{ε_0}	δ_a	δ_{e^i}	$\Theta^i(^\circ)$	δ_b	$\tilde{\mathcal{E}}_1'$	$\varepsilon_{\varepsilon_1'}$
-.1	-.1	-.1	-.1	2	-.1	0.283	-0.8584
.1	-.1	-.1	-.1	2	-.1	0.286	-0.8570
-.1	.1	-.1	-.1	2	-.1	0.344	-0.8279
.1	.1	-.1	-.1	2	-.1	0.346	-0.8269
-.1	-.1	.1	-.1	2	-.1	0.435	-0.7825
.1	-.1	.1	-.1	2	-.1	0.437	-0.7813
-.1	.1	.1	-.1	2	-.1	0.530	-0.7351
.1	.1	.1	-.1	2	-.1	0.532	-0.7342
-.1	-.1	-.1	.1	2	-.1	1.658	-0.1710
.1	-.1	-.1	.1	2	-.1	1.658	-0.1708
-.1	.1	-.1	.1	2	-.1	2.027	0.0132
.1	.1	-.1	.1	2	-.1	2.027	0.0132
-.1	-.1	.1	.1	2	-.1	1.347	-0.3265
.1	-.1	.1	.1	2	-.1	1.348	-0.3260
-.1	.1	.1	.1	2	-.1	1.646	-0.1772
.1	.1	.1	.1	2	-.1	1.646	-0.1768
-.1	-.1	-.1	-.1	2	.1	2.328	0.1638
.1	-.1	-.1	-.1	2	.1	2.326	0.1632
-.1	.1	-.1	-.1	2	.1	2.846	0.4321
.1	.1	-.1	-.1	2	.1	2.845	0.4224
-.1	-.1	.1	-.1	2	.1	1.658	-0.1710
.1	-.1	.1	-.1	2	.1	1.658	-0.1708
-.1	.1	.1	-.1	2	.1	2.027	0.0132
.1	.1	.1	-.1	2	.1	2.027	0.0132
-.1	-.1	-.1	.1	2	.1	∞	∞
.1	-.1	-.1	.1	2	.1	∞	∞
-.1	.1	-.1	.1	2	.1	∞	∞
.1	.1	-.1	.1	2	.1	∞	∞
-.1	-.1	.1	.1	2	.1	59.61	28.806
.1	-.1	.1	.1	2	.1	59.59	28.794
-.1	.1	.1	.1	2	.1	72.88	35.442
.1	.1	.1	.1	2	.1	72.86	35.430

Table 3: Retrieval of ε_1' when five nuisance parameters (excepting Θ^i) are $\delta = \pm 10\%$ uncertain.

7.9 Table of the influence of uncertainty regarding five nuisance parameters, the sixth nuisance parameter being certain, on the accuracy of the retrieval of ε_1''

In table 4 we give the numerical values of $\tilde{\mathcal{E}}_1''$ and $\varepsilon_{\varepsilon_1''}$ (obtained by numerical minimization, via the Simplex scheme, of $\mathcal{K}^{(3)}$) in all of the 32 possible cases in which five nuisance parameters are $\delta = \pm 10\%$ uncertain at a time.
This table reveals that in 22 of these cases, $|\varepsilon_{\varepsilon_1'}| > 5|\delta|$, and in 12 of these cases, $|\varepsilon_{\varepsilon_1'}| >> |\delta|$ (due to combined nuisance parameter uncertainty-induced instability). The comparison of table 4 with table 3 shows that the pattern of retrieval error of $\mathcal{E}_1''$ is substantially the same as that of $\mathcal{E}_1'$.

$\delta_{\varepsilon_1'}$	δ_{ε_0}	δ_a	δ_{e^i}	$\Theta^i(^\circ)$	δ_b	$\tilde{\mathcal{E}}_1'$	$\varepsilon_{\varepsilon_1'}$
-.1	-.1	-.1	-.1	2	-.1	0.031	-0.6899
.1	-.1	-.1	-.1	2	-.1	0.034	-0.6561
-.1	.1	-.1	-.1	2	-.1	0.035	-0.6532
.1	.1	-.1	-.1	2	-.1	0.038	-0.6210
-.1	-.1	.1	-.1	2	-.1	0.024	-0.7569
.1	-.1	.1	-.1	2	-.1	0.027	-0.7322
-.1	.1	.1	-.1	2	-.1	0.027	-0.7265
.1	.1	.1	-.1	2	-.1	0.030	-0.7030
-.1	-.1	-.1	.1	2	-.1	0.082	-0.1818
.1	-.1	-.1	.1	2	-.1	0.084	-0.1583
-.1	.1	-.1	.1	2	-.1	0.100	0.0034
.1	.1	-.1	.1	2	-.1	0.100	0.0002
-.1	-.1	.1	.1	2	-.1	0.043	-0.5670
.1	-.1	.1	.1	2	-.1	0.046	-0.5448
-.1	.1	.1	.1	2	-.1	0.052	-0.4843
.1	.1	.1	.1	2	-.1	0.053	-0.4707
-.1	-.1	-.1	-.1	2	.1	0.202	1.0169
.1	-.1	-.1	-.1	2	.1	0.194	0.9444
-.1	.1	-.1	-.1	2	.1	0.872	1.7205
.1	.1	-.1	-.1	2	.1	0.247	1.4651
-.1	-.1	.1	-.1	2	.1	0.082	-0.1818
.1	-.1	.1	-.1	2	.1	0.084	-0.1583
-.1	.1	.1	-.1	2	.1	0.100	0.0034
.1	.1	.1	-.1	2	.1	0.100	0.0002
-.1	-.1	-.1	.1	2	.1	154.3	1542.0
.1	-.1	-.1	.1	2	.1	167.4	1673.3
-.1	.1	-.1	.1	2	.1	175.5	1753.5
.1	.1	-.1	.1	2	.1	188.6	1884.9
-.1	-.1	.1	.1	2	.1	89.46	893.60
.1	-.1	.1	.1	2	.1	88.19	880.93
-.1	.1	.1	.1	2	.1	110.6	1105.1
.1	.1	.1	.1	2	.1	109.3	1092.4

Table 4: Retrieval of ε_1'' when five nuisance parameters (exceting Θ^i) are $\delta = \pm 10\%$ uncertain.

8 Conclusion

The inverse problem we set out to solve was the retrieval of one of the seven parameters (either the real (ε_1') or imaginary (ε_1'') part of the permittivity of a cylinder) that enter into a 2D quasistatic electricity configuration. The exact solution of the forward problem was obtained by separation of variables and employed to furnish the data serving as the input to the inverse problem. The retrieval model also relied on the separation of variables solution, but with one of the seven true parameters thereof replaced by a variable ε_1' or ε_1' and the remaining six (called nuisance) parameters by more or less well-known values. We solved the inverse problem in four manners: 1) by mathematically searching for the minimum of the cost functional $\mathcal{K}$ relative to continuous data on a measurement circle, 2) by mathematically searching for the minimum of the cost functional $\mathcal{K}^{(N)}$ relative to discrete data registered at N sensors on the measurement circle, 3) by numerically searching (via the Simplex algorithm) for the minimum of $\mathcal{K}^{(N)}$, 4) by numerically solving the quartic eqution precluding the mathermatical solution. *The first two manners led to exact, mathematically-explicit solutions which lend themselves to a complete mathematical analysis of the way in which the retrieval error varies as a function of the nuisance parameter uncertainties.* The second manner led to the result that $N = 3$ sensors, equispaced over the angular range $[0, 2\pi[$, are necessary and sufficient to provide the required data for the inversion. The second, third and fourth manners led to identical numerical results and the latter were identical to those of the first manner for $N \geq 3$. It was shown, in addition to the existence and uniqueness of the inverse problem solution, that the latter is unstable with respect to uncertainties concerning the nuisance parameters A, E^i and B, acting individually or in combination. These instabilities manifest themselves by extremely-large retrieval error in the neighborhoods of certain values of these nuisance parameters. It was also shown that, even quite far from these neighborhoods, the retrieval error $|\varepsilon_{\varepsilon_1}|$ can be much larger than a generic nuisance parameter uncertainty $|\delta_g|$. Finally, it was found numerically, in agreement with the theory, that the pattern of retrieval error of ε_1'' is much the same as that of ε_1', notably as concerns the instability issue; moreover the relative retrieval error for M uncertain parameters turned out to be roughly proportional to M (outside of the instability regions, and for both the real and imaginary parts of the permittivity).

This investigation underlines the necessity, in parameter-retrieval inverse problems, to take account of nuisance parameter uncertainty in order to evaluate the accuracy of the retrieved parameter(s). In our study, only one parameter was retrieved at a time, while from one to five parameters were uncertain. It may be possible to reduce the global retrieval error by retrieving two or more parameters at a time while considering the remaining parameters to be uncertain, but this issue is out of the scope of the present study.

References

[1] Abbe E., *Neue Apparate zur Bestimmung des Brechungs und Zerstreuungsvermögens fester und flüssiger Körper*. Mauke Verlag, Jena (1874).

[2] Abelès F., *Détermination de l'indice et de l'épaisseur de couches minces*, C.R.Acad.Sci, 228, 553-558 (1949).

[3] Abelès F., *Methods for determining optical parameters of thin films*, in Advanced Optical Techniques, Van Heel A.C.S. (ed.), North Holland, Amsterdam (1967).

[4] Abramowitz M. and Stegun I.S., *Handbook of Mahtematical Functions*, Dover, New York (1968).

[5] Artemev A., Parnovski L. and Polterovich I., *Inverse electrostatic and elasticity problems for checkered distributions*, Inverse Probs., 29, 075010 (2013).

[6] Alessandrini G., *Examples of instability in inverse boundary-value problems*, Inverse Probs, 13, 887-897 (1997).

[7] Banks H.T. and Bihari K.L., *Modelling and estimating uncertainty in parameter estimation*, Inverse Probs., 17, 95-102 (2001).

[8] Banks H.T. and Kunisch K., *Estimation Techniques for Distributed Parameter Systems*, Birkhauser, Boston (1989).

[9] Bauer N., Fajans K. and Lewin S.Z., *Refractometry*, in Physical Methods of Organic Chemistry, Weissberger A. (ed.) Interscience, New York (1960).

[10] Bohren C.F. and Huffman D.R. *Absorption and Scattering of Light by Small Particles*, Wiley, New York (1983).

[11] Buchanan J.L., Gilbert R.P. and Ou M.-J.Y., *Recovery of the parameters of cancellous bone by inversion of effective velocities, and transmission and* reflection coefficients, Inverse Probs., 27, 125006 (2011).

[12] Chen L., Zhenya L., Yang R., Shi X. and Jiawei Zhang J., *Determining the effective electromagnetic parameters of bianisotropic metamaterials with periodic structures*, Progr.Electromagnetics Res. M, 29, 79-93 (2013).

[13] Chen X., Grzegorczyk T.M., Wu B.-I., Pacheco Jr. J. and Kong J.A., *Robust method to retrieve the constitutive effective parameters of metamaterials*, Phys.Rev. E 70, 016608 (2004).

[14] Chylek P., Ramaswamy V., Ashkin A. and Dziedzic J.M. *Simultaneous determination of refractive index and size of spherical dielectric particles from light scattering data*, Appl.Opt., 22, 2302-2307 (1983).

[15] Coleman H.W. and Steele W.G., *Experimentation, Validation, and Uncertainty Analysis for Engineers*, Wiley & Sons, Hoboken (2009).

[16] Devlin J. F., *A simple and powerful method of parameter estimation using simplex optimization*, Ground Water, 32, 323-327 (1994).

[17] Emery A.F., *The effect of correlations and uncertain parameters on the efficiency of estimating and the precision of estimated parameters*, in Inverse Engineering Handbook, Woodbury K.A. (ed.), CRC Press, Boca Raton (2003).

[18] Hadamard, J.S., *Lectures on Cauchy's Problem in Linear Partial Differential Equations*, Oxford University Press, Oxford (1923).

[19] Hasar, U. C., J. J. Barroso, C. Sabah, Y. Kaya, and M. Ertugrul, *Differential uncertainty analysis for evaluating the accuracy of S-parameter retrieval methods for electromagnetic properties of metamaterial slabs*, Opt.Express, 20, 29002-29022 (2012).

[20] Hasar U.C., Barroso J.J., Ertugrul M., Sabah C. and Cavusoglu B., *Application of a useful uncertainty analysis as a metric tool for assessing the performance of electromagnetic properties retrieval methods of bianisotropic metamaterials*, Prog.In Electromagn.Res., 128, 365-380 (2014).

[21] Heubrandtner T., Schnizer B. and Riegler W., *The quasi-static approximation for weakly conducting media and applications*, Proc. 11th Intl. IGTE Symposium on Numerical Field Calculation in Electrical Engineering, TU Graz, Graz, 138-143 (2004).

[22] Hu L., Toyoda K. and Ihara I., *Dielectric properties of edible oils and fatty acids as a function of frequency, temperature, moisture and composition*, J.Food Engrg., 88, 151158 (2008).

[23] Isakov V., *Inverse obstacle problems*, Inverse Probs., 25, 123002 (2009).

[24] Johnson M.L. and Lindsay M. Faunt L.M., *Parameter estimation by least-squares methods*, in Numerical Computer Methods, Brand L. and Johnson M.L. (eds.), Academic, New York (1992).

[25] Lagarias J., Reeds J., Wright M. and Wright P., *Convergence properties of the Nelder-Mead Simplex method in low dimensions*, SIAM J.Optim., 9, 112-147 (1998).

[26] Lee T.S. and Wei-Fang S., *Non-contacting method of determining DC dielectric constant for a thin insulating polymer layer* J.Electrostat., 44, 97-104 (1998).

[27] Lefeuve-Mesgouez G., Mesgouez A., Ogam E., Scotti T. and Wirgin A., *Retrieval of the physical properties of an anelastic solid half space from seismic data*, J.Appl.Geophys., 88, 70-82 (2013).

[28] Mamishev A.V., Takahashi A.R., Du Y., Lesieutre B.C. and Zahn M., *Parameter estimation in dielectrometry measurements*, J.Electrostat., 56, 465-492 (2002).

[29] Morabito F.C. and Coccorese E., *A fuzzy modeling approach for the solution of an inverse electrostatic problem*, IEEE Trans. Magnetics, 32, 1330-1333 (1996).

[30] Morse P.M. and Feshbach H., *Methods of Theoretical Phyics*, Mc Graw-Hill, New York (1953).

[31] Neittaanmaki P., Rudnicki M. and Savini A., *Inverse Problems and Optimal Design in Electricity and Magnetism*, Clarendon Press, Oxford (1996).

[32] Nelder J. A. and Mead R., *A Simplex method for function minimization*, The Comput.J., 7, 308-313 (1965).

[33] Nesvadba P., Houasska M. , Wolf W., Gekas V., Jarvis D. and Sadd P.A., *Database of physical properties of agro-food materials*, J.Food Engrg., 61, 497-503 (2004).

[34] Pluchino A B., Goldberg S.S., Dowling J.N. and Randall C.M., *Refractive-index measurements of single micron-sized carbon particles*, Appl.Opt., 19, 3370-3372 (1980).

[35] Preis K., Biro O., Supancic P. and Ticar I., *Time-domain analysis of quasistatic electric fields in media with frequency- dependent permittivity*, IEEE Trans. Magnetics, 40, 1302-1305 (2004).

[36] Reagan J.A. and Herman B.M. *Light scattering by irregularly shaped particles versus spheres: what are some of the problems presented in remote sensing of atmospheric aerosols?*, in Light Scattering by Irregularly Shaped Particles, Schuerman D.W. (ed.), Plenum, New York (1980).

[37] Sambuelli L., *Uncertainty propagation using some common mixing rules for the modelling and interpretation of electromagnetic data*, Near Surf.Geophys., 7, 285-296 (2009).

[38] Scotti T. and Wirgin A., *Multiparameter identification of a lossy fluid-like object from its transient acoustic response*, Inverse Prob.Sci.Engrg., 22, 1228-1258 (2014).

[39] Sebaa N., Fellah Z.E.A., Fellah M., Ogam E., Mitri F.G., Depollier C. and Lauriks W., *Application of the Biot model to ultrasound in bone: inverse problem*, IEEE Trans.Ultrason.Ferroelec.Freq.Contr., 55, 1516-1523 (2008).

[40] Seitz F., *The Modern Theory of Solids*, Dover, New York (1987).

[41] Shivola A., *Mixing models for heterogeneous and granular Media*, in Advances in Electromagnetics of Complex Media and Metamaterials, Zouhdi S., Sihvola A. and Arsalane M. (eds.), Kluwer, Amsterdam (2002).

[42] Smith D.R., Schultz S., Marko P. and Soukoulis C.M., *Determination of effective permittivity and permeability of metamaterials from reflection and transmission coefficients*, Phys.Rev. B, 65, 195104, (2002).

[43] Smith D.R., Vier D.C., Koschny T., and Soukoulis C.M., *Electromagnetic parameter retrieval from inhomogeneous metamaterials*, Phys.Rev. E, 71, 036617 (2005).

[44] Soltani M., Alimardani R. and Omid M., *Evaluating banana ripening status from measuring dielectric properties*, J.Food Engrg., 105, 625-631 (2011).

[45] Stratton J.A., Electromagnetic Theory, Mc Graw-Hill, New York (1941).

[46] Tomick J.J., *On convergence of the Nelder-Mead simplex algorithm for unconstrained stochastic optimization*, Phd thesis, Pennsylvania State University, College Park (1995).

[47] Trefethen L.N. and Bau D., *Numerical Linear Algebra*, SIAM, Philadelphia (1997).

[48] Von Hippel A.R., *Dielectrics and Waves*, Chapman & Hall, London (1954).

[49] Vuye G. and Lopez-Rios T., *Precision in the ellipsometric determination of the optical constants of very thin films*, Appl.Opt., 21, 2968-2971 (1982).

[50] Wirgin A., *Ill-posedness and accuracy in connection with the recovery of a single parameter from a single measurement*, Inv.Probs.Engrg., 10, 105-115 (2002).

[51] Yeh C.-C. and Yang C.-H., *Characterization of mechanical and geometrical properties of a tube with axial and circumferential guided waves*, Ultrasonics, 51, 472-479 (2011).

[52] Yilmaz T., Foster R. and Hao Y. *Detecting vital signs with wearable wireless sensors*, Sensors, 10, 10837-10862 (2010).

[53] Young J. and Ridzal D., *An application of random projection to parameter estimation in partial differential equations*, SIAM J.Sci.Comput., 34, A2344-A2365 (2012).

[54] Young K.F. and Frederikse H.P.R., *Compilation of the static dielectric constant of inorganic solids*, J.Chem.Phys.Ref.Data, 2, 313-408 (1973).